Numerical modeling of wave transmission over a living breakwater

Kimon Kadoglou

reefy
Innovation for nature

TU Delft

Deltares

Numerical modeling of wave transmission over a living breakwater

by

Kimon Kadoglou

To obtain the degree of master of Science
at the Delft University of Technology,
to be defended publicly on May 10th, 2023, at 15:15 PM.

Student number: 5384761

Thesis Committee:

Prof. dr. ir. M. van Gent (Chair)	TU Delft
Dr. M.F.S. Tissier	TU Delft
Dr. ir. S.G.Pearson	TU Delft
Ir. D. Houtzager	Reefy
Ir. M.P. de Ridder	Deltares

An electronic version of this thesis is available at https://repository.tudelft.nl/

Cover picture: Reefy breakwater. Credit: Reefy

reefy Innovation for nature

TU Delft

Deltares

Abstract

Living Breakwaters have evolved from traditional breakwaters to create multi-purpose structures that provide environmental and social benefits. These breakwaters promote a healthy habitat for flora and fauna, while achieving the same structural capabilities as conventional structures. *Reefy* has developed a modular living breakwater that can serve both as an artificial reef and a stable breakwater. This study aims to model the impact of a Reefy breakwater on the transmitted wave height, using a process-based numerical model, namely XBeach.

This study builds upon a previous one conducted by van den Brekel [2021], where scaled experiments were performed in a physical wave flume, to investigate the hydrodynamic and ecological functionalities of the Reefy breakwater. In the wave flume experiments a total of 15 structure configurations together with 35 wave conditions, both regular and irregular, were tested. The first 7 of the configurations were 2D structures with a relatively simple shape and a porosity of 20%, and the rest were complex 3D structures with a porosity above 20%. The wave flume was recreated within the numerical model. The influence of the breakwaters on the wave heights are examined through the comparison between the calculated transmission coefficient of the wave flume and the numerical model. However, XBeach, and more specifically XBeach non hydrostatic+ mode which was used, does not resolve the complex interaction between waves, friction and porosity of the structures. As a result, a simple method had to be found to compensate for the loss of these phenomena, while successfully calculating the transmission coefficient.

The findings of this analysis demonstrate that treating the breakwater as an impermeable change in bathymetry, coupled with a 15% reduction in structure height, produces the desired outcomes. From the 35 wave conditions only the 8 irregular wave conditions were chosen to be of interest due to time constraints. Among these 8 wave conditions that were used as an input in XBeach, only 5 of them were satisfying the criterion that describes the range for which the numerical model should produce accurate results ($kd<2$). The transmission coefficient was defined as the ratio of the transmitted wave height behind the breakwater, and incident wave height in front of the structure. The wave decomposition method used was a modified Guza split method. In pursuit of finding a valid solution, the breakwaters were modeled firstly as impermeable structures with a decreased height, secondly as impermeable structures with a decreased width, thirdly as vegetation with the help of the vegetation module,and lastly the maximum wave steepness criterion as applied in the model was increased (*maxbrsteep* up to 1.4), without modifying the structure height.

Among the suggested solutions and after being validated for 13 experiments with both simple and complex structures, decreasing the width did not achieve the desired results while the vegetation module failed to produce consistent outcomes. As far as transmission coefficient is of interest, a 15% decrease in the structure height had the smallest mean absolute percentage error of almost 10% and a root mean square error of 8.2%. On the other hand, choosing to increase the maximum wave steepness (to a value of 1.4) is not a valid option for the complex 3D structures, but illustrates even better behavior than a change in the structure height when simple structures with 20% porosity are concerned. To summarize, this thesis provides alternatives to replicate in a simplified way the impact of porous structures, such as Reefy breakwaters, without the need of an extensive and time expensive numerical model.

Acknowledgements

After a challenging two and a half years, my journey at TUDelft is coming to a close. This journey has been filled with both ups and (lock)downs. I am immensely grateful for the unwavering support of both my old and new friends. Living with roommates for the first time, I could not have found better people to share my experience with. To my friends at the university, who always found time to chat by the coffee machines, my days at the university would have been dull without you.

Even before I joined TU Delft, I was fascinated by nature-based solutions, so when the opportunity arose to do my thesis project with Reefy, I applied instantly. I was pleasantly surprised to meet a team full of passionate people with a common goal, working together to bring the Reefy breakwater to life. I am grateful to Jaime Ascencio for trusting me and letting me be a part of the Reefy team, where I felt welcomed from the moment I walked into their office in Rotterdam. It is amazing to see the team expanding with more people and upgrading their offices from Rotterdam to Delft. I am sure the future of Reefy is bright, and I can't wait to see their next accomplishments.

I was very fortunate with my thesis committee members, who showed endless patience and provided useful feedback and support. Daan Houtzager helped me in every step of my thesis, from coding to writing, and was there for me every single day. Without Menno de Ridder, I would not have been able to set up XBeach and analyze the results. His patience and willingness to help and answer my countless emails are truly admirable. Stuart Pearson was even more enthusiastic and optimistic than I was and provided me not only with valuable literature but also helped me organize my thoughts and write them. Marion Tissier was always on point with her feedback on my results and teaching me to be critical of my results. Without her guidance, I would still not be able to define my end goal. Marcel van Gent helped me with the important decisions I had to make through my thesis and provided constructive input on the topic.

Lastly, I am greatly appreciative of my brother who was there with me every day, and with whom I could share all the bad and good moments of my journey. I always had unlimited support and love from my family, despite being 2,000 kilometers away. Thank you for always being there for me.

Kimon Kadoglou

Delft, May 2023

...

Contents

List of Figures

List of Tables

1. Introduction

1.1. Background

In December of 2015, the Paris Agreement was signed by 175 parties, including the countries of the European Union. According to the Paris agreement, the parties agreed, based on Article 2, to adopt measures to maintain the increase of the global average temperature by 1.5 degrees Celsius above pre-industrial level, in a way to minimize the possible climate change impacts [UNFCCC, 2016]. Contrary to temperature, within the agreement there is no reference to sea level rise. Even if the Paris Agreement targets are full filled, sea levels will continue to rise steadily [Toimil et al., 2020]. For the scenario of maintaining the temperature rise between 1,5 °C and 2 °C, the global sea level is expected to rise between 0,74 and 0,80 meters [Brown et al., 2021]. Based on a study of 5 different coastal areas in the East USA coast, it was found out that the magnitude of coastal erosion is two times bigger than the rate of the increase of sea level rise [P.Leatherman, 2000]. This means that the existing problems humanity is facing at the moment regarding coastal safety and erosion will only be exacerbated in the not so distant future.

The common practice (e.g. Salman et al. [2004]; Airoldi et al. [2005]) to facilitate the coastal development around the globe for many years has been to construct hard structures, such as sea walls, groins, breakwaters, revetments etc. However, these structures come along with many negative effects, such as alteration of the coast's natural system or detrimental visual effects on the landscape. Such an alteration could be the change of flow acceleration (e.g a shore normal structure) that may prevent sessile creatures from attaching at the inter tidal zone or block the along shore movement of fauna and sand [Schoonees et al., 2019]. Through the years, the use of such structures has been highly challenged by both governmental institutions and the public opinion (e.g. Singhvi et al. [2022]; European Commission and Directorate-General for Research and Innovation [2015]; Spalding et al. [2014]). Given the need to act pro-actively and under public pressure for a more sustainable future, the solutions that coastal engineers have to provide must be flexible, long-lasting, multi-functional, and financially feasible. For these reasons, engineers have focused on the use of ecosystems and their role in coastal management. The utilization of the ecosystems provide natural alternatives to support coastal communities, while offering even more considerable benefits than the traditional hard structures, including preservation of nature, development of recreational areas,capture of carbon,enhancement of water quality, the production of fisheries, etc. [Gracia et al., 2018]. Restoration of mangroves and salt marshes can be up to five times less expensive than a breakwater, and they may even prove to be more cost-effective than a series of groynes, according to a study that examined the costs and advantages of 52 ecosystem-based coastal erosion management projects from around the world [Narayan et al., 2016]. Beck et al. [2022] suggest that over the lifetime of a project, restored natural infrastructure can offer flood protection benefits of $100,000 per hectare, under conservative estimations and utilizing risk-industry methods for the area of the Caribbean Sea (20 countries). At they same time, they provided valuable information regarding funding options to decrease flood risk through habitat restoration.

One of the most important natural coastal ecosystems are coral reefs. They are the equivalent of a rainforest, providing high structural complexity, high species diversity and are an important source of protein for the human population that inhabit the tropical latitudes. These tropical regions are also the

ones that experiencing rapid population growth, adding to the need for a sustainable managing plan for the reef ecosystems [Reaka-Kudla, 1997]. Coral reefs, comprising of fore reef, reef crest and coral flat, can help with the wave attenuation, by reducing the incoming wave energy up by an average of up to 97% [Ferrario et al., 2014]. Moreover, coral reefs have the ability of natural vertical accretion, even though with the current rate, sea level rise is expected to exceed new reef flat accretion [Quataert et al., 2015]. Coral reefs are in danger of increased and repeated events of extreme temperatures. The frequency of these events, render the reefs incapable of significant recovery [Sheppard et al., 2005]. When the corals die, the reef then starts to degrade and erosion takes place. Additionally, apart from the resulting deepening of the reef, it also loses its natural surface roughness. In the coral reef of Roi-Namur, the decrease of the roughness together with an increase of higher offshore water level resulted in an astonishing 200% increase of the wave runup (Figure 1.1 [Quataert et al., 2015].

Based on the aforementioned information and in the wake of the need to not only protect, but also enhance the natural ecosystems, focus has shifted from armoring the coastlines with hard structures to a holistic approach that includes ecosystem services that are being provided by nature. Such solutions are referred as *Living Shorelines* that incorporate coastal natural habitats and provide opportunities for restoration of the ecosystem and at the same time protect the shore from erosion [Bilkovic et al., 2016]. These solutions apart from their ability to counter coastal erosion and secure coastal security, can also survive sea level rise by natural accretion, as long as they are not overtaken by the accelerating rate of sea level rise. One should note though that introducing structures to create such shoreline may induce some trade-offs which can induce loss or transformation of local fauna [Bilkovic and Mitchell, 2013].

For the Living Shorelines to exist, traditional design of breakwaters had to be evolved to accommodate the needs of the community that pursues of a sustainable management of the coasts. That is how the creation of *Multi-purpose* or *Living-Breakwaters* has come to existence. Traditional breakwaters usually mimic stone shorelines and have detrimental effects to aesthetics and water quality [Diplarakos, 2016]. On the contrary, living breakwaters display environmental (by providing habitat for the marine environment), social (e.g better water quality near shore,tourism) benefits while achieving the same structural capabilities of conventional structures. A successful instalment of living breakwater took place in Brooklyn, New York, where after a 3-year monitoring program, Manson et al. [2018] observed that the artificial reefs that were installed there provided the expected rehabilitation results, despite the lack of initial natural environment (Figure 1.2). It is very important for these kind of breakwaters to promote a healthy and complex coral growth, by considering their location on the shore, their material, texture and structural characteristics. Harris et al. [2018] has reported findings which indicate that even in an increased sea water level, healthy and complex coral reefs decreased the wave height of the back reef by three times. Such Living breakwaters could be put in front of existing breakwaters or dikes to lessen the impact on the structures. Submerged and permeable breakwaters have been proven to work, without the need of modifying the height of existing infrastructure [Liang et al., 2015]. An example of a living breakwater that offer opportunities for corals establishment is ***Reefy Living Breakwater***.

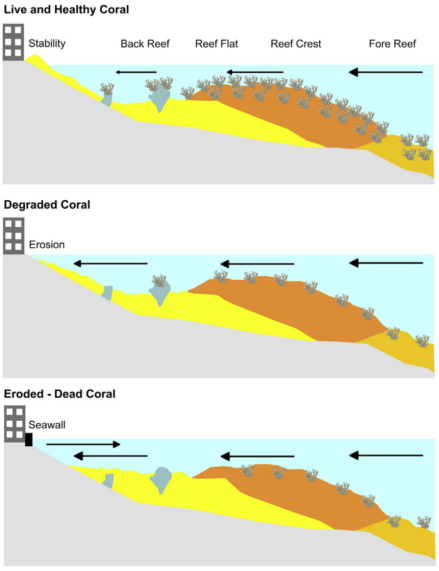

Figure 1.1.: How the change from healthy to eroded corals affects the shore. [Gracia et al., 2018]

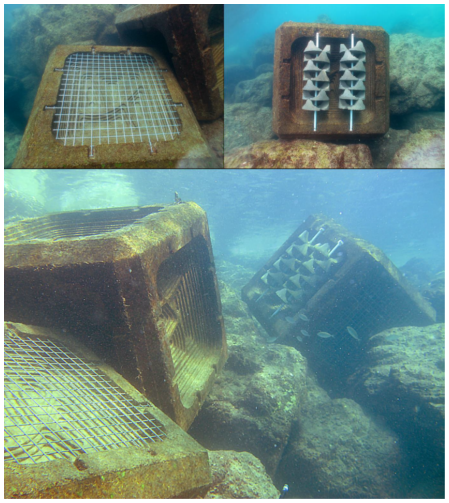

Figure 1.2.: Example of the installation of the units used for the creation of Living Breakwaters in New York at the start of the project. [Manson et al., 2018]

1.2. Reefy

The start up Reefy has come up with a design of a modular living breakwater. A breakwater made by Reefy modules is shown in Figure 1.3. Due to its architecture, the unit based on which the breakwater is built, allows the creation of necessary cavities where fish can nest or be protected from predators and extreme hydrodynamic conditions. The empty spaces help to achieve high porosity of the structure and ensure the flow of nutrients through it. Reefy blocks have a coarse texture and can be manufactured with geopolymer or circular (recycled) concrete based on the requirements of the project. These characteristics help with the establishment of organisms that need a hard substrate, such as corals or oysters. What makes Reefy unique is the combination of creating an artificial reef and creating a stable breakwater that can survive wave induced loading during storms.

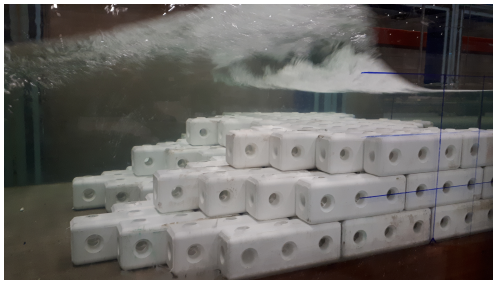

Figure 1.3.: Scaled ($n_l = 15$) Breakwater constructed of Reefy blocks.

Figure 1.4.: An example of a Reefy module scaled to actual size.

1.3. Prior Study & Scope

Reefy has already done tests with the blocks and the breakwater at the facilities of Deltares. In the Eastern Scheldt wave flume, the Reefy team conducted a number of experiments where 15 different configurations of the Reefy breakwater were tested, with the purpose of testing its hydrodynamic performance under daily conditions [van den Brekel, 2021]. Likewise, ecological performance was evaluated through the study of the velocities near the structures, since the flow velocities around the structure determine whether or not different organisms could grow on the breakwater. By doing so, they manage to formulate some initial guidelines and provide knowledge about the relevant physical processes that govern wave attenuation by the structure. A more detailed description of the flume experiment will be given in Chapter 2.

The next phase of the study would be to recreate the physical experiments in a numerical model. A numerical model is needed to achieve a better understating of the hydrodynamics around the proposed breakwater. For example, a numerical model can will provide information that would be useful to access the wave impact on the shore and the possible fauna and flora that would inhabit the area. Having this information will help to design breakwaters that are site-specific and cost-effective. The model is already chosen to be XBeach [Roelvink et al., 2009] and specifically the XBeach Non-Hydrostatic+ (XB-NH+) version of the model [Smit et al., 2014b]. The focus of this thesis is to access the effect of the breakwater on the transmitted wave field through the examination of the wave transmission coefficient. To do so, a way must be found for the breakwater to be successfully simulated within the domain, even though XBeach offers no possible option to simulate a porous submerged structure.

1.4. Objectives and Research questions

The main purpose of this thesis is to show the applicability of XBeach numerical model in modeling the Reefy breakwater with the intention of providing insight into the effect of the breakwater on wave transmission. Understanding the influence that design configurations of the breakwater have on the transmitted flow field is critical for determining the quality of the results. Thus, the study is aiming to answer the following question:

> In what way and how accurately can we simulate the impact on wave transmission of a Reefy breakwater using the process-based numerical model (XBeach Non hydrostatic+)?

The research question is subdivided into 2 subquestions that will help with answering the main question:

1. *How does the physical geometry of the breakwater affect the accuracy of XBeach Non hydrostatic+ simulation results?*
2. *In what ways can the breakwater and the impact on the transmitted wave heights be simulated within XBeach and how accurate are these other strategies?*

1.5. Thesis outline

The thesis is divided in 7 Sections. So far in Section 1 the motivation behind the thesis together with the scope has been defined. The following chapters will be aimed to develop a better understanding of the theoretical background, set up of the XBeach simulations, and then provide the necessary explanation to answer the research questions. Section 2 will provide a more thorough explanation of the wave flume experiment that was conducted before the current thesis. An overview of the relevant literature will be given that will help with understanding the effects of porous breakwaters on the wave field, the modeling of a porous breakwater and the inner workings of XBeach. In Section 3, the data that will be used together with the parameters and tools that are needed for the analysis will be provided. Furthermore, the model set up, both of the wave flume and the breakwater, will take place. Following that, in Section 4, the results of different simulations along with the validation of different structures from the experiment will take place. Section 5 an application of XBeach to verify the behavior of the model. Finally, Section 6 provides a discussion of the results, Section 7 the conclusion, and Section 8 recommendations.

2. Literature Study

An overview of the available literature is given in this Section. Insight and background information will be provided that is needed to comprehend the knowledge of previous studies. This knowledge is required to evaluate and understand the findings of the current thesis. In Section 2.1 the layout of the wave flume experiment and the main key observations are given. In Section 2.2 the hydrodynamic behavior of a porous structure and an analysis of the main methods that are being used to model porous breakwaters are explained. Lastly, Section 2.3 describes the formulation and applicability of XBeach and lastly

2.1. Preceding research and physical model

This section provides a summary of the previous thesis and introduces the data that will be used in the present study. The prior research conducted by van den Brekel [2021] serves as the foundation for the current thesis, as it lays the groundwork for the research to be conducted

2.1.1. Scaled Model

van den Brekel [2021] executed a scaled wave flume experiment with a total of 15 configurations and 36 wave conditions. The law of scaling that was used is based on a constant Froude number:

$$Fr = \frac{u}{\sqrt{gd}} \tag{2.1}$$

For the test, a scale factor of $n_l = 15$ was chosen, which translates to a model whose lengths are 15 times smaller compared to reality. The set up of the model is given in the Figure 2.1.

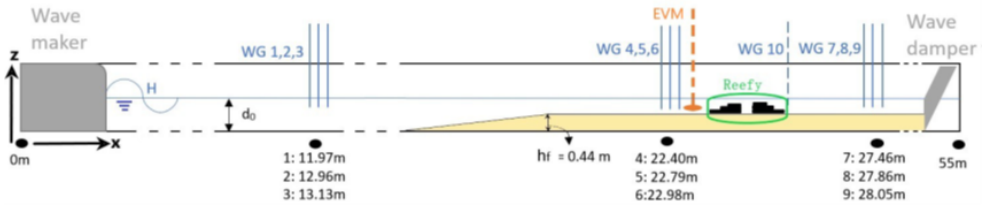

Figure 2.1.: A figure of the cross-section where the set up is visible. An explanation of the symbols is given in the following paragraphs. The flume can be divided in 3 parts: the deep part that is located at the left side of the flume and ranges from x=0m to x=19.5m, the foreshore located between x=19.5m to x=22m, and finally the shallow part until x=55m. At x=55m a parabolic wave damper was installed.

The following notations were used, which will be used again in this thesis with the same meaning:

- H= the wave height (m)
- d_o= deep water depth (m)
- h_f= the foreshore height (m)
- d_f= depth at the toe of the structure (m)
- h_c= height of the breakwater
- $R_c = d_f - h_c$= relative freeboard which will be positive for submerged structures
- WG = Wave gauges to record waves characteristics
- EVM = Electromagnetic liquid velocity meter to measure water velocities

The total length of the set up was 55 meters, the width was 1 meter and the total height 1.2 meters. The wave maker was installed at the left side (x=0m). It was a piston type wave generator with reflection compensation activated throughout the study and was also able to produce second order waves. At the end of the flume a parabolic wave damper was situated (x=55m). The deepest area in front of the foreshore had a varied depth of 0.61m, 0.68m and 0.75m (based on a pilot project) and where the first 3 wave gauges are located. The foreshore had a height of 0.44m with a slope of 1:10 to recreate the non-linear phenomena, namely due to shoaling and the breaking of the waves. This results in the generation of shorter, smaller waves which are phase-locked with the primary wave and are released during breaking. The wave spectrum also experiences changes, with energy transferring from peak frequencies to lower frequencies and higher harmonics [Lamberti and Burcharth, 2004] . In each test, the breakwater was constructed between gauges 6 (wave gauge group of 4-5-6) and 7 (wave gauge group of 7-8-9), with the front located about x=25.1m, changing among the experiments about 10cm. The extra wave gauge, namely WG 10, was only present for structures 4,5,6 and 7 to measure set up, with position 26.93m and 26.16m.

The waves conditions varied between regular and irregular. For the regular wave tests the target steepness s(0.02-0.04), wave height H(m) and period T(s) had to be defined. On the other hand, for the irregular wave test the target steepness s(0.02-0.04) significant wave height Hs(m) and peak period Tp(s) were used to create a JONSWAP spectrum with a peak enhancement factor γ=3.30. A description of the non-linearity of the tests at wave gauges 4 to 6 is given at Figure 2.2. For every combination of s and d_o the wave height was increased until just under the point of breaking. The goal was to have tests where the waves did not break at all before they reach the structure. The regular waves that were breaking before the structure where of no interested for the study. An overview of the wave conditions are given in Appendix A Table A.1

The first 6 structures were **2D** structures, in which there is no change in the structure width-wise, and the rest are **3D** structures where the block-void composition and/or the orientation change along the width. Structures 8 to 12 are actually comprised of 2 structures with a channel between them. This channel had a varied length among the different experiments. An overview of all design is given in Figure 2.3. For the description of the different configurations the following abbreviations were used:

- h_c= crest of the breakwater (m)
- B= width of the crest (m)
- α= front slope ($^\circ$)
- L_{ch}= Channel length (m)
- S_{ch}= Spacing between the middle of front - back crest width (m)

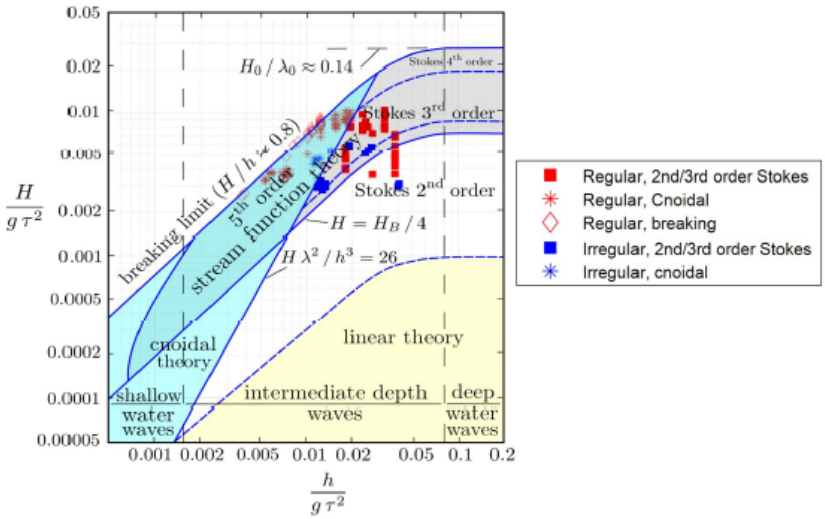

Figure 2.2.: In this figure the steepness of the waves against the relative water depth is plotted for the incoming waves at wave gauges 4,5,6 (in front of the location of the breakwater). The points are plotted above the diagram of [Méhauté, 1976] that describes the applicability of different wave theories. The red marks depict regular wave condition whereas blue marks depict the irregular wave conditions. [van den Brekel, 2021].

- A_{tot}= total surface area of cross section (m^2)
- Φ= Porosity, estimated as $\frac{V_{voids}}{V_{total}} = \frac{V_{total} - V_{material}}{V_{total}}$. The V_{total} is assumed equal to $A_{total} * 3$

Furthermore, the effect of coral growth was simulated by either adding 3D printed corals or PVC pipes. This structures are the 8-I-3D and 8-I-PVC, with "I" meaning that the channel length is equal to 1m (in a full scaled model). Likewise, "II" means that the channel length is 2m etc. Lastly, in structure 2-BH, the effect of the blockage of the holes due to growth of vegetation was simulated. In Appendix A, and in Table A.2, Table A.3, the details of the characteristics of each structure are given.

2.1.2. Data Processing

Both for regular and irregular wave tests the significant wave height H_{m0} (based on the total variance) was used to measure the transmission and reflection coefficients (as per, Zanuttigh and van der Meer [2008]). The following equations were used for the transmission and reflection coefficient:

- Firstly, tests were done without the structure and measurements were taken at the position of the wave gauges. These tests are symbolized with an f. Afterwards, the tests were repeated with the structure, and measurements were taken at the same positions. These tests are symbolized with s,f. The transmission coefficient is estimated as the the transmitted wave height behind the structure relative to the test without the structure. Both measurements were taken at Wave Gauges 7,8,9 (Figure 2.1).

$$K_t(s) = \frac{H_{m0,i,WG789(s,f)}}{H_{m0,i,WG789(f)}} \tag{2.2}$$

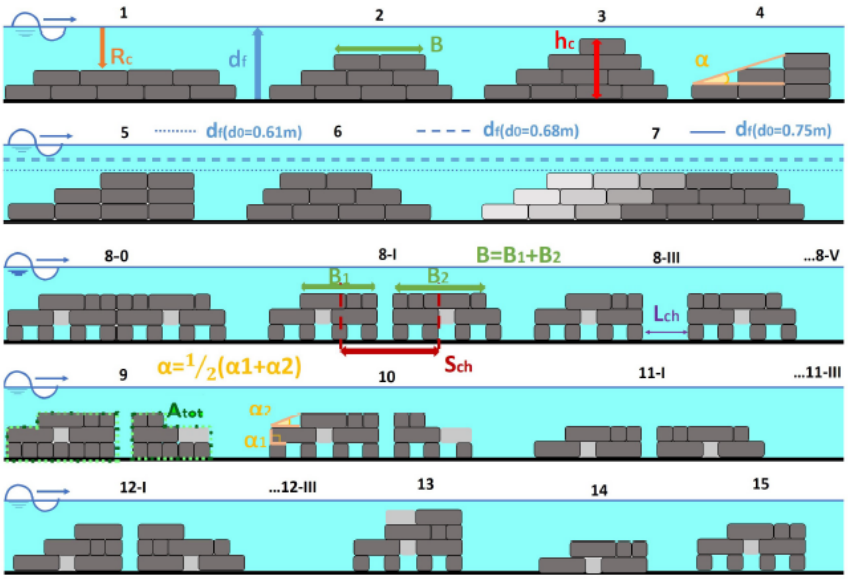

Figure 2.3.: Simplified illustrations of all the side views of all the configurations. Above each structure, the corresponding number is given. The holes of the modules are not shown here. Lighter shades of grey mean change of the orientation width wise, meaning shark-tooth/zigzag orientation [van den Brekel, 2021].

- For the wave reflection the coefficient was defined by measuring the reflected and the incoming wave height at the Wave Gauges 4,5,6 (Figure 2.1), assuming that the wave damper located at the end of flume is not influencing the results.

$$K_r(s) = \frac{H_{m0,r,WG456(s,f)}}{H_{m0,i,WG456(s,f)}} \tag{2.3}$$

For the wave decomposition method, Zelt&Skjelbreia (Z&S) [Zelt and Skjelbreia, 1992] method was used. With the help of Z&S method the reflected time signal was identified and subtracted from the total wave signal, resulting in the incoming wave signal. Subsequently the mean of the variances (incoming and reflected) were used to estimate the $H_{m0,r}$ and $H_{m0,i}$. It is worth noting that this method is used based on the fact that the reflection wave is small enough to be consider linear. If the reflected and incident wave heights were non-linear, for example during extreme conditions, the results would be unreliable. In consequence, only the cnoidals and stokes waves were into consideration during the optimization process of the empirical equations (Section 2.1.3) and not the breaking ones. The optimization was mainly performed with the regular wave tests because they were more than the irregular tests.

van den Brekel [2021] did an extensive literature review on the existing formulae on wave transmission and reflection of submerged breakwaters, based on which the following design variables were used to evaluate their impact the hydrodynamic performance (the parameters are defined at Section 2.1.1):

- Relative structure height $\frac{h_c}{d_f}$
- Relative freeboard $\frac{R_c}{H_{m0,i}}$

- Relative crest width $\frac{B}{L_0}$
- Porosity Φ
- Surf similarity parameter $\frac{tan(a_{front})}{\sqrt{s_{0,m-1,0}}}$
- Relative channel spacing $\frac{S_{ch}}{L_0}$
- Surface roughness

2.1.3. Hydrodynamic performance

Following the tests, van den Brekel [2021] compared the results to the existing formulae to find out the best fit. The best fit was achieved with the formula of van der Meer et al. [2005], which subsequently was optimized using a non linear regression analysis to get a smaller relative error. The resulting equations are:

- for $\xi \geq 3$

$$K_t = 0.325\frac{R_c}{H_{s,i}} + 0.679\left(\frac{B}{H_{s,i}}\right)^{-0.24}\left(1 - e^{(-10.511)*\xi_{0,m-1,0}}\right) \tag{2.4}$$

- for $\xi < 3$

$$K_t = 0.189\frac{R_c}{H_{s,i}} + 0.498\left(\frac{h_c}{d_f}\right)^{-0.358}\left(1 - e^{(-1.919)*\xi_{0,m-1,0}}\right) \tag{2.5}$$

Equation 2.4 was created from both regular and irregular wave conditions, but Equation 2.5 was based only on regular wave conditions, due to the fact that only four tests had $\xi < 3$ of the irregular wave tests, while more were needed. In both equations, the freeboard relatively to the incoming wave height has the largest impact on the transmission coefficient. Even though the roughness and the porosity of the breakwater are not within these equations, it was found they can also affect the transmission coefficient, but to a lesser extent compared to the other variables.

An overview of the key results will be given here. For further information one should look at van den Brekel [2021]:

1. Transmission
    - An increase in roughness of the structure decreases the transmission, with the effect being more important for steeper waves.
    - Increasing the porosity results in an increased transmission, specifically for longer waves. Likewise, decreasing porosity by blocking the modules holes with PVC decreases transmission.
    - For a given number of blocks, a wider crest is more effective in decreasing wave transmission than smaller porosity.
    - No correlation was found between transmission and channel spacing.
    - Increasing structure height decreases transmission.
    - Decreasing slope steepness decreases the transmission (more profound effect for smaller wave steepness).

- Surface roughness decrease the energy in first and second harmonic if the relative structure height is big enough.
- Zigzag/sharktooth orientation 1.3 didn't affect the transmitted spectrum.

2. Reflection coefficient
   - Reflection increases for increasing relative channel length.
   - Decreasing block porosity increases the reflection. However, when compared to the other factors, the effect is minimal.
   - Crest width and roughness had too little impact on the reflection.
   - Zigzag orientation resulted in less reflection compared to a straight one.
   - Increasing structure height increases reflection.
   - Like transmission, decreasing slope steepness decreases the reflection (more profound effect for smaller wave steepness).

2.2. Analysis of Porous Breakwaters

In this Section, the interaction between a porous breakwater and incoming waves will be discussed through the analysis of transmission and reflection coefficients, followed by an overview of how to model such a breakwater. Reefy breakwater is a porous structure itself and based on Table A.2 the porosity of the tested breakwaters varied between 0.20 and 0.46. The distinctiveness of a permeable structure arises from 2 characteristics. The first one is porosity, which is the proportion of the total volume of the structure that is occupied by voids or openings. The second one is friction, which refers to the resistance to the movement that the water faces as it flows through the pores of the structure. The amount of friction depends on the size and shape of the porous media.

2.2.1. Transmission and reflection above porous breakwaters

The objective of permeable breakwaters is the same as every coastal protection structure, to dissipate the incoming wave energy and protect, the shore or another structure, from heavy wave loading. They do so, by reflecting waves and causing wave breaking that reduces transmitted wave heights. For permeable breakwaters, there is additional dissipation of energy due to flow friction inside the porous structure.

Dick and Res [1968] were one of the first to investigate the behavior of permeable submerged structures against impermeable structures, through experimental work. They conducted experiments with rectangular breakwaters made of nested tubes. It was observed that permeable breakwaters behaved differently than impermeable ones: the reflection coefficient was smaller than the respective solid structures, and the transmission coefficient was smaller. Thus permeable breakwaters could dissipate more wave energy with increasing porosity values. However, for very shallow depths of submergence, both breakwaters were similar in their behavior.

On the other hand, Dattatri et al. [1978] reported that the behavior between permeable and impermeable breakwaters was not that different. Numerous laboratory investigations were conducted on porous structures of different shapes, porosity and submergence depths. In their report, the most important characteristics of the structures that influenced the behavior of the transmitted wave heights were the

width and the submerged height, while the porosity (tested values of 0, 0.41, 0.42 and 1) was of less importance for larger depths of submergence. Moreover, the shape of the breakwaters had only an effect on the reflection coefficient and not the transmission coefficient. Dattatri et al. [1978] account for the difference in their findings compared to Dick and Res [1968] on the fact that they used crushed stones as porous media, rather than tubes.

Gu and Wang [1992] created a numerical model to study permeable breakwaters of irregular shape and concluded that, if designed properly, porous breakwaters can dissipate more wave energy than impermeable structures, but for breaking waves, depth submergence played a more dominant role.

? studied the effect of the incident wave obliqueness together with breakwater shape characteristics and porosity. The results indicated that wave obliqueness has a lesser role compared to porosity and structure submergence on the reflection and transmission coefficient and that structure width is more important than structure slope.

Twu et al. [2001] investigated the behavior of a deeply submerged porous structure consisting of multiple vertical slices of porous material. Compared to a single-slice breakwater, in deep waters, a multi-sliced breakwater can decrease wave transmission more effectively. The submerged breakwater's porosity contributes more to wave dampening than the friction coefficient (inside the structure), because wave penetration would occur at both the submerged structure's front vertical face and upper horizontal face.

A numerical model was developed from Huang et al. [2003] to model the interaction between a solitary wave and a submerged permeable breakwater, where they found that there is a favorable value of porosity where the wave transmission is minimized, namely 0.52. Above this value, the transmission coefficient is increased again. Similarly, Hieu and Tanimoto [2006] estimated in their numerical model that a value of 0.56 was the most effective for reducing the wave transmission for a submerged porous breakwater under regular wave loading.

The interaction between a solitary wave and a submerged permeable breakwater was examined again by Lin and Karunarathna [2007]. They report that the more porosity values increase, the more the wave transmission values are increased. Nonetheless, there is a window of porosity values, $0.3 \leq n \leq 0.7$, where the energy dissipation increases with increasing porosity. On the contrary, the reflection coefficient decreases with increasing porosity values. Lin and Karunarathna [2007] also investigate in their work the effect of the breakwater length, for a given particle size of the porous media. The transmission coefficient tends to decrease with increasing the length of the breakwater, reaching the value of 0, since more energy is damped inside the structure. The reflection coefficient though, increases with increasing breakwater length, until it reaches a constant value and remains steady despite any further increase, meaning that the incoming energy dissipates at the frontal part of the structure. A finding that was also confirmed by Wu et al. [2012]; Wu and Hsiao [2013]. Therefore, there is an optimal thickness for the structure where efficiency is maximized.

Metallinos et al. [2016] designed a numerical model and illustrated the difference between an impermeable and permeable structure under breaking waves. They concluded that structures with low porosity, or impermeable structures, are more efficient in reducing incoming wave energy since flow through porous media is not able to reduce the energy through friction, to the same levels that of wave breaking. The transmitted waves are "squeezed" by the structure in impermeable conditions, allowing them to flow through the freeboard and over the crest. As a result, all of the wave energy is concentrated in the free depth above the structure. Wave breaking thus becomes more intense for the solid structure, resulting in lower transmission coefficient.

Qu et al. [2022] examined the effect of a permeable breakwater under extreme wave conditions by constructing a numerical wave model and using focused wave groups. The permeable breakwater resulted in bigger energy losses, up to 38% more than the impermeable structure.

Lastly, Kurdistani et al. [2022] formulated and calibrated an empirical formula to predict wave transmission, taking into account the pore pressure distribution inside the mound and the resulting wave damping. The suggested formula for the wave transmission coefficient shows a logarithmic descending trend for increasing porosity. In their formula, porosity has a weak effect on wave transmission, with the main influence originating from the relative submergence depth. Equation 2.6 shows the calibrated formula where z is the seaward slope, $\omega = (1/2\pi)\tanh(2\pi d_f/L)$, $\varphi = (n0.5d_f x)/(B_c H_i)$, n is the porosity of the structure and x is the horizontal coordinate inside the breakwater. For submerged breakwaters B_{eff} equals to [(4 × crest width + bottom width)/5].

$$K_t = 0.576 \ln\left(0.428\,(1+z)^{0.042}\left(1+\frac{R_c}{H_i}\right)^{0.75}\left(\frac{B_{eff}}{D_{n50}}\right)^{0.125}\left(\frac{L}{B_{eff}}\right)^{0.39}\omega^{0.413}\varphi^{-0.18}\right)+0.923 \tag{2.6}$$

Everything considered, in terms of the transmission coefficient for the porous structure, increasing the porosity generates higher energy dissipation due to flow friction inside the porous structure, lowering the transmitted wave height. On the other hand, increased porosity allows more energy to penetrate the structure, increasing the transmitted wave height. These two elements balance each other out. [Huang et al., 2003] Porosity seems to have a bigger impact on the reflection coefficient, but only the frontal part of the structure influences the outcome since most of the energy is dissipated in face of the structure.

Based on the aforementioned literature, porosity itself is not the most important factor that regulates wave transmission, but rather the submergence depth and width of the breakwater, mainly for breaking wave regimes above the structure. This is in agreement with the findings of van den Brekel [2021], where after the analysis of the experiments and optimized equations she came to the conclusion that porosity has a lesser effect on the transmission, with the submergence depth and width having a major impact.

Likewise, there is an agreement between the findings of previous studies and the results of the physical model regarding the reflection coefficient. As reported in the key results of the previous study, it was found that crest width had no serious impact on reflection, implying that the width of the breakwater was wide enough already and the reflection coefficient had reached a steady value. Zigzag orientation compared to a straight orientation has a bigger area where the incoming wave can dissipate and produce less reflection, further explaining the findings of van den Brekel [2021].

2.2.2. Overview of porosity models

A major difficulty in the understating the hydrodynamics of porous breakwater is the impact of the porosity on the flow that runs through it. Modelling porous media flow would also be very computationally demanding and possibly unnecessary if bulk results are desired. Usually, the porous breakwater, or any porous structure, is assumed to be uniform with one average porous parameter describing the porosity. To estimate the flow resistance and energy dissipation generated by porosity, semi-analytical porosity models with empirical parameters have been created. The hydrodynamic conditions of a porous breakwater are defined usually by a boundary value problem which requires a main equation

together with suitable boundary conditions [Han and Wang, 2022]. Normally such porous solutions suggest:

1. A fitting boundary condition of a simplified porous flow model.
2. An estimation of the empirical parameters, for example empirical viscous parameters or parameters to approximate the flow resistance and energy dissipation caused by porosity.

The first one to investigate the flow through porous media was Darcy [1856]. Following the formulation of the Darcy law, Forchheimer [1901] extended the equation to include inertial effects for higher Reynolds number flows. One of the first studies on wave transmission and reflection of porous breakwaters was performed by Sollitt and Cross [1972], of whom the proposed momentum equations are still widely used [Huang et al., 2003]. They recommended a linearized theory that arises from the momentum equations together with additional terms of inertia and nonlinear resistance forces to explain the frictional forces exerted by the porous media. The resulting linear equation, based on linear wave theory, was formulated as:

$$S\frac{\partial q}{\partial t} = -\frac{1}{\rho} \bigtriangledown (p + \gamma z) - f\sigma q \tag{2.7}$$

with S the inertial coefficient, q is the instantaneous Eulerian velocity vector, p is the corresponding pressure, ρ the fluid mass density, γ fluid weight density, z the vertical coordinate, σ the angular frequency of the wave and f is the linearized friction coefficient which is written as:

$$f = \frac{1}{\sigma} \frac{\int_V dV \int_t^{t+T} \varepsilon^2 \left\{ \frac{\nu q^2}{K_p} + \frac{C_f}{K_p} \left| q^3 \right| \right\} dt}{\int_V dV \int_t^{t+T} \varepsilon q^2 dt} \tag{2.8}$$

where V is the flow field where f is constant, T the wave period, ε is the porosity ratio, K_p the intrinsic permeability and C_f dimensionless turbulence coefficient.

After the study of Sollitt and Cross numerous numerical models were created to examine the interaction of porous structures with waves. One set of equations that were used from numerous models are the mild slope equations. One example is Rojanakamthorn et al. [1989] who modified Sollitt and Cross [1972] findings to develop a modified mild slope equation (by utilizing vertical eigenfunctions) to examine non-breaking waves over a finite porous bed. Other numerical models that were created based on mild slope equations are that of [Losada et al., 1991; Méndez et al., 2001; Hsu et al., 2008]. Just like mild slope approaches, shallow water equations (e.g.,Kobayashi et al. [1987]; Wurjanto and Kobayashi [1993]; van Gent [1994]), Boussinesq equations (e.g.,Hsiao et al. [2009]; Chen [2006]; Er et al. [1997]; Madsen and Sørensen [1992]) and extended Boussinesq equations [Metallinos et al., 2019, 2016] are widely used to model the flow in and out of a permeable structure.

All the previous numerical models are based on the notion of potential flow, which assumed that that the fluid is incompressible, non-viscous and the fluid motion is irrotational [Han and Wang, 2022]. The theory of potential flow upholds as long as the waves are not breaking. Nonetheless, wave breaking processes, turbulent flow, non-linear effects and structure-wave interaction need to be accounted for. Van Gent [1995] created a model based on Reynolds- Averaged Navier-Stokes equations to examine the wave motion outside and inside of the structure, by considering linear and nonlinear frictional forces. Furthermore Van Gent [1995] modified the Navier Stokes equations to include porous media flow. For a two dimensional incompressible flow with a constant fluid mass density through a homogenous isotropic porous medium, the equations are formulated as [Van Gent, 1993, 1995]:

$$\frac{1+C_A}{ng}\frac{\partial u}{\partial t}+\frac{1}{n^2 g}\left(\frac{\partial u^2}{\partial x}+\frac{\partial uw}{\partial z}\right)+\frac{1}{\rho g}\frac{\partial p}{\partial x}=-au-bu\sqrt{(u^2+w^2)} \tag{2.9}$$

$$\frac{1+C_A}{ng}\frac{\partial w}{\partial t}+\frac{1}{n^2 g}\left(\frac{\partial uw}{\partial x}+\frac{\partial w^2}{\partial z}\right)+\frac{1}{\rho g}\frac{\partial p}{\partial z}=-aw-bw\sqrt{(u^2+w^2)}-g \tag{2.10}$$

where:

- u and w are the filter velocities in x and z direction respectively
- n is the porosity
- C_A is a coefficient for added mass
- a is a dimensional coefficient (s/m)
- b is a dimensional coefficient (s^2/m^2)

Equations Eq.2.9 and Eq.2.10 can also be rewritten for one-dimensional porous flow as:

$$\frac{1+C_A}{ng}\frac{\partial u}{\partial t}+\frac{1}{n^2 g}u\frac{\partial u}{\partial x}+\frac{1}{\rho g}\frac{\partial p}{\partial x}=-au-bu|u| \tag{2.11}$$

The dimensional parameters a,b and C_A are computed as:

$$a=\alpha\frac{(1-n)^2}{n^3}\frac{\nu}{gD_{n50}^2} \tag{2.12}$$

$$b=\beta_c\left(1+\frac{7.5}{KC}\right)\frac{1-n}{n^3}\frac{1}{gD_{n50}^2} \tag{2.13}$$

$$C_A=\frac{1+\frac{1-n}{n}\left(0.85-\frac{0.015}{A_c}\right)}{ng} \tag{2.14}$$

where $KC=\frac{uT}{nD_{n50}}$, $A_c=\frac{u}{ngT}$ while α and β_c are empirical parameters

Following the work of Van Gent, Hsu et al. [2002] created a mathematical model on the basis of Volume-Averaged/Reynolds Averaged Navier-Stokes (VARANS) equations this time to depict sea surface for both impermeable, permeable structures or a combination of both. By taking the standard $k-\varepsilon$ equations and due to the volume-averaging process, the effects of the small-scale turbulence was managed to be included in the model. Another way to modify the Navier-Stokes equations is to additionally time average the VARANS equations [De Lemos, 2012].

The last step, so far, regarding the numerical modelling of porous flow is to model 3D processes like wave refraction or diffraction, something not possible with the previous studies presented here. For that reason del Jesus et al. [2012] constructed a new set of equations based on VARANS, the multiphase VARANS equations, where the turbulence once more is being modeled by $k-\varepsilon$ equations and Volume of Fluid Method (VOF) was used to simulate the water surface. The importance of a fully 3D model comes from the fact that the porosity actually may change along a porous structure such a breakwater. The model was validated from del Jesus et al. and was found out to demonstrate high level of agreement with previous experimental data.

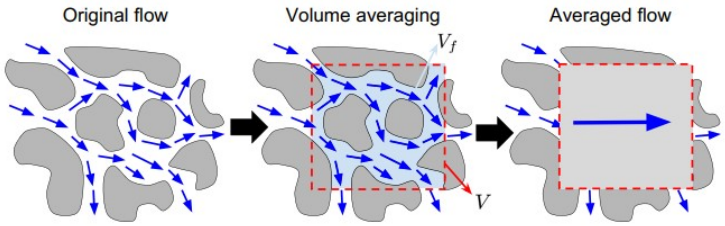

Figure 2.4.: The volume-averaging process used to resolve the porous flow [Losada et al., 2016]

Based on the existing literature, several techniques including design equations, analytical methods, numerical modelling and model testing, have been used to examine the influence of porous materials on the performance of breakwaters. For every different approach to the problem, a set of assumptions (e.g, physical or first estimation of parameters) and equations are applied that then are carried on from subsequent authors that expand their work. The difference between the way of approaching the porous flow and processing the steps needed to create a numerical model proves that there is no common agreement on modelling porous media flow [del Jesus et al., 2012]. Different models may be suitable for different structures and applications. Han and Wang [2022] suggest three factors to choose a fitting porous flow model:

1. Simplicity and robustness: When the early stages of conceptual development are concerned or when the study's focus is elsewhere rather than on the specific effects of porosity, simple models can be used. When qualitative rather than quantitative results are desired, models that are not complex and computationally expensive are sufficient enough.
2. Flow regime: Once the focus of the study is on understanding the energy dissipation of a porous breakwater, physical aspects may need to be considered to avoid unrealistic results. Different flow regimes (e.g., laminar, turbulent) affect the resistance force terms. Each model's applicability is determined by the relative importance of the resistance terms, which is determined by the flow characteristics.
3. Comparison with experimental data: Whether or not a porosity model is applicable to a given flow regime and structure, can be evaluated by comparing the results with experimental data. It is better to choose a porous model that has already been validated for the given structure.

2.3. Numerical Model

The theory behind the numerical model helps with recognizing the shortcomings and strengths that accompany it. Initially, the general description of XBeach is given with the governing equations, followed by the description of the XBeach non hydrostatic+ edition of the model, which is going to be used for the simulations.

2.3.1. Modelling with XBeach

The given model is XBeach, an open source process-based model [Roelvink et al., 2009], which was originally developed to simulate nearshore hydrodynamics such as the impact of erosion on dune and sandy beaches. Based on the desired time scale in which the model resolves the hydrodynamic processes, three model options are available:

- Stationary mode: wave-averaged equations but not taking into account infragravity waves.
- Surfbeat mode (XB-SB): both short wave variations and the long waves associated with them are computed on a group scale (instationary).
- Non-hydrostatic mode (XB-NH): models the propagation of and decay of individual waves (wave resolving).

For this thesis the Non-hydrostatic mode, and more specifically the Non-hydrostatic + mode (XB-NH+), was already decided since it has been thoroughly verified for reef hydrodynamics [Pearson, 2016; Quataert, 2015; Pomeroy et al., 2012; Van Dongeren et al., 2012; Lashley et al., 2018; De Ridder, 2018]. This is important because this means that XBeach Non-hydrostatic + is able to successfully reproduce wave transformations, such as shoaling, breaking and spectral energy allocation.

2.3.2. Non-hydrostatic + XBeach mode

Using non hydrostatic numerical schemes to model wave propagation has been applied before, with the most common models being SWASH [Zijlema et al., 2011] and NHWAVE [Ma et al., 2014]. Both models were applied to simulate porous structures with satisfactory agreement between experimental and numerical results. The advantage of these models is that they can model with better accuracy the structure-wave interaction. The disadvantages are that to compute the non-hydrostatic effects, a large number of grid cells are needed.

For the non-hydrostatic mode of XBeach, the non-linear shallow water equations together with a non-hydrostatic pressure are used to calculate the depth-averaged flow due to waves and currents. However, this model is not suitable for deep water waves because an error in the wave celerity arises in the deep water. The frequency dispersion behaviour can be captured sufficiently up to a certain degree with the depth-averaged and phase-resolving formulations, usually up to a relative depth of about kh=1, where k is the wave number and h the water depth. This limitation can be confining and force the boundary to be located in a region where kh$\leq$ 1, which can be for example the surfzone [de Ridder et al., 2021]. Contrary to Non-hydrostatic mode, which is a 1 layer model, Non-hydrostatic+ mode has 2 (reduced) vertical layers, similar to the work of Rijnsdorp et al. [2017]; Zijlema et al. [2011]. Adding an extra vertical layer increases the model's capabilities of computing the dispersive behaviour, while at the same time increases the computational costs. Cui et al. [2014] developed a reduced 2 layer model which still represents the dispersive behaviour better than a 1-layer model, but is less computationally costly.

De Ridder [2018] formulated in detail the equations used in the XB-NH and XB-NH+ versions, where he also validated them with laboratory data from previous cases. Here only the governing equations will be shown while for further details one should refer to De Ridder [2018]. The initial point for the derivation of the equations is the swallow water equations together with the inclusion of the non-hydrostatic pressure (for uniform flow in the y direction):

$$\frac{\partial u}{\partial t} + \frac{\partial uu}{\partial x} + \frac{\partial wu}{\partial z} = -\frac{1}{\rho}\frac{\partial (p_{nh} + p_h)}{\partial x} + \frac{\partial \tau}{\partial z} \tag{2.15}$$

$$\frac{\partial w}{\partial t} + \frac{\partial uw}{\partial x} + \frac{\partial ww}{\partial z} = -\frac{1}{\rho}\frac{\partial q}{\partial z} \tag{2.16}$$

$$\frac{\partial u}{\partial x} + \frac{\partial w}{\partial z} = 0 \tag{2.17}$$

where:

- t is time
- u horizontal Eulerian velocity
- w vertical Eulerian velocity
- t the shear stress
- p_{nh} non hydrostatic pressure
- $p_h = \rho g(\xi - z)$ hydrostatic pressure
- z=0 still water level, ξ the free surface elevation and d the water depth.

The above equations are bound by a constant pressure at the free surface and the following kinematic conditions:

$$w = \frac{\partial \xi}{\partial t} + u\frac{\xi}{\partial x} \quad \text{for} \quad z = \xi \tag{2.18}$$

$$w = -u\frac{\partial d}{\partial x} \quad \text{for} \quad z = -d \tag{2.19}$$

XBeach Non-hydrostatic+ , follows the reduced 2 layer model, where the domain is divided in the vertical into two layers, namely $\Delta z_1 = \alpha h$ and $\Delta z_2 = (1-\alpha)h$ with α the layer distribution parameter and h the total water depth. The normalized non-hydrostatic pressure q is given as p_{nh}/ρ. Vertical velocities and non-hydrostatic pressure are at the cell face, whereas horizontal flow velocities are along the layers' centers. The difference in velocity between the 2 layers is assumed small, which in terms of depth averaged velocity U means Δu/U $\ll$1.

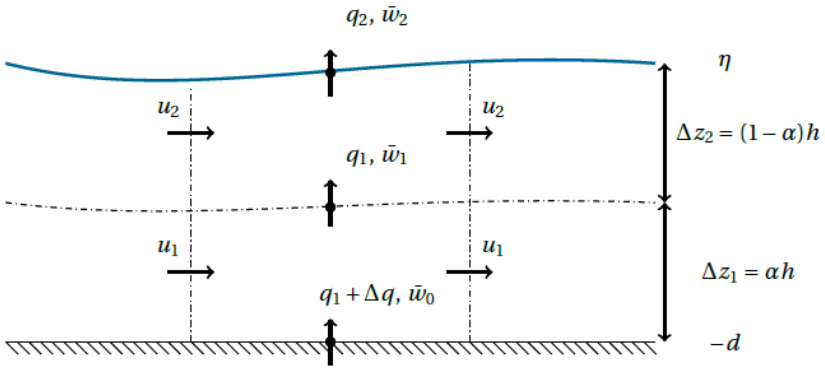

Figure 2.5.: Representation of the XBeach-nh+ grid. The bottom non-hydrostatic pressure is expressed as $q_0 = q_1 + \Delta q$ [De Ridder, 2018].

In the reduced two layer system, in the bottom layer (Δz_2) the non-hydrostatic pressure is constant, which means that Δq can be omitted, while the vertical velocity of the interface $\bar{w_1}$ is assumed to be of the same order such as Δu. The constant non-hydrostatic pressure can be justified from Equation 2.20 [Cui et al., 2014] which shows that the non-hydrostatic profile tends to become constant near the bottom, mainly for increasing kh values.

$$q = \rho h \eta \left(1 - \frac{coshk(z+d)}{coshkd}\right) \tag{2.20}$$

with

- q non-hydrostatic pressure profile
- h the free surface level
- η wave height
- d still water level

As a consequence of the simplifications made for the reduced 2 layers, only the continuity relation for the upper layer (Equation 2.21), the global continuity equation (Equation 2.22), the equation for the mean vertical momentum equation in the top layer (Equation 2.23) and the two horizontal momentum equations (Equations 2.24 and 2.25) are required. Through these equations U, Δu, w_2, ξ and q are possible to be calculated.

$$\frac{\partial}{\partial x}[(1+a)hU + (1+a)ha\Delta u] + 2w_2 - \bar{u_2}\frac{\partial \xi}{\partial x} - \bar{u_1}\frac{\partial z_1}{\partial x} = 0 \tag{2.21}$$

$$\frac{\partial \xi}{\partial x} + \frac{\partial hU}{\partial x} = 0 \tag{2.22}$$

$$\frac{\partial hw_2}{\partial t} + \frac{\partial hUw_2}{\partial x} - \frac{q}{1-a} = 0 \tag{2.23}$$

$$\frac{\partial hU}{\partial t} + gh\frac{\partial \xi}{\partial x} + \frac{\partial}{\partial x}(hU^2) + \frac{1+a}{2}\frac{\partial hq}{\partial x} - q\frac{\partial d}{\partial x} = 0 \tag{2.24}$$

$$h\frac{\partial \Delta u}{\partial t} + \frac{\partial U\Delta u}{\partial x} + \frac{1}{2}\frac{\partial hq}{\partial x} + \frac{q}{(1-a)}\frac{\partial \xi}{\partial x} = -\tau_0 - \nu\frac{2\Delta u}{a(1-a)h} \tag{2.25}$$

The location and the breaking of the waves are estimated with the hydrostatic front approximation [Smit et al., 2014a], in which the model is locally transformed to a shallow water model where the pressure distribution under breaking bores is assumed to be hydrostatic. With the hydrostatic front approximation the vertical structure of the flow is not explicitly computed as XBeach is depth-averaged. Based on the XBeach manual, a cell is considered hydrostatic when $\frac{\partial \xi}{\partial t} > 0.6$, i.e the steepness of the wave is above 0.6. Higher steepness values mean steeper wave faces before the limit of breaking. The cell will become non-hydrostatic once $\frac{\partial \xi}{\partial t} < 0.3$, which stands for the passing of the wave crest. In XBeach, this value is calibrated through the *maxbrsteep* parameter. Through validation with 2 different cases, de Ridder et al. [2021] concluded that the XB-NH+ can correctly simulate the bulk wave statistics and the spectral properties, with extended applicability up to kh=5, but for kh bigger than 2 the surface amplitude deviates from linear wave theory. On the contrary, XB-NH is applicable up until kh=1.

3. Methodology

In Chapter 2 a short summary was given of the work van den Brekel [2021] had conducted and will provide the present thesis with data. In Section 3.1 all the necessary data together with the parameters and techniques with which the analysis of the data shall take place will be shown. In Section 3.2 the set up of the wave flume and the breakwater within XBeach non-hydrostatic+ will take place. The breakwater will be simulated with a variety of options in the pursuit of reaching an agreement between the modeled transmitted wave heights and the reference wave heights from the wave flume.

3.1. Data

In this section, the parameters and the analysis tools will be introduced, followed by the selection of data that is going to be used in the next sections.

3.1.1. Data processing

To compare and analyze the data of both the wave flume and XBeach, the following 3 wave parameters are be computed:

$$\text{Significant wave height} \quad H_{m0} = 4 * \sqrt{m_0} \quad [m] \tag{3.1}$$

$$\text{Spectral Periods} \begin{cases} T_{m0,1} = \left(\frac{m_0}{m_1}\right) & [s] \\ T_{m-1,0} = \left(\frac{m_{-1}}{m_0}\right) & [s] \end{cases} \tag{3.2}$$

with:

- m_0 zero order moment of the spectrum (variance)
- m_1 first order moment of the spectrum
- m_{-1} minus one order moment of the spectrum

The moments are computed by integrating the variance density spectrum and are defined as:

$$m_n = \int_0^3 f^n E(f) df \quad \left[m^2/s^n\right] \quad \text{for} \quad n = -1, 0, 1 \tag{3.3}$$

The boundaries of the integration was 0-3 Hz, based on the fact that almost all of the energy of the computed frequency spectra was located within this range. From the surface elevation time series, the energy spectra are computed with the help of Welch's average periodogram method [Welch, 1967].

The variance is computed with the composite trapezoidal rule. In Appendix B, more information is given on the Welch method and a short analysis is done on the spectral resolution.

To distinguish between incoming and reflected wave signals a python script based on the method of Guza et al. [1984] is used. This method distinguishes the incoming and reflected signal using Equation 3.4, which is a relationship between the surface elevation and the cross-shore depth average velocity.

$$C_{\pm} = (\eta c \pm hu)/2c \tag{3.4}$$

with:

- $C_{\pm}$ the positive (incoming) and negative (reflected) wave signals
- η surface elevation
- u depth averaged current
- h local depth
- c the wave celerity. In its original form, this method assumes shallow water conditions and therefore the celerity is computed as $c = \sqrt{gh}$. However, for the given wave conditions and depths, the waters can be characterized as either deep waters or intermediate (swallow waters when d/L < 0.05). For this reason, the celerity was modified based on the dispersion relationship as followed: $c = 2\pi/T_p k$ where k is computed iteratively through the dispersion relationship $(2\pi/T_p)^2 = gktanh(kh)$. As an input for the wave period, the peak period of each wave condition was used.

Lastly, to assess the results of all the different simulations and computations, the root mean square error (RMSE Equation 3.5) and the mean average percentage error (MAPE Equation 3.6) will be used.

$$RMSE = \sqrt{\frac{\sum_{i=1}^{N}(\widetilde{y^i} - y^i)^2}{N}} \tag{3.5}$$

$$MAPE = \frac{100\%}{N}\sum_{i=1}^{N}\left|\frac{\tilde{y^i} - y^i}{y^i}\right| \tag{3.6}$$

where $\widetilde{y^i}$ are the computed values of XBeach, y^i are the observed values of the wave flume and N is the number of observations. RMSE is a measure of the average magnitude of the error while MAPE is a measure of the error relative to the physical model values. Additionally, the error plots, where the predicted values are plotted against the actual values, will also be given for each solution. It is worth noting that from the physical model test, only the surface elevation is known, and the measured wave parameters in the wave gauges. There is no information about the incoming wave spectra, or information about locations within the wave flume that were no wave gauges.

3.1.2. Wave Conditions

In Appendix A Table A.1 an overview of all the wave conditions is shown, both regular and irregular, that were tested in the wave flume experiment. In this thesis though, only the irregular conditions will be of interest, mainly for 2 reasons. Firstly, in the ocean and in real-life conditions the wave field is irregular. Secondly, due to time constraints, choices should be made on which conditions would be of interest. The table only with the irregular wave conditions is given at Table 3.1. For every wave condition, tests with and without the structure took place. As it can been seen from the same table not every structure was tested for every wave condition. The structure that was tested the most was the structure with number 8-I, a double-row structure with a channel in between and zig-zag orientation. (Figure 3.2). Structure 8-I along with Structure 2 will be the 2 main configurations with which the computations in the next sections will take place, for a solution to be found. Structure 2 (Figure 3.1), in contrast to Structure 8-I, is a single unit with a constant orientation over the width. It has the most plain shape among the structures that were tested for irregular wave conditions. After a solution is found, a validation will take place with configurations that were not tested.

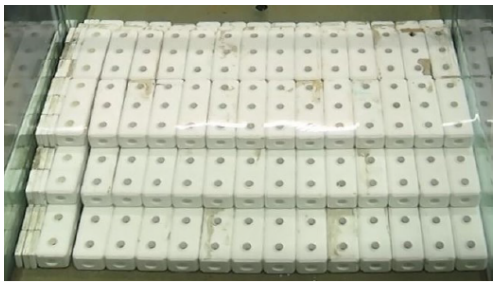

Figure 3.1.: Structure 2

Figure 3.2.: Structure 8-I

In Appendix A there are pictures of all the structures that were tested. The side view of all the structures was also given in Figure 2.3.

Wave conditions	d_0 [m]	T_{target} [s]	H_{target} [m]	s [-]	Structure number
5	0.61	1.16	0.04	0.02	11-I
					11-III
					12-I
					12-III
					14
16	0.68	1.47	0.06	0.02	2
					8-0
					8-I
					8-V
					13
					15
					8-I-PVC(69&169)
17	0.68	0.8	0.02	0.02	8-I
					15
18	0.68	1.31	0.1	0.04	11-I
					11-III
					12-I
					12-III
					14
19	0.68	1.15	0.08	0.04	8-I
					13.8-I-PVC
20	0.68	0.98	0.06	0.04	8-0
					8-I
					8-V
					8-I-PVC(169&3D)
35	0.75	1.6	0.14	0.04	2
					2-BH
					4
					5
					6
					7
					8-I
					8-I-PVC(38&69&169)
36	0.75	1.45	0.12	0.04	8-I

Table 3.1.: Overview of the Irregular wave conditions tests. T_{target} is the peak period T_p and H_{target} is the significant wave height H_s that were used to generate a JONSWAP spectrum that was the input of the wave generator. d_0 is the water depth at the wave paddle, which was located at the deep part of the flume (Figure 2.1). In some tests, a number of tubes (38,69 or 169) or 3D printed corals were installed at the holes of the top blocks to increase the friction of the breakwater (Figure A.8, Figure A.9, Figure A.10, Figure A.11). In one structure, structure 2-BH, the vertical holes were blocked with pipes to mimic fauna growth (Figure A.2). Note that these pipes didn't completely block the holes.

In Section 2.3.2, XBeach was described as a model made initially to compute nearshore processes and eventually was modified to be able to capture processes of intermediate waters with the XBeach non-hydrostatic+ mode. The wave conditions that were used as input (Table 3.1) have to go through an analysis to evaluate whether they satisfy the boundary conditions of XBeach. The analysis was done by computing whether for the given combination of wave height, wave period and depth, the waters in the flume can be characterized as deep, intermediate, or shallow. According to Holthuijsen [2007] and based on the ratio of depth/wave length or wave number times depth, the limits are:

- Deep water: d/L $>$ 0.5, or kd $>$ 3
- Intermediate water: 0.5 $>$ d/L $>$ 0.05, or 3$>$ kd $>$ 0.3
- Shallow water: 0.05 $>$ d/L, or 0.3 $>$ kd

XB-NH+ can be applied for boundary conditions up to kd=5, but an error is introduced at the surface amplitudes for kd bigger than 2. For this thesis, wave conditions that correspond to kd $>$ 2 will not be considered for the following sections and chapters as the results are expected not to be valid. In Table 3.2 the kd values of the wave conditions for the deep and shallow part of the wave flume are estimated (Figure 2.1).

	Wave characteristics			Deep Part		Shallow Part	
	d_0 [m]	T_{target} [m]	H_{target} [m]	d/L [-]	kd [-]	d/L [-]	kd [-]
WC 5	0.61	1.16	0.04	0.30	1.90	0.12	0.78
WC 16	0.68	1.47	0.06	0.22	1.42	0.11	0.72
WC 17	0.68	0.8	0.02	0.68	4.27	0.25	1.63
WC 18	0.68	1.31	0.10	0.27	1.70	0.13	0.82
WC 19	0.68	1.15	0.08	0.33	2.12	0.15	0.97
WC 20	0.68	0.98	0.06	0.45	2.80	0.19	1.20
WC 35	0.75	1.60	0.14	0.21	1.34	0.12	0.76
WC 36	0.75	1.45	0.12	0.24	1.56	0.13	0.85

Table 3.2.: The different wave conditions together with the computed characteristics.

There are 3 wave conditions, in which the kd values exceed the limit of 2, namely wave conditions 17, 19 and 20. For wave condition 17 specifically kd equals 4.27, which is the highest among the different wave conditions and with a value of d/L=0.68 the only wave condition in which the wave flume can be characterized as deep waters. The other two wave conditions have also high kd values. Therefore, these 3 wave conditions will not be of interest. A more extensive explanation is given in Appendix B and Table B.2

It is worth noting that the values used in Table 3.1 are the inputs that were used at the wave paddle at the start of the flume to produce the different wave conditions. At the wave gauges, different values were measured. In Table 3.3, Table 3.4 and Table 3.5, the significant wave height and the spectral periods are shown for each irregular wave condition without the structure. These values are computed from the surface elevation time series recorded at all the 9 wave gauges (WMH) that were installed at the physical model. The selection of the input for model will be based on these recorded values as explained in Section 3.2.1

	H_{m0} of all wave gauges [m]											
	d_0 [m]	T_{target} [s]	H_{target} [s]	WMH01	WMH02	WMH03	WMH04	WMH05	WMH06	WMH07	WMH08	WMH09
WC 5	0.61	1.16	0.04	0.038	0.038	0.038	0.036	0.036	0.036	0.035	0.035	0.035
WC 16	0.68	1.47	0.06	0.057	0.058	0.057	0.058	0.057	0.057	0.057	0.056	0.056
WC 18	0.68	1.31	0.10	0.093	0.094	0.093	0.088	0.087	0.087	0.085	0.084	0.084
WC 35	0.75	1.60	0.14	0.131	0.132	0.130	0.127	0.124	0.124	0.120	0.119	0.119
WC 36	0.75	1.45	0.12	0.112	0.113	0.112	0.108	0.107	0.107	0.104	0.103	0.103

Table 3.3.: Overview of H_{m0} per wave gauge and wave condition for the physical model. This is the significant wave height, computed through the measured surface elevation, including incident and reflected signals, which are not separated.

	$T_{m0,1}$ of all wave gauges [s]											
	d_0 [m]	T_{target} [s]	H_{target} [s]	WMH01	WMH02	WMH03	WMH04	WMH05	WMH06	WMH07	WMH08	WMH09
WC 5	0.61	1.16	0.04	1.00	1.00	1.00	1.00	1.01	1.01	1.03	1.04	1.03
WC 16	0.68	1.47	0.06	1.24	1.24	1.24	1.22	1.23	1.23	1.27	1.28	1.27
WC 18	0.68	1.31	0.10	1.13	1.13	1.13	1.08	1.10	1.11	1.17	1.17	1.17
WC 35	0.75	1.60	0.14	1.36	1.36	1.36	1.24	1.25	1.26	1.36	1.38	1.38
WC 36	0.75	1.45	0.12	1.24	1.24	1.25	1.19	1.20	1.21	1.27	1.27	1.27

Table 3.4.: Overview of $T_{m0,1}$ per wave gauge and wave condition for the physical model

	$T_{m-1,0}$ of all wave gauges [s]											
	d_0 [m]	T_{target} [s]	H_{target} [m]	WMH01	WMH02	WMH03	WMH04	WMH05	WMH06	WMH07	WMH08	WMH09
WC 5	0.61	1.16	0.04	1.07	1.08	1.08	1.11	1.12	1.13	1.18	1.18	1.18
WC 16	0.68	1.47	0.06	1.36	1.35	1.35	1.39	1.39	1.40	1.46	1.47	1.46
WC 18	0.68	1.31	0.10	1.24	1.24	1.24	1.30	1.32	1.33	1.44	1.44	1.44
WC 35	0.75	1.60	0.14	1.51	1.51	1.51	1.52	1.53	1.53	1.65	1.67	1.67
WC 36	0.75	1.45	0.12	1.36	1.36	1.36	1.39	1.41	1.41	1.49	1.50	1.50

Table 3.5.: Overview of $T_{m-1,0}$ per wave gauge and wave condition for the physical model.

3.2. Model setup

Now that the wave conditions that will be used as forced conditions at the boundary of XBeach are defined and the structures that will be used to be in the simulations have been chosen, the setup of the numerical model can be realized. At first, in Section 3.2.1, the setup of the wave flume will be completed. This includes grid sensitivity analysis that determine the results' resolution, tuning the forced conditions on the boundary as well as simulating the bathymetry that represents the physical model. The next step is to simulate the breakwater inside. As an Original case, the breakwaters will be represented as a simple change in the bathymetry, followed by modifying their size to reach the desired results. The maximum wave steepness parameter will also be part of the solution, as it regulates the wave breaking behavior. In the end, the vegetation module of XBeach will be tested to investigate whether modeling the breakwater as vegetation is possible.

3.2.1. Wave flume setup

Output locations

Regarding the output locations (e.g the locations within the domain where data is stored), in all the grid points both the depth average velocity u and the instantaneous sea surface z_s are stored. Additionally, fixed output points are chosen by the user for specific locations and XBeach links the point to the nearest grid point. The number of fixed output points in total will be 11 points, 9 are the water gauges as they were located at the physical model and another 2 output points in various parts of the model. An overview of the points and the location of each is given Figure 3.3.

Grid & Points per wavelength

The grid that was used as an input for XBeach, and the corresponding bathymetry, were computed using the XBeach Toolbox Python script provided by Deltares. The toolbox uses the bathymetry as an input, the desired points per wavelength, the wave period, and in the end produces a variably spaced grid (non-equidistant) that minimizes the computational costs.

To make sure that all the wave components are accurately resolved to the desired resolution, the cross-shore grid spacing has to be specified. The denser the grid, the better the resolution, but at expense of the computational effort. Within one wavelength there should be enough grid points to simulate the wave shape without losing information. 5 different values of the grid points per wavelength were used to examine which of the 5 values would represent the wave parameters the best. To accurately find a value that describes all the conditions, as an input the wave period of Wave condition 5 was used because according to the dispersion relation, it has the shortest wavelength and the grid must be sufficient enough to represent it. The number of grid points per wavelength and the resulting number of total grid points are given in Table 3.6.

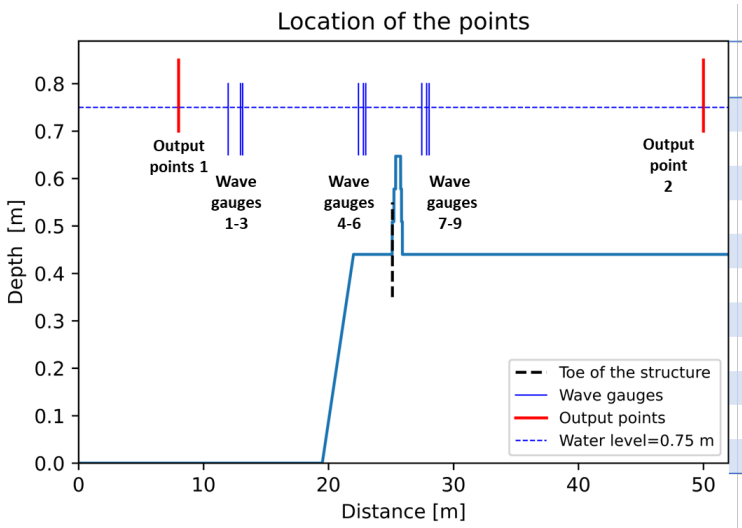

Points	Location [m]
Output point 1	8
Wave gauge 1	11.97
Wave gauge 2	12.96
Wave gauge 3	13.13
Wave gauge 4	22.4
Wave gauge 5	22.79
Wave gauge 6	22.79
Wave gauge 7	27.46
Wave gauge 8	27.86
Wave gauge 9	28.05
Output point 2	50

Figure 3.3.: Location of the output points within the domain. Structure 2 is also visible for reference. The toe of the different structures is at a distance of 25.1 m. At the end and after location x=55 m a 1-3 slope is present to mimic the wave damper as was installed in the physical model.

Points per wavelength	Total grid points
20	474
40	893
60	1333
80	1773
100	2215

Table 3.6.: Overview of the points per wavelength and the total grid points that XBeach Toolkit produced.

In Figure 3.4 and Figure 3.5, the significant wave height for all grid points is given together with the variance spectra of the first wave gauge for wave condition 5. It can be seen that after 80 grid points per wavelength both parameters seem to stabilize regarding their values. Most importantly, from Figure 3.4 it can be seen a steep decrease of the significant wave height at the boundary of the domain. This decrease is there for all runs and wave conditions. This behavior of XBeach is known and is also visible in other studies (e.g Pearson [2016]). Another noticeable trend is the mild damping of the wave height across the domain, which can be an effect of friction.

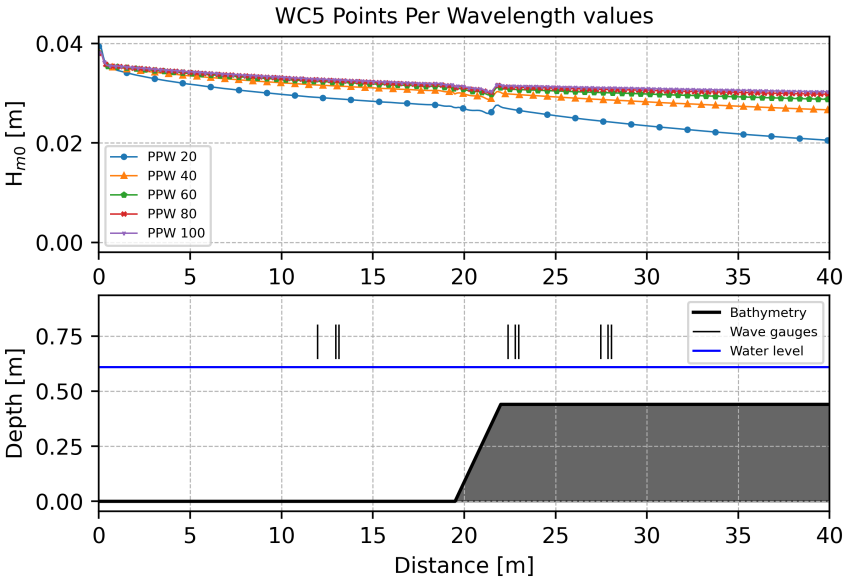

Figure 3.4.: Significant wave height for all grid points for different points per wavelength (PPW) values and for wave condition 5.

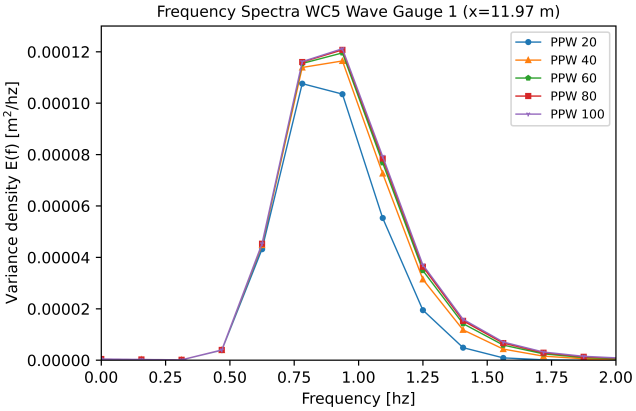

Figure 3.5.: Variance spectra of wave gauge 1 for different points per wavelength values and for wave condition 5.

Boundary conditions

At the boundary, a JONSWAP spectrum is forced with a wave height and peak period as defined in Table 3.1. For the upper frequency, a Nyquist frequency of 3 Hz will be used. This is due to the fact that a scale model is being simulated and setting the Nyquist frequency above the default values (which is 0.2-1 Hz) is needed to cover all the frequencies in the boundary condition.

In Figure 3.4 a steep decline in the wave heights is visible at the start of the domain. For that reason, the input of the wave heights was increased until the resulting significant wave height in wave gauges

1-3 is about the same as the significant wave height that was measured at the wave flume (Table 3.3). The new wave heights, that are going to be used to create the JONSWAP spectra, are computed as the ones shown in Table 3.7

Wave conditions	d_0 [m]	T_{input} [s]	H_{input} [s]	s[-]	Structure number
5	0.61	1.16	0.047	0.02	11-I
					11-III
					12-I
					12-III
					14
16	0.68	1.47	0.066	0.02	2
					8-0
					8-I
					8-V
					13
					15
					8-I-PVC(69&169)
18	0.68	1.31	0.119	0.04	11-I
					11-III
					12-I
					12-III
					14
35	0.75	1.6	0.15	0.04	2
					2-BH
					4
					5
					6
					7
					8-I
					8-I-PVC(32&69&169)
36	0.75	1.45	0.136	0.04	8-I

Table 3.7.: The new forced conditions that are applied at the boundary of XBeach for the irregular wave conditions. These 5 wave conditions will be used in the subsequent analyses, after screening out wave conditions not meeting the kd criteria. With blue color, are the structures that are used for the calibration while green colored are the additional structures to be used for the validation. The validation will take place with both blue and green coloured structures.

Slope at the end

At location x=55 m of the physical wave flume (Figure 2.1) a parabolic wave damper was installed. In the pursuit of successfully representing the physical model, the wave damper will be represented as a slope. Measured during the physical experiment, the reflection coefficient of the parabolic wave damper was about 20%. For the numerical model, it was tested for different values (Table 3.8), that a slope of 1:3 produces on average 20% for the different wave conditions.

Slope	Reflection
1:1	0.38
1:2	0.30
1:3	0.18
1:5	0.06
1:10	0.03

Table 3.8.: Overview of the reflection for different slope values. The reflection is defined as $K_r = \frac{H_{reflected}}{H_{incoming}}$.

The rest of the parameters used in XBeach and that were not referred will have the default values suggested in the XBeach User manual. The friction coefficient is going to be within the limits proposed by the XBeach User manual likewise. More specifically, after a sensitivity analysis was conducted in Appendix B Section B.4, it was concluded that a geometrical roughness of Nikuradse k_s equal to 0.01 m, using the White-Colebrook formulation, resulted in the best results. The results of the wave flume set up without the breakwater are presented in Section B.4. Only for one solution will there be a change in the settings,as explained in Section 3.2.2.

3.2.2. Schematization of the breakwater in the numerical model

A breakwater constructed by Reefy blocks is porous and can have a complicated 3D shape that changes horizontally or vertically. In this thesis, the different breakwater configurations will only be examined in the cross-shore profile, as conducted in the physical experiments. However, such a 1D approach, together with the capabilities of XBeach, imposes limitations on the level of detail that the breakwater can be represented with. XBeach has no features to specifically model porous structures. Therefore different options will be investigated to simulate the breakwater.

Breakwater as a change in the bathymetry (Original case)

The first option is to represent the breakwater as a simple change in the bathymetry. This option recreates the breakwater as an impermeable structure and does not consider the porosity and friction of the structure. Figure 3.12 and Figure 3.13 show Structure 2 and Structure 8-I modeled as changes in the bathymetry.

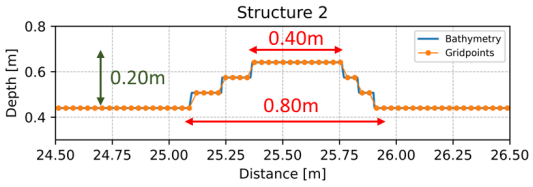

Figure 3.6.: Bathymetry and grid points of structure 2.

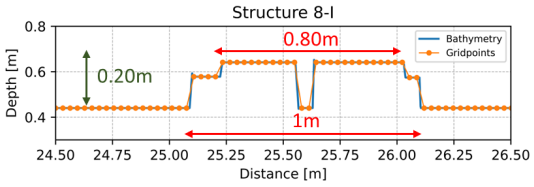

Figure 3.7.: Bathymetry and grid points of structure 8-I.

Decreased structure height

In the previous option, the effect of the porosity and friction of the porous media is not taken into account. In Section 2.2.1 the difference between a permeable against an impermeable structure was

explained in detail. Just like Metallinos et al. [2016] described in their model, it is expected that since the waves break above the breakwater, modeling it as an impermeable structure will result in too much energy dissipation through wave breaking. Structure height controls depth breaking and thus it will be examined whether lowering the height will produce the desired agreement between the results of the model and physical test. For both structures, the following levels of structure height decrease were modeled: 10%, 15%, 20%, 25% 35%, and 45% (Figure 3.8 and Figure 3.9)

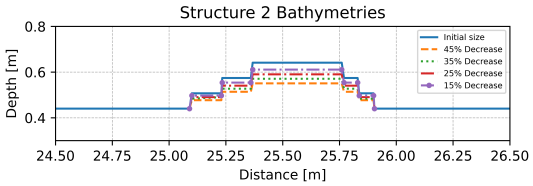

Figure 3.8.: Decreased heights for structure 2.

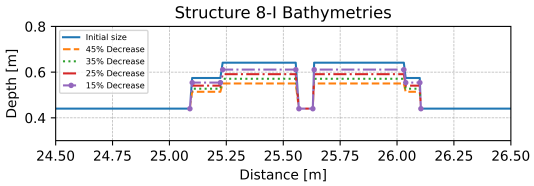

Figure 3.9.: Decreased heights for structure 8-I.

Change in wave steepness parameter

Another method to influence the breaking process is to delay the wave breaking by changing the maximum wave steepness parameter *maxbrsteep*. The maxbrsteep parameter was also explained in Section 2.3.2 and controls the location and magnitude of wave breaking. When the local surface steepness exceeds the value of *maxbrsteep*, the nonhydrostatic pressure correction term is turned off and the pressure is assumed to be hydrostatic (hydrostatic front assumption). The default value is 0.4 and for this solution, it was increased to values of 0.6, 0.8, 1, 1.2 and 1.4. Higher maxbrsteep values allow for steeper wave faces prior to wave-breaking. Increasing the parameter to too-high values will result in even steeper waves. To compute such steep waves the grid points per wavelength should also be increased to capture the wave transformation. For the present thesis, the number of grid points reminded the same despite the value of *maxbrsteep*. The advantage of this solution compared to the others is that *maxbrsteep* is a setting of the numerical model, and thus there is no need to modify the structure in any way.

Decreased structure width

Even though depth by breaking is the main cause of energy loss, structure width also influences wave transmission above the breakwater. Structure width is not such an important factor as structure height so it is expected that the impact on the transmitted wave heights is going to be less pronounced. For both structures, the width is going to be decreased by 5%, 10%, 15% and 20% (Figure 3.10 and Figure 3.11).

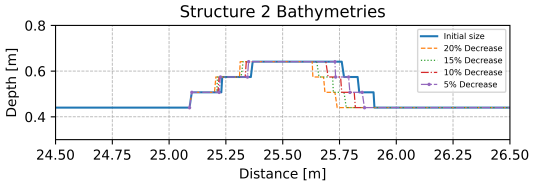

Figure 3.10.: Decreased widths for structure 2.

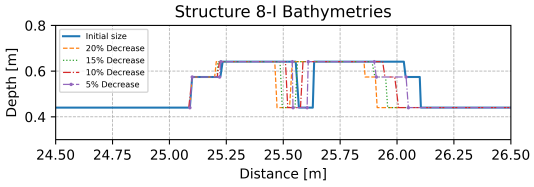

Figure 3.11.: Decreased widths for structure 8-I.

Vegetation module

XBeach gives the ability to model the effect of the vegetation on the waves. Even though it is not specifically designed to model porous breakwaters, an attempt will be made to adapt it to simulate the effects of a porous breakwater. By adjusting the parameters needed to reflect the hydraulic properties of the breakwater material, vegetation will be used as a porous medium. The vegetation module models the drag force exerted by vegetation on the flow, by defining the properties of the vegetation. This drag force (Equation 3.7) is added to the momentum equations.

$$\text{Drag Force} \quad F_d = \frac{1}{2}\rho C_d b_v h_v N u |u| \quad [N] \tag{3.7}$$

with

- C_d drag coefficient
- b_v stem diameter
- h_v stem height
- N density in the cross section
- u wave velocity

The multiplication of $b_v * h_v * N$ gives the surface of the structure that is vertical to the flow in the 1D cross section. Both structures will be modeled as one layer of vegetation, with a number of different options and combinations of C_d and N, while h_v and b_v will be for both structures equal to 0.20m and 0.0536m respectively. The individual Reefy block has a porosity of 20%. This percentage was taken out from the initial width of the block, resulting in the aforementioned value of b_v.

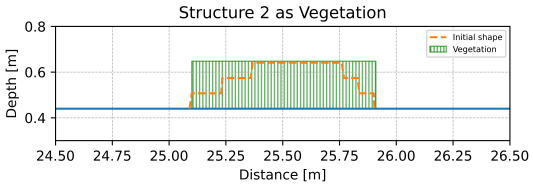

Figure 3.12.: Structure 2 as Vegetation.

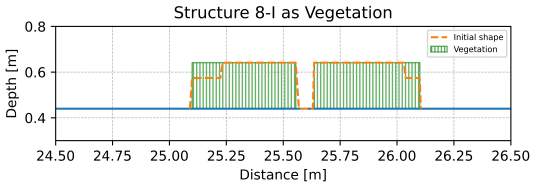

Figure 3.13.: Structure 8-I as Vegetation.

4. Results

This chapter is structured into 4 parts, each with a specific focus. The first part, Section 4.1, reports the results obtained for all the proposed solutions to model the breakwaters suggested in Section 3.2, including the results for the wave flume without the breakwater inside. The accuracy of each solution is evaluated using Root Mean Square Error (RMSE) and Mean Absolute Percentage Error (MAPE), providing a quantitative assessment of their performance. Based on the results obtained in Section 4.1, the most accurate solution is selected and employed to model various breakwater configurations that were not considered in Section 3.2. Section 4.2 focuses on validating the chosen model using these new configurations. Section 4.3 provides a small overview of the selected solution before a comparison is being done in Section 4.4 with the empirical formulas of van den Brekel [2021] (Equation 2.4, Equation 2.5) and Kurdistani et al. [2022] (Equation 2.6) to verify the efficiency and reliability of the model.

4.1. Numerical modelling

The results of the original case, the change in the wave steepness parameter, the modified structure and the structure as vegetation will all be presented in this section. For the original case, both figures regarding the significant wave height evolution and error plots will be given. For the vegetation module only the significant wave height evolution will be shown. For the rest of the solutions, the focus will be on the error plots, while the wave height evolution figures will be showcased in Appendix C.

Regarding the computed errors, since the focus of this thesis is on the transmitted wave field the following errors will be computed: the error in the total wave height as measured in wave gauge 7 (Figure 3.3), the error in the transmitted wave height as measured in wave gauge 7, the transmission coefficient error, the errors in spectral periods $T_{m-1,0}$ and $T_{m0,1}$, for the transmitted wave height, again for wave gauge 7. Lastly, the error in the reflection coefficient, for wave gauge 4, will also be presented for a brief examination. The error plots show the errors for both structures and for all the wave conditions that were tested. This means that on the plots there are 5 points, 2 points for the two wave conditions Structure 2 was tested, and 3 points for the wave conditions Structure 8-I were tested (Table 3.7).

The transmission coefficient is defined at the wave gauge 7 as: $$K_t = \frac{H_{transmitted}}{H_{incoming}} \quad [-] \tag{4.1}$$

The reflection coefficient is defined at the wave gauge 4 as: $$K_r = \frac{H_{reflected}}{H_{incoming}} \quad [-] \tag{4.2}$$

4.1.1. Wave flume - No breakwater

In this section the results for the wave flume set-up without the breakwater inside are given. The error plots are shown in Figure 4.5. Concerning the total wave height, the model overestimates the results (MAPE 7.2%), but on the other hand the incoming heights are measured with great detail, with an mean average percentage error of just 2.4%. This overestimation is a result of the increased heights used as an input, which had to be increased so the incoming waves can be modeled accurately. Because the wave input had to be increased for the incoming wave heights to be correct, this means that the Guza split method underestimate slightly the incoming wave characteristics. In a similar way, the spectral periods, which are based on the incoming wave spectra, are also overestimated, with the MAPE error being for both spectral periods below 6%.

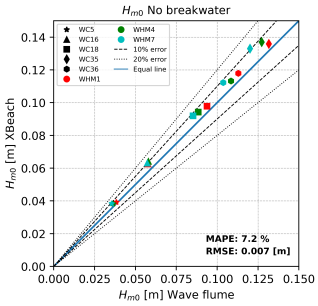

Figure 4.1.: H_{m0} error without the structure.

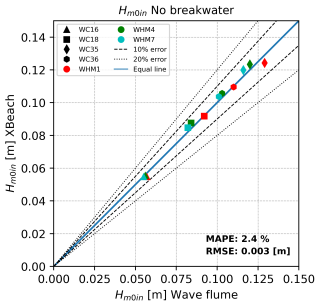

Figure 4.2.: H_{m0in} error without the structure.

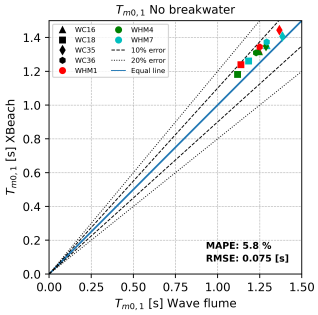

Figure 4.3.: $T_{m0,1}$ error without the structure.

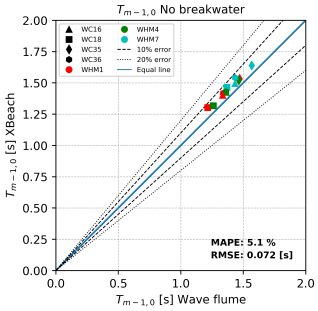

Figure 4.4.: $T_{m-1,0}$ error without the structure.

Figure 4.5.: Errors of the wave flume without the breakwater, for the different wave conditions and for wave gauges 1-4-7. For wave condition 5 there was no available data for the incoming parameters form the physical model.

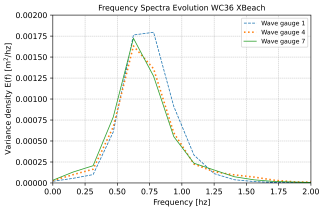

Figure 4.6.: Total frequency spectra evolution for WC36.

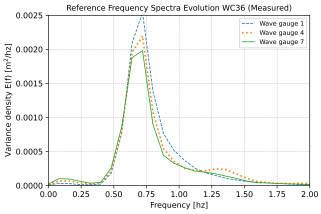

Figure 4.7.: Measured total frequency spectra evolution for WC36.

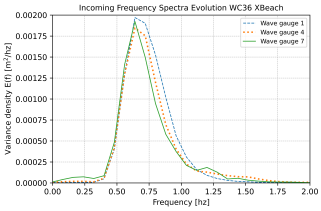

Figure 4.8.: Incoming frequency spectra evolution for WC36.

Figure 4.9.: Evolution of the frequency spectra between wave gauges 1-4-7 and for wave condition 36. Input parameters: $T_{input} = 1.45$ [s], $H_{input} = 0.136$ [m].

Figure 4.9 shows the evolution of the wave spectra from wave gauge 1 to wave gauge 7, for wave condition 36. The computed spectra, the total and incoming produced by XBeach, exhibit the same behavior, where the energy from the higher frequencies is dissipated and the peak is transferred to the lower frequencies. The same holds true also for the measured spectra, even though the peak frequency remains steady. The computed total spectra are wider than the measured spectra, but the peak variance density is smaller than the measured one. This could be explained by the different γ factor that was used (which was equal to 1) compared to the one chosen for the wave flume experiments, which was 3.3. There is no information about the measured incoming spectra. It is assumed that the computed incoming spectra are wider than the spectra in the physical model tests, based on the relation between the computed-measured total spectra. The wider measured incoming spectra would explain why the spectral periods are also overestimated. In the incoming spectra, a small peak is also visible around 1.2 Hz, in the last wave gauge 7. This can be result of an energy transfer from the main peak towards higher harmonics. This small peak is not visible in the computed total spectra, probably because it is masked from the energy in lower frequencies, which have more energy compared to the higher frequencies of the incoming spectra. For reference, Figure 4.10 shows the wave evolution within the wave flume for wave condition 36. The rest wave conditions are in Appendix B.

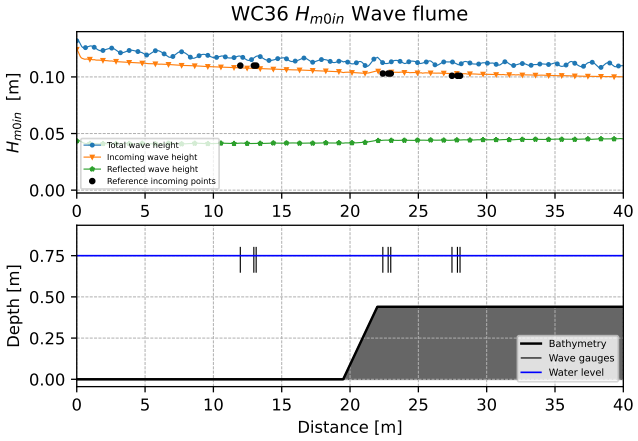

Figure 4.10.: Total, incoming and reflected significant wave height evolution for wave condition 36 and without a structure.

4.1.2. Original case

Before Structure - Wave gauge 4

For the original case error plots were computed also before the structure to provide insight and confirm the ability of XBeach on computing the wave transformation in the domain. In Figure 4.15 the error plots are given for wave gauge 4.

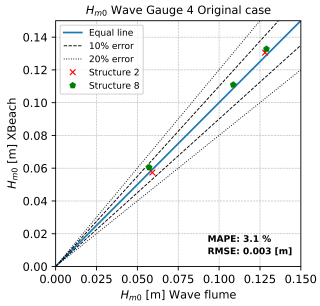

Figure 4.11.: H_{m0} error Original case before structure.

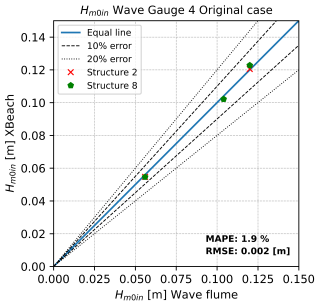

Figure 4.12.: H_{m0in} error Original case before structure.

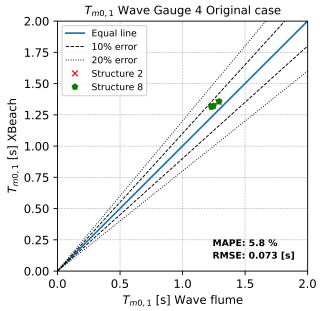

Figure 4.13.: $T_{m0,1}$ error Original case before structure.

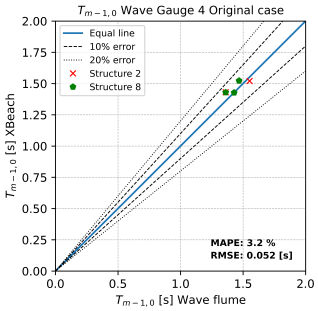

Figure 4.14.: $T_{m-1,0}$ error Original case before structure.

Figure 4.15.: Wave parameters for Wave gauge 4 and Original case.

All the errors are within an acceptable error of MAPE <6 %. The biggest errors are reported for the spectral periods, which are slightly overestimated. The total and incoming variance density for Wave condition 35 is given for both structures since it was tested for both structures.

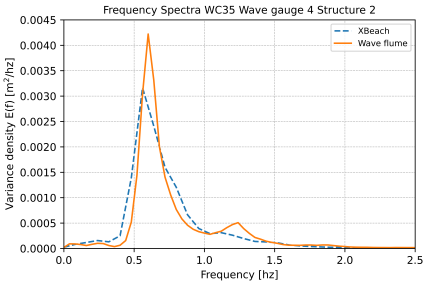

Figure 4.16.: Frequency Spectra WC35 Wave gauge 4 Structure 2 Original case.

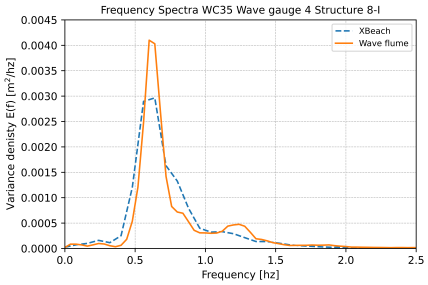

Figure 4.17.: Frequency Spectra WC35 Wave gauge 4 Structure 8-I Original case.

Figure 4.18.: Total frequency spectra for wave condition 35 before the structure for the Original case. Input parameters: $T_{input} = 1.6$ [s], $H_{input} = 0.15$ [m].

Both structures show the same results for Wave gauge 4, as depicted in Figure 4.16 and Figure 4.17. The computed total spectra of XBeach has smaller peak frequency, but is more wide. Furthermore, in the wave flume experiment, there is second smaller peak around 1.25 Hz, which is barely visible in the computed spectra. A comparison in also made with the incoming wave spectra in Figure 4.21. This time, in the incoming frequency spectra, the small peak at 1.25 Hz is also visible in both structures.

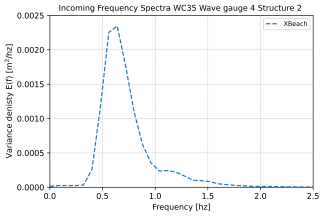

Figure 4.19.: Computed incoming frequency spectra WC35 Wave gauge 4 Structure 2.

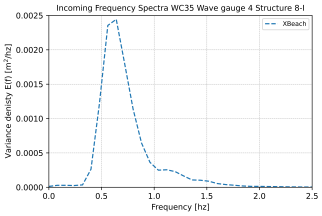

Figure 4.20.: Computed incoming spectra WC35 Wave gauge 4 Structure 8-I.

Figure 4.21.: Incoming frequency spectra for wave condition 35 before the structure for the Original case.

After Structure - Wave gauge 7

The original case refers to the structure as a simple change in the bathymetry. In Figures 4.22 to 4.27 the error plots are given. The settings used in the original case are the default values proposed by the XBeach manual as explained in Section 3.2.

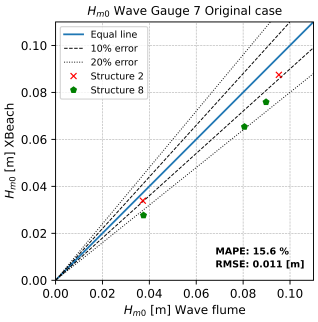

Figure 4.22.: H_{m0} error Original case.

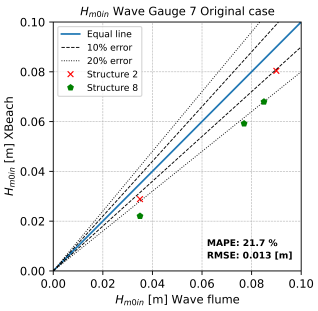

Figure 4.23.: H_{m0in} error Original case.

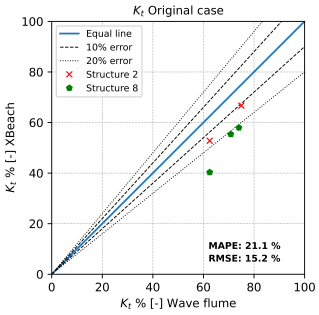

Figure 4.24.: Kt error Original case.

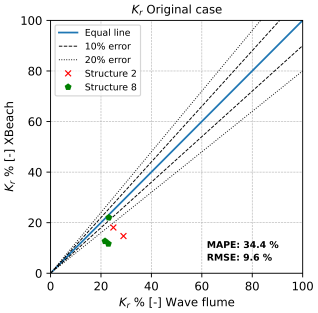

Figure 4.25.: K_r error Original case.

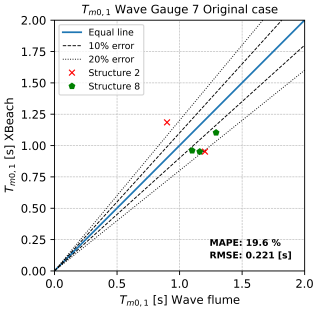

Figure 4.26.: $T_{m0,1}$ error Original case.

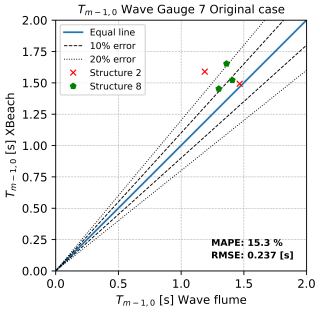

Figure 4.27.: $T_{m-1,0}$ error Original case.

Figure 4.28.: Error plots for the Original case.

It can be seen that for the original case, the MAPE for the total wave heights and for both structures is about 15%, and the RMSE is 0.01m. Based on Figure 4.22, the results for structure 2 are better than structure 8-I, with the percentage error of the former lies within the 10% error line. The errors for the incoming significant wave heights, as measured in wave gauge 7, show larger error values, with 21.7% and 0.013m MAPE and RMSE respectively. The MAPE error for the transmission coefficient is of the same order as the error for the incoming significant wave height.

The error plots show that the model, XBeach, computed smaller wave heights after the structure resulting in an underestimation of the transmission coefficient, compared to the physical model. The smaller wave is a consequence of the overestimation of the wave breaking above the structure. This is in line with what was expected as reported in Chapter 2 and Section 2.2.1. Therefore the model behaves as intended.

The reflection coefficient seems to present the biggest errors, with MAPE equal to 34,4% and a RMSE equal to 9.6%. Just like the transmission coefficient, the reflection coefficient is also underestimated for both structures.

The spectral periods $T_{m0,1}$ and $T_{m-1,0}$ seem to behave differently. $T_{m0,1}$ is on average underestimated. On the other hand, $T_{m-1,0}$ is overestimated. In general, spectral periods are used to describe the energy distribution in the wave spectrum over the different frequencies. $T_{m0,1}$ represents the center of gravity of the 1D wave spectrum while $T_{m-1,0}$, also called mean energy wave period [Hofland et al., 2017], gives more weight on lower frequencies (longer periods). An example of the energy spectra is given in Figure 4.31. Based on the definitions of the spectral periods and the comparison of the computed variance spectra, the error plots can be explained. Regarding the overestimation of the $T_{m-1,0}$ period, the model overestimates the energy concentrated at the lower frequencies, resulting in a total overestimation of the spectral period. On the contrary, the model underestimates the total energy in the higher frequencies, resulting in a smaller energy distribution among the different frequencies, and a smaller center of gravity, and thus underestimates the $T_{m0,1}$ spectral period. Note that the frequency spectra figures presented here are illustrating the total wave signal, while the spectral periods are computed for the incident wave signal. It is assumed that the same behavior would be observed to both signals.

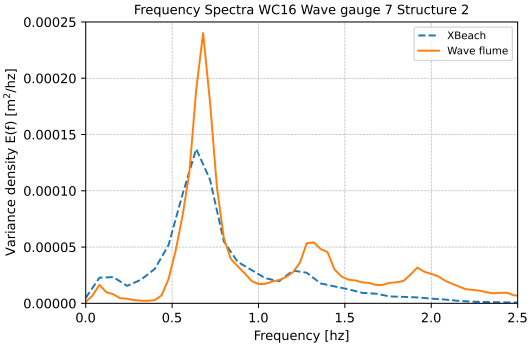

Figure 4.29.: Frequency Spectra for Structure 2.

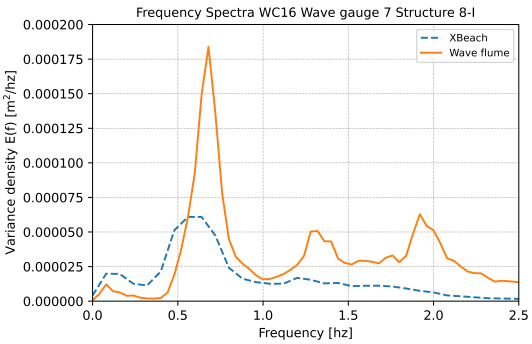

Figure 4.30.: Frequency Spectra for Structure 8-I.

Figure 4.31.: Total frequency spectra in wave gauge 7 for both structures and wave condition 16. Input parameters: $T_{input} = 1.6$ [s], $H_{input} = 0.15$ [m].

After both structures, 2 more peaks are visible, at around 1.25 Hz and 1.9 Hz. The peak around 1.25 Hz is also visible computed total spectra this time, implying energy transfer to higher frequencies past the breakwater. In the measured total spectra the peaks are more pronounced and more energy is located in the higher frequency region.

4.1.3. Modified structure

Now that the overestimation of the wave breaking is established, the solutions that can affect the breaking phenomenon can be examined. In this section, the structure is modified, by decreasing the height or the width of the structure. Here, from the different changes that were examined, only the best results will be shown.

Decrease in Structure height

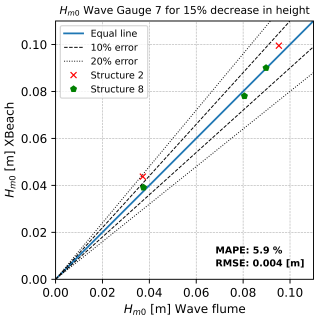

Figure 4.32.: H_{m0} error 15% height decrease.

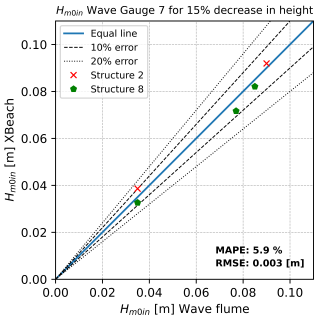

Figure 4.33.: H_{m0in} error 15% height decrease.

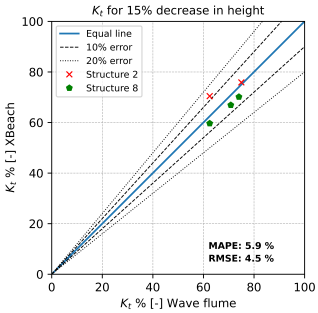

Figure 4.34.: K_t error 15% height decrease.

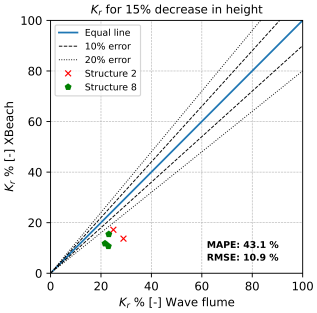

Figure 4.35.: K_r error 15% height decrease.

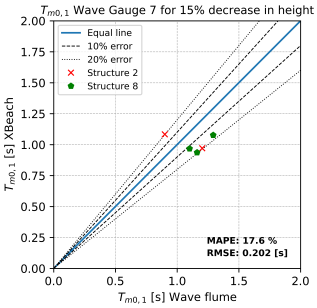

Figure 4.36.: $T_{m0,1}$ error 15% height decrease.

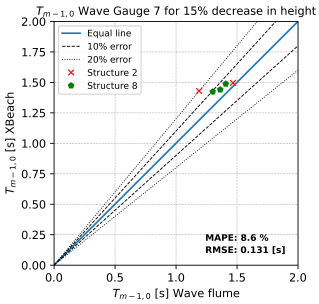

Figure 4.37.: $T_{m-1,0}$ error 15% height decrease.

Figure 4.38.: Error for a 15% decrease in structure height.

A decrease of 15% in the structure height shows the best results among the different values tested. Overall, the same trends observed in the Original case in Section 4.1.2 are also visible in the error plots shown in Figures 4.32 to 4.37. The errors are all smaller than the Original case, with a MAPE equal to 5.9% and RMSE equal to 0.003m for the error in the measured significant wave height after the structure. The error in the reflection coefficient is the only one where the values of the MAPE and RMSE increased. In the original case, the reflection coefficient was underestimated with a MAPE of about 34%. By decreasing the structure height the frontal area where the wave can be reflected is also decreased. Therefore, the underestimation is amplified and reaches a MAPE value of 43%.

Decrease in structure width

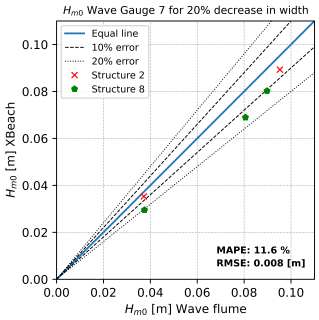

Figure 4.39.: H_{m0} error 20% width decrease.

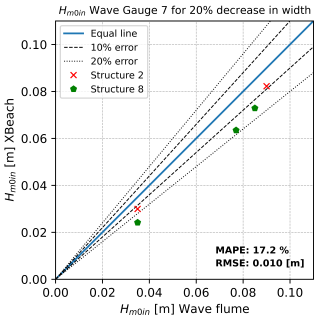

Figure 4.40.: H_{m0in} error 20% width decrease.

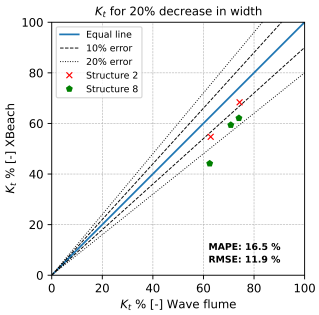

Figure 4.41.: K_t error 20% width decrease.

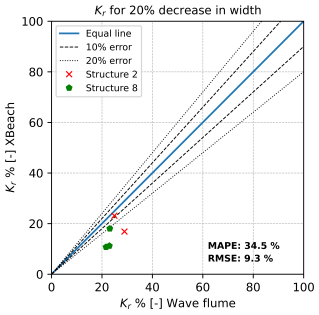

Figure 4.42.: K_r error 20% width decrease.

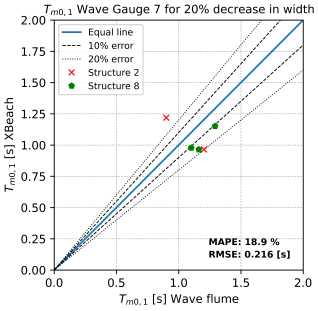

Figure 4.43.: $T_{m0,1}$ error 20% width decrease.

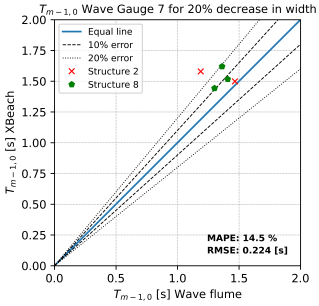

Figure 4.44.: $T_{m-1,0}$ error 20% width decrease.

Figure 4.45.: Error plots for a 20% decrease in structure width.

Among the 4 different values, a decrease in width of 20% gives the best results for both structures. The errors show a slight improvement compared to the Original case. The error in the transmitted wave, as measured in wave gauge 7, has 17.2% MAPE and 0.01m RMSE. The MAPE error of the transmission coefficient decreased from 21.1% in the Original case to 16.5%. Nonetheless, the errors in the reflection coefficient and spectral periods remained almost the same with the initial representation of the structure.

Comparing the effects of changing the height or the width of the structures, the former gives much better results. Changing the width influences the wave breaking but not as much as changing the structure heights. In Appendix C it can be seen that changing the width had a small impact on the wave height evolution, for all the tested values. On the other hand, a change in the structure height, even for a small one, had a noticeable impact.

4.1.4. Change in the wave steepness parameter

This is the only option where the settings of XBeach are not the ones recommended. In this solution, the structures are modeled with their original dimensions but the wave breaking process is delayed, by changing the wave steepness parameter Maxbrsteep. Like explained before in Section 3.2.2, the value of this setting was not increased further than 1.4 because then the points per wavelength should also be increased. In the following figures (Figure 4.46 to 4.51) the error plots are displayed.

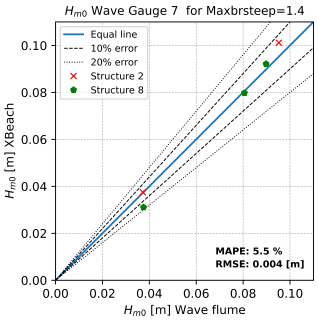

Figure 4.46.: H_{m0} error Maxbrsteep=1.4.

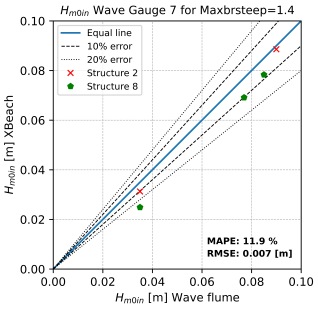

Figure 4.47.: H_{m0in} error Maxbrsteep=1.4.

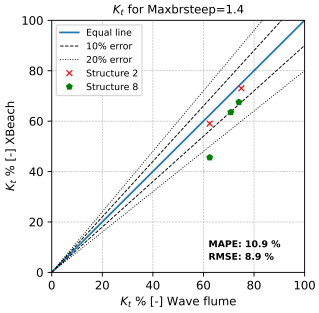

Figure 4.48.: K_t error Maxbrsteep=1.4.

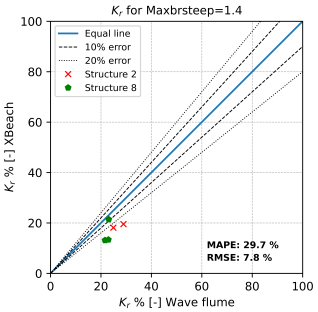

Figure 4.49.: K_r error Maxbrsteep=1.4.

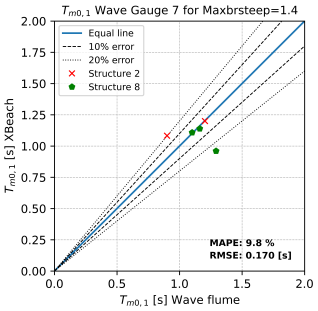

Figure 4.50.: $T_{m0,1}$ error Maxbrsteep=1.4.

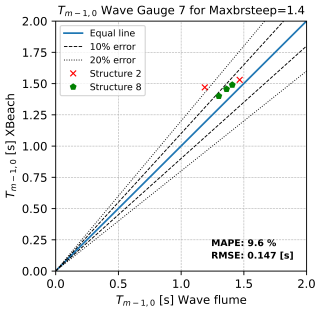

Figure 4.51.: $T_{m-1,0}$ error Maxbrsteep=1.4.

Figure 4.52.: Error plots for Maxbrsteep=1.4.

In contrast with the Original case, the results are highly improved. The MAPE error in the transmitted wave height is almost 12%, and the RMSE is 0.007m. Likewise, the MAPE and RMSE errors are equal to 10,9% and 8.9% for the transmission coefficient. The error of the reflection coefficient has also decreased to almost 30% MAPE, compared to about 35% of the Original case. The spectral periods' errors also have decreased, with both $T_{m0,1}$ and $T_{m-1,0}$ having a MAPE of about 10%. Once more structure 2 shows better results within the error plots compared to structure 8-I.

4.1.5. Structure as vegetation

For the vegetation module, the error plots will not be given, but rather the incoming significant wave height evolution. The results between the two structures and wave conditions vary a lot and therefore a comparison can not be made. There were 2 values that could be changed: Cd or one value of the 3 values that their multiplication equal to surface area ($b_v * h_v * N$). It was decided that density N was deemed preferable to be investigated as the other two are connected directly to the size of the tested breakwater. The drag coefficient of a structure is usually already known either from physical model tests or numerical modeling, but this is not the case for the current analysis therefore various values were tested ranging from 1 to 15. The initial value for the density N was 14, which is the number of columns in the cross-section as placed in the physical model. The density was increased afterward up to the value of 600.

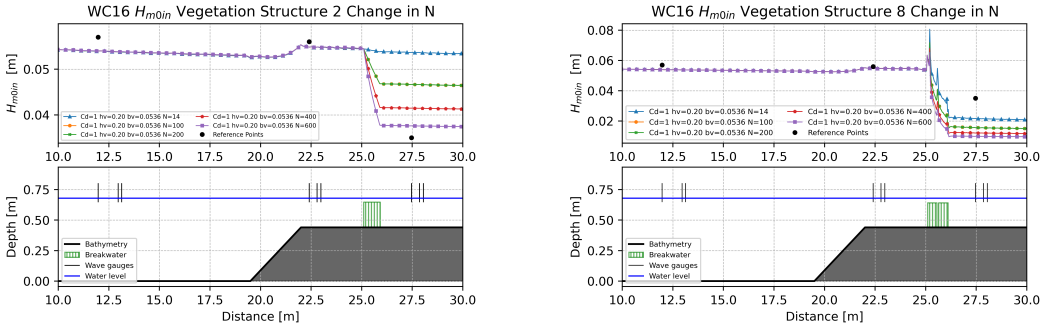

Figure 4.53.: Comparison between the incoming wave heights evolution for both Structure 2 and Structure 8-I, for WC16 and change in N.

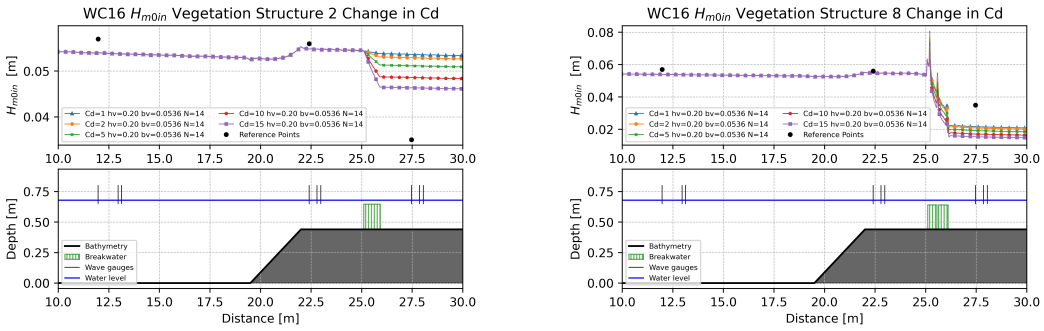

Figure 4.54.: Comparison between the incoming wave heights evolution for both Structure 2 and Structure 8-I, for WC16 and change in Cd.

In Figure 4.53 and Figure 4.54 the different behavior between the 2 structures is visible. For Structure 2, no matter the values of N and Cd, the transmitted wave heights are overestimated and not able to reach the value of the desired Original point. Additionally, the waves are not breaking. On the other hand, Structure 8 produces too much dissipation above the structure and the transmitted wave height is underestimated for all the tested values, while the waves are breaking on the structure. Furthermore, the wave height evolution is quite different between the structures. In Appendix C results are also given

for wave condition 35. Since the waves dont break for structure 2, other processes like set up are also not modelled, leading to wrong wave evolution within the domain. XBeach divides the domain into water columns, on which the vegetation modules adds an extra force, just like friction does. By not taking into account breaking by depth, the module is not able to produce the expected outcomes.

4.1.6. Choosing representation method

The breakwaters as a simple change in the bathymetry behaved as expected, with increased wave breaking and underestimation of the transmitted wave heights past the breakwaters. The effect was more noticeable for Structure 8-I. Structure 8-I is not only wider than Structure 2, but is also a more porous breakwater, with a porosity of 45%, while Structure 2 has only 20%. Even though wave breaking is the main process that regulated the transmitted wave heights, the fact that the less porous structure displayed better behavior in being modeled as impermeable implies that porosity does indeed affect the end results to a lesser extent. Structure 2 had consistently better results than Structure 8-I in all the different methods used.

Based on the above errors the best solution can be determined. To start with, the solutions that did not show good results will be discussed. The vegetation module failed to produce reasonable outcomes. The results were not only different between the 2 structures, but there was also quite a variability between different wave conditions of the same configurations. One possible explanation for the difference between the 2 structures is that the length of the structure parallel to the 1D section plays an important role for the effect of the vegetation to become important.

Increasing the width of the structure also did not have the expected improvement in the transmitted wave heights. The impact the changing of the values had, was minimal. Compared to decreasing structure height, changing the width is not as effective and therefore not suggested.

The last two options both had favorable outcomes. The first one, the decrease in structure height, had the strongest impact in increasing the transmitted wave heights and therefore the smallest errors in the transmission coefficient. On the other hand, increasing the wave steepness parameter to 1.4, also had good results on the transmission coefficient errors, but bigger errors compared to a decrease in height. Noticeably, the errors in the spectral periods were minimum for the change in the steepness parameter, as well as the error in the reflection coefficient. An overview of the errors for the different parameters is given in the Table 4.1.

Errors Summary		H_{m0} [m]	H_{m0in} [m]	K_t % [-]	K_r % [-]	$T_{m0,1}$ [s]	$T_{m-1,0}$ [s]
Original case	MAPE [%]	15.6	21.7	21.1	34.4	19.6	15.3
	RMSE	0.011	0.013	15.2	9.6	0.221	0.237
15% Structure height decrease	MAPE [%]	**5.9**	5.9	5.9	43.1	17.6	8.6
	RMSE	0.004	0.003	4.5	10.9	0.202	0.131
20% Structure width decrease	MAPE [%]	11.6	17.2	16.5	34.5	18.9	14.5
	RMSE	0.008	0.01	11.9	9.3	0.216	0.224
Max steepness parameter = 1.4	MAPE [%]	5.5	11.9	10.9	29.7	9.8	9.6
	RMSE	0.004	0.007	8.9	7.8	0.17	0.147

Table 4.1.: Overview of the MAPE and RMSE errors for the different solutions. The results with the minimum error per parameter are coloured with green. Apart from $T_{m-1,0}$ which is overestimated, the rest parameters are all underestimated.

Given the fact that half of the parameters perform better for the 15% decrease in height, and half for the increase of the Max steepness parameter both these options will be chosen for the validation that follows in the next section. The reason is that all the parameters are important to assess the possible impact of the breakwater on the transmitted wave height and characteristics.

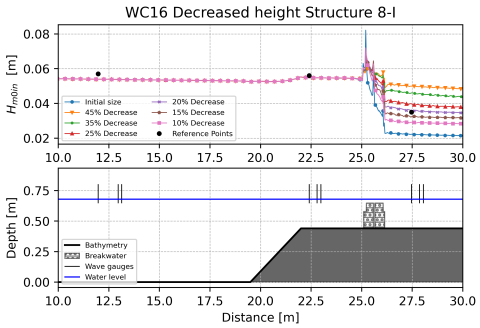

Figure 4.55.: Incoming wave heights for WC16 change in height.

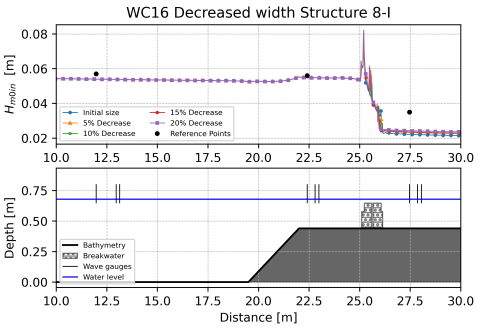

Figure 4.56.: Incoming wave heights for WC16 change in width.

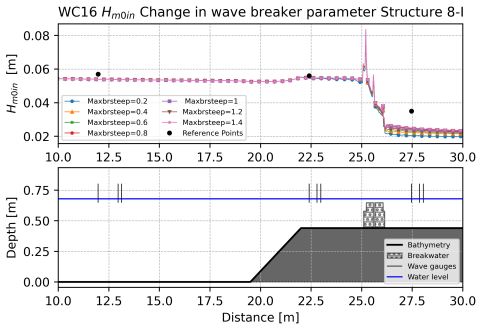

Figure 4.57.: Incoming wave heights for WC16 change in Maxbrsteep.

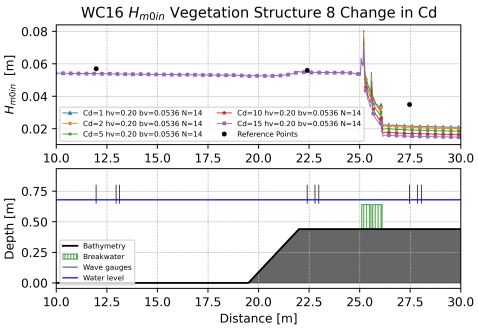

Figure 4.58.: Vegetation module for WC35.

Figure 4.59.: Comparison of incoming wave height evolution for all the proposed solutions and for structure 8, wave condition 16. Input parameters: $T_{input} = 1.6$ [s], $H_{input} = 0.15$ [m].

Figure 4.59 shows a comparison of all the solutions for Structure 8-I. Only the change in the structure height produces the desired outcomes on the incoming wave height evolution. Changing the width had almost no effect, while increasing the wave steepness also failed to have a big impact on the transmitted wave height. On the contrary, wave steepness showed better results for structure 2. Structure 8-I has a channel in between the 2 structures that comprises the breakwater. The effect of the channel is visible in the wave evolution, after the waves initially break when they reach the breakwater, then they re-organize in the channel, and break again just above the structure, producing these wave height peaks due to wave shoaling.

4.2. Solution Validation

For the validation technique structures that were not tested in the previous section will be used. From the simple 2D structures, Structure 4, Structure 5 and Structure 7 were decided to be used. The first two have a simple shape, while Structure 7 resembles Structure 2 but has a different orientation. From the complex 3D structures, Structure 8-V, Structure 11, Structure 12 and Structure 14 were used. Structure 11 and Structure 14 are both chosen due their small structure height, while Structure 12 was chosen because it is emerged during one of the wave conditions it was tested. Ideally, Structure 13, which is the tallest structure and emerged, would also be tested, but there is no data from the wave flume on the incoming wave heights. Lastly, to examine the effect of the channel length on the errors, Structure 8-V will be modeled. The cross sections of the structures was given at figure while in Appendix C images of the structures as where illustrated in XBeach are given.

In this Section, error plots for the two solutions will be given for all the structures combined. In Appendix C the significant wave height evolution for all the structures are given as well as the errors for the Original case of all the structures.

Decrease in Structure height

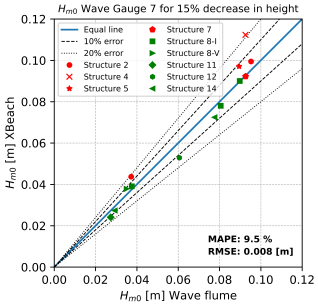

Figure 4.60.: H_{m0} error for 15% height decrease.

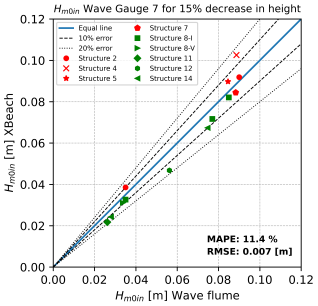

Figure 4.61.: H_{m0in} error for 15% height decrease.

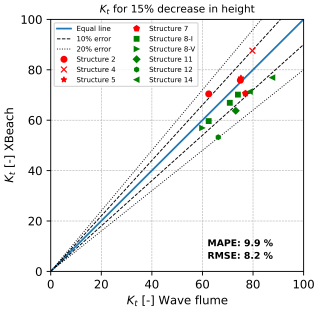

Figure 4.62.: K_t error for 15% height decrease.

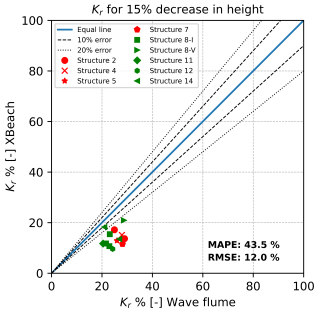

Figure 4.63.: K_r error for 15% height decrease.

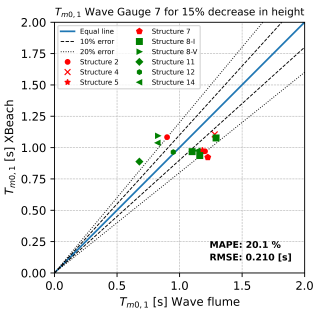

Figure 4.64.: $T_{m0,1}$ error for 15% height decrease.

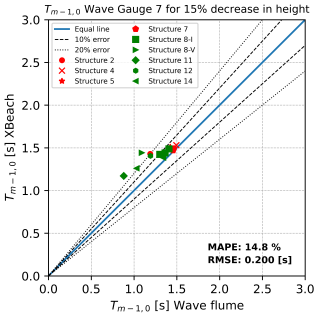

Figure 4.65.: $T_{m-1,0}$ error for 15% height decrease.

Change in wave steepness parameter

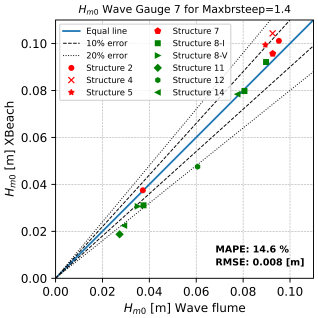

Figure 4.66.: H_{m0} error for Maxbrsteep=1.4.

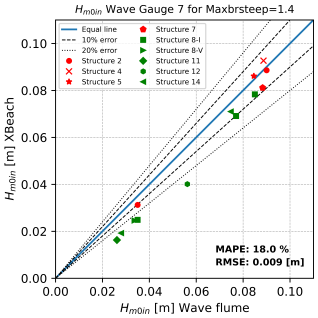

Figure 4.67.: H_{m0in} error for Maxbrsteep=1.4

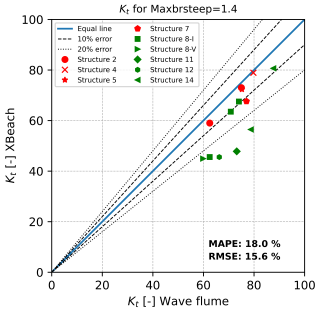

Figure 4.68.: K_t error for Maxbrsteep=1.4

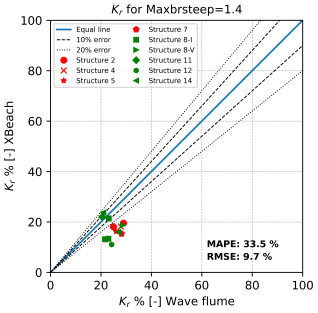

Figure 4.69.: K_r error for Maxbrsteep=1.4

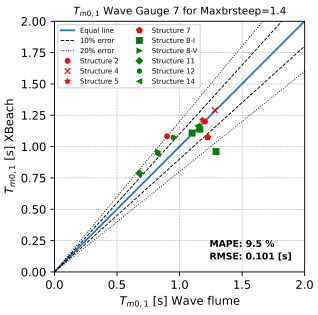

Figure 4.70.: $T_{m0,1}$ error for Maxbrsteep=1.4

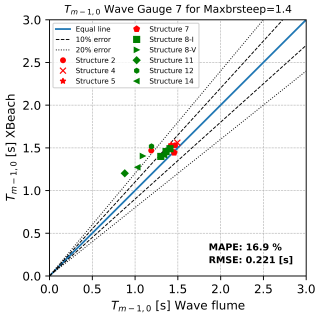

Figure 4.71.: $T_{m-1,0}$ error for Maxbrsteep=1.4

It is evident from the figures above that the errors for both solutions have quite increased, and that the change in Maxbrsteep has greatly under performed compared to Section 4.1.4 where only structures 2 and 8-I were tested. Red colors indicate the markers of the simple 2D structures and with green the markers of complex 3D structures. A synopsis of the results was created in Table 4.2. For Structure 12 it was decided not to use wave condition 5, because Guza split was not able to compute the incoming parameters. In Appendix C and Figure C.46 it can be seen that when the structure is emerged no safe calculations can be made for the wave characteristics.

Errors-Validation Summary		H_{m0} [m]	H_{m0in} [m]	K_t % [-]	K_r % [-]	$T_{m0,1}$ [s]	$T_{m-1,0}$ [s]
Original case	MAPE [%]	20.2	26.5	27.6	40.1	23	23.5
	RMSE	0.011	0.014	21.5	11.7	0.237	0.334
15% Structure height decrease	MAPE [%]	9.5	11.4	9.9	43.4	20.1	14.8
	RMSE	0.008	0.007	8.2	12.1	0.21	0.2
Max steepness parameter = 1.4	MAPE [%]	14.6	18	18	33.5	9.5	16.9
	RMSE	0.008	0.009	15.6	9.7	0.101	0.221

Table 4.2.: Overview of the MAPE and RMSE errors for the validation. The results with the minimum error per parameter are coloured with green. $T_{m-1,0}$ is overestimated while $T_{m0,1}$ shows no clear relation. The rest parameters are mainly underestimated, for all the solutions.

The main behaviour of the error plots that were shown in Section 4.1.3 and 4.1.4 are still illustrated here. The only difference is the results in the spectral period $T_{m0,1}$. In the previous sections, there was an underestimation of the spectral period, while in this section and taking into account all the structures, (Figure 4.64 and Figure 4.70) this is not visible. There seems to be a trend that the complex 3D structures (green colours) show an overestimation of the spectral period $T_{m0,1}$ while the opposite is true for the simple 2D structures (red colour).

As a whole, the findings in Table 4.2 suggest that a 15% decrease in structure height still gives the best results. The MAPE and RMSE errors for the transmission coefficient are almost 10% and 8% respectively. The biggest error values are again the error in the reflection coefficient. Interestingly enough, all structures considered, the decrease in the structure height also computes better the $T_{m-1,0}$ spectral period, with MAPE equal to about 15% and RMSE 0.2 sec. The change in the wave steepness parameter can still calculate $T_{m0,1}$ better than the change in the height, with a 9.5% MAPE, compared to a 20.1% MAPE of the latter. An increase in the Maxbrsteep setting is still a valid option to model the breakwater since all the MAPE errors are below 20% except for the reflection coefficient. Still, the 15% height decrease performs the best it is a more favorable solution, as long as the reflection is not of interest.

4.3. Preliminary conclusions

In this chapter, the results from Chapter 3 were given, mainly in the form of plots that illustrate the error for the different methods that were used to model the breakwater. The Original case for all the structures is the representation of them as a change in the bathymetry, with the same dimensions as the wave flume experiment. Modeling the breakwaters this way resulted in an overestimation of the breaking process and thus an underestimation of the transmitted wave height. To decrease the amount of wave breaking, the structures were modified either by decreasing the width or the height. Another option that was used, was to increase the wave steepness parameter setting to 1.4, instead of 0.4 which is the default value. Additionally, the vegetation module was also explored as a modeling option, but it showed inconsistencies and was deemed unsuitable for this study. The initial tests were conducted on structures 2 and 8-I, and the most successful methods were found to be the decrease in height and the increase in the wave steepness parameter.

The methods that worked the best were the change in height and the increase of the wave steepness parameter. The change in width was not sufficient to impact the results while the vegetation module showed many inconsistencies to be used as a possible solution. These two methods were then tested for a bigger number of structures to validate the results. The smallest error values were computed when

the structures were modeled with a 15% decreased height. The change in Maxbrsteep setting is also a good option with relatively small computed errors, but it still under performs compared to the modified structure option. Therefore as proposed solution, a decrease of 15% is suggested.

Among the different structures, there was a trend in which simple 2D structures performed better than the respective 3D structures, which indicated that porosity does play a lesser role in modeling the breakwaters. More specifically, 2D structures can also be modeled with great outcomes by only changing the Maxbrsteep setting equal to 1.4, while for the more complex structures, only a decrease in the structure height can produce the desired outcomes.

4.4. Comparison with empirical equations

A comparison will take place in this section between the results of XBeach and the empirical formulas of van den Brekel [2021] (Equation 2.4, Equation 2.5) and Kurdistani et al. [2022] (Equation 2.6), to prove the effectiveness of the numerical model. These equations are analyzed in Section 2. The results are given in Figure 4.72 and the errors are given in Table 4.3. The formulas were tested for all the breakwaters, simple and complex, that were used in the above Sections.

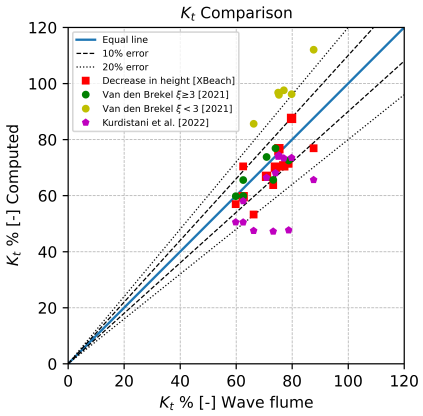

Figure 4.72.: Comparison with empirical formulas.

Errors - Comparison with empirical equations		K_t % [-]
15% Structure height decrease	MAPE [%]	9.3
	RMSE	7.7
van den Brekel [2021]	MAPE [%]	16.11
	RMSE	14.4
Kurdistani et al. [2022]	MAPE [%]	17.37
	RMSE	15.3

Table 4.3.: Overview of the MAPE and RMSE errors for the empirical formulas. The results with the minimum error are coloured with green.

XBeach is the most effective in calculating the wave transmission over the breakwater. The equations of van den Brekel [2021] illustrate good behavior for $\xi \geq 3$ but fail to do so for $\xi < 3$. This was expected as Equation 2.5 was not optimized for irregular wave conditions. The MAPE error for the optimized equations was 16.11% and the RMSE was 14.4% . Kurdistani et al. [2022] on the other hand, strongly underestimates the wave transmission, mainly for the complex breakwaters that had porosity 45%. Equation 2.6 had no limitations of applicability. The underestimation of the wave transmission coefficient has MAPE 17,37 % and RMSE of 15.3%. Therefore for the existing dataset, Kurdistani et al. [2022] is not suitable to describe the wave transmission coefficient due to an overestimation of the porosity's effect. For $\xi \geq 3$, Equation 2.4 can be used for a quick assessment of the resulting transmission coefficient, but a numerical model would still be needed to compute wave transmission when $\xi < 3$. Based on the errors, XBeach is better equipped to make wave transmission computation compared to the existing empirical formulas.

5. Application

In the previous chapters, it was shown that XBeach could simulate the wave flume within reasonable error limits and compute the transmitted wave height past the breakwater. The solution was further validated by simulating more structures and analyzing the results. Now that the solution has been validated, it is the turn of XBeach to undergo a brief validation check by examining the behavior of the model under the effect of a simple breakwater. The focus is once more on the transmission coefficient, so a comparison can be made with the behavior that is recorded in the literature in Section 2.2.1 and with the results of the previous thesis. In Section 5.1 the model and its input parameters are explained and in Section 5.2 the results will be given to assess whether XBeach is producing reliable results that can be used to draw meaningful conclusions and make informed decisions.

5.1. Set-Up

For the application, a simple trapezoidal structure will be used, with the same dimensions as Structure 8-I that was used in the previous chapters. The structure is given at Figure 5.1. The wave condition that is going to be used in wave condition 35, with a significant wave height input 0.14 m, target period is Tp 1.6 sec and depth equal to 0.75 m. This wave condition was chosen because it has one of the lowest kd values (Table 3.2) and XBeach can better simulate the wave evolution, while it was also extensively used in the previous chapters. The bathymetry is the same like the one that was used in the wave flume (Figure 3.3).

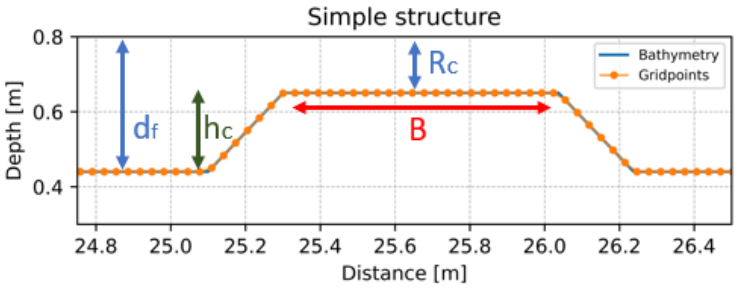

Figure 5.1.: Simple structure together with notations that going to be used for the consistency check.

The notations that are being used are the same as the ones described in Section 2.1.1 and were also used with the same meaning in the physical model experiments.

To evaluate the performance of XBeach, the following parameters and ratios are going to be modified and their impact on the transmission coefficient will be examined:

1. Relative structure height h_c / d_f.

2. Relative freeboard $R_c / H_{m0,i}$.

   The effect of the height of the structure can be assessed with both dimensionless ratios above. Checking the relative structure height and relative freeboard of a submerged breakwater is an important aspect of evaluating its performance and effectiveness given the fact that structure height dominated other structure characteristics on wave transmission.

3. Relative width $B / L_{m-1,0}$.

   With this ratio, the effect of the crest on the transmission can be investigated. The width is made dimensionless by dividing it by the incoming wavelength. With this ratio will be investigated not only the effect of the width but the effect of the wave period likewise. Modifying the wave period also translates to different wave steepness values and varying wavelength values. The wave period that will be used for the computations is the spectral period $T_{m-1,0}$

4. Slope of the structure.

   The simple breakwater has a slope of 1:1, which is quite steep. For this reason values up to 1:5 will be tested.

5. Changing structure height versus changing structure width.

   In the previous chapters, it was shown that the structure height can more effectively regulate wave transmission above the breakwater, compared to width. For this reason, both the effect of height and width will be plotted on the same figures to easily make comparisons between the two.

5.2. Results

Relative structure height h_c / d_f

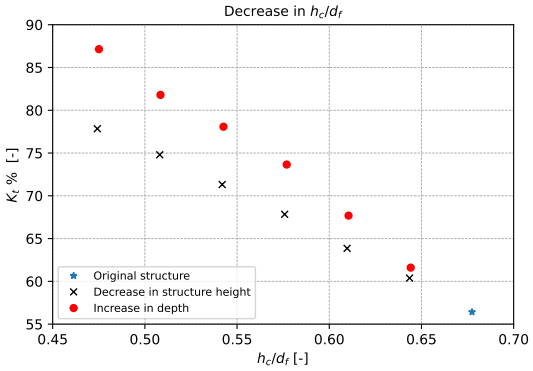

Figure 5.2.: Change in K_t for decreasing h_c / d_f.

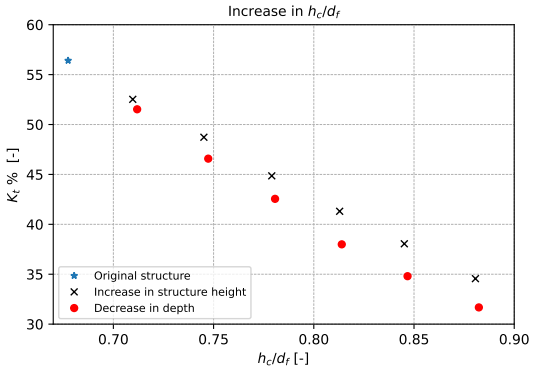

Figure 5.3.: Change in K_t for increasing h_c / d_f.

In Figure 5.2 and Figure 5.3 the h_c / d_f takes values from about 0.45 to almost 0.90. No emerged configurations were tested. To examine the effect of the foreshore, both the structure height and the total water depth were changed. The ratio can be increased either by increasing the structure height or by decreasing the water depth. Likewise, the ratio can decrease by decreasing the structure height

or increasing the water depth. If only the structure height is changed, then the effect of the foreshore would not have any impact on the wave field.

It is noticeable that the further the ratio increases or decreases, the transmission coefficient starts to differ for the same values of h_c/d_f. The difference can be as high as almost 10% when the ratio is smaller than 0.5. This highlights the impact of the foreshore. Bathymetry plays an important role in wave evolution and thus only modifying the structure height alone could lead to distorted results. In this particular bathymetry, it seems like for the initial depth of 0.75 m the waves feel the impact of the foreshore by having their wave heights influenced. A change in the wave height means a change in the wave steepness and thus a different breaking pattern above the breakwater. If the depth increases, the waves propagate within the domain freely without being influenced.

The same is observed for a decrease in the water depth in Figure 5.3. Smaller depths mean a stronger impact of the foreshore on the incoming waves and thus even more wave breaking on the structure. Although, the difference in the transmission values is not that prominent, compared with increasing the structure height.

In the physical model test, it is reported that the smallest transmission results ($K_t < 0.6$) were observed for values $h_c/d_f > 0.68$. In this particular configuration, the transmission coefficient reaches values of less than 60% a bit earlier than $h_c/d_f = 0.68$, but this can be explained by the fact that this structure is impermeable, while the ones in van den Brekel [2021] are all porous. Therefore XBeach shows the expected behavior.

Relative freeboard $R_c/H_{m0,i}$

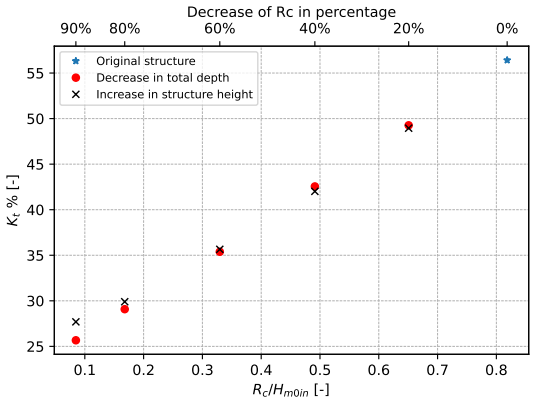

Figure 5.4.: Change in K_t for decreasing R_c/H_{m0in}.

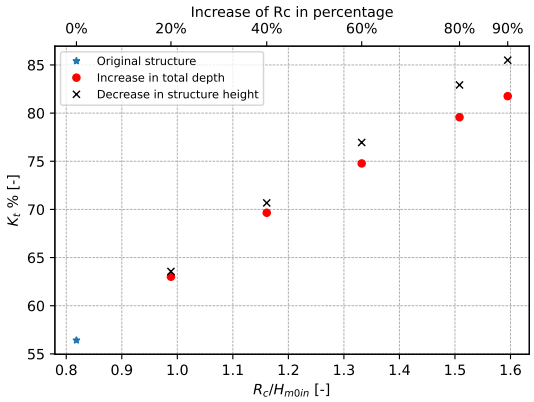

Figure 5.5.: Change in K_t for increasing R_c/H_{m0in}.

In a similar way to that of Relative structure height h_c/d_f, there are two ways to modify the freeboard and subsequently $R_c/H_{m0,i}$ ratio. Either the depth can increase or decrease, or, in the same manner the structure height. The incoming wave height was decided to remain constant because changing the input wave height, for example, 5%, will not produce an equal 5% change in the incoming wave height, making the computations time expensive. Therefore only the freeboard R_c was changed, as it can be seen in Figure 5.4 and Figure 5.5.

Compared to relative structure height, relative freeboard demonstrates relatively the same behavior for altering the structure height or total depth. Only for values of $R_c/H_{m0,i}$ above 1.2 there seem to be a small difference of about 1-3%. Every 20% change in R_c seems to produce an equal change in the transmission coefficient of about 6% in both figures. Contrary, in the physical wave flume, it is reported that increasing $R_c/H_{m0,i}$, K_t increases at first more rapidly and then more slowly. An example of the recorded $R_c/H_{m0,i}$ values within the physical model is given in Figure 5.6, where the change in the transmission coefficient is illustrated. One possible explanation for the differences between the figures for the simple structure and the figures from the physical model can be can be due to the inconsistencies between the configurations that were tested in the wave flume, as well as the change of the period and steepness of the waves among the different wave conditions. This is not true for the simple structure, since the wave period, wave height and structure shape remained constant, resulting in an almost linear change of K_t.

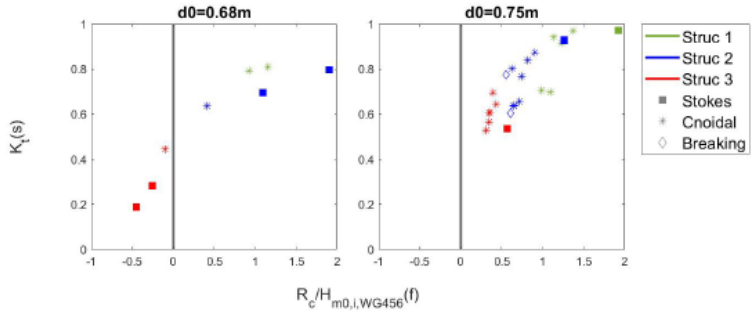

Figure 5.6.: Change of the $R_c/H_{m0,i}$ ratio for different depths and structures.

Relative width $B/L_{m-1,0}$

With this ratio, both the change in width will be investigated, and the change in wave steepness, by changing the input wave period. In the wave flume the input parameters used resulted in wave steepness that was varying from 0.02 to 0.04 (s_{Tinput}). This time the wave steepness is varied between 0.02 to about 0.07, to take into account a wide range of steepnesses that can be attributed to storm waves, but this time the spectral period $T_{m-1,0}$ will be used to calculate the wave steepness.

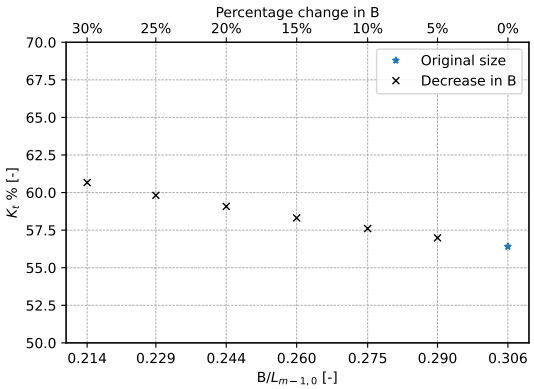

Figure 5.7.: Change in K_t for decreasing $B/L_{m-1,0}$.

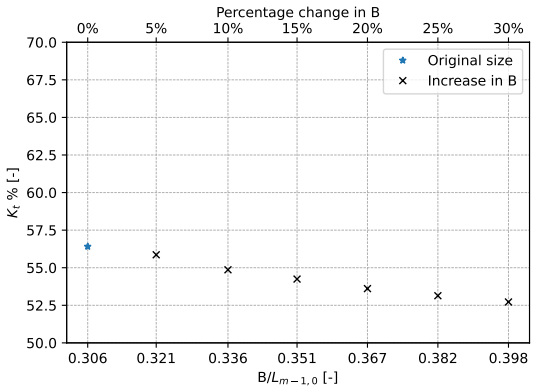

Figure 5.8.: Change in K_t for increasing $B/L_{m-1,0}$.

Firstly, the change in the width is given in Figure 5.7 and Figure 5.8. As expected from the previous chapters, changing the width has little influence on the transmission coefficient. The same findings where reported in the previous thesis, although there seemed to be a bit stronger relation. This can be a result of different freeboard between the tests.

Below the change in wave steepness is given. The effect of wave steepness seems to not be strong enough, for decreasing wave periods. For values $B/L_{m-1,0} > 0.3$ the transmission coefficient stabilizes around 57%. On the other hand, Figure 5.8 shows that for an increase in the ratio, K_t continues to decrease. Increasing the wave period results in an initial decrease of the transmission coefficient, and then an increase (Figure 5.9). Through increasing the wave periods, the waves become longer, and the crest of the breakwater is not wide enough to dissipate them.

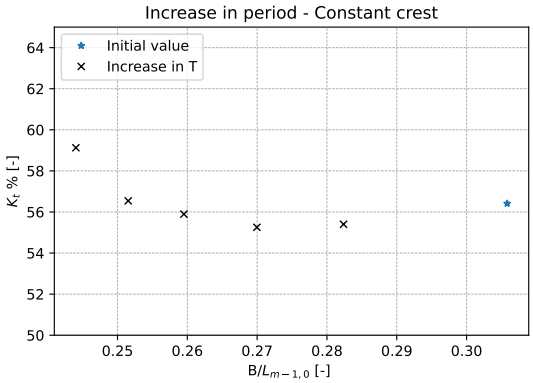

Figure 5.9.: Change in K_t for decreasing $B/L_{m-1,0}$.

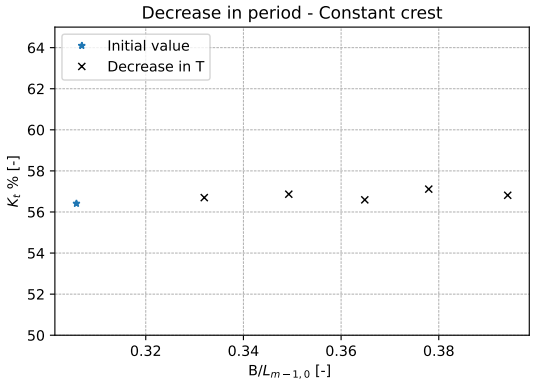

Figure 5.10.: Change in K_t for increasing $B/L_{m-1,0}$.

Slope of the structure

The findings that are presented here regarding the slope of the structure can not be directly compared to that of the previous thesis, due to the reason that the structures used by van den Brekel [2021] had steep fronts and were not slopped. For this reason, the surf similarity parameter was used to examine the effect of slope and wave steepness. On the contrary, in this section, only the slope of the structure was modified to reach a value of up to 1:5. The results are shown in Figure 5.11. As expected the change of slope did not had a strong impact on the transmission coefficient. It is worth mentioning that the wave is breaking above the breakwater and thus changing the slope would change the breaking point. In regular wave conditions without wave breaking, the effect of the slope could also be minimal. The effect of the slope could become more important for even milder slopes, but such slopes are not common for submerged breakwaters.

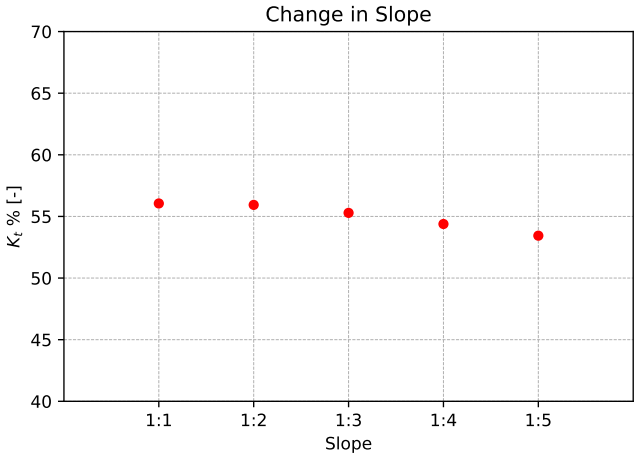

Figure 5.11.: Change of the slope.

Changing structure height versus changing structure width

The impact of the structure height on wave transmission has been established within this study by looking both at previous literature and present results. Likewise, the weak impact of the structure width was also highlighted. In Figure 5.12 and Figure 5.13, these two structure characteristics are plotted against each other to illustrate the differences.

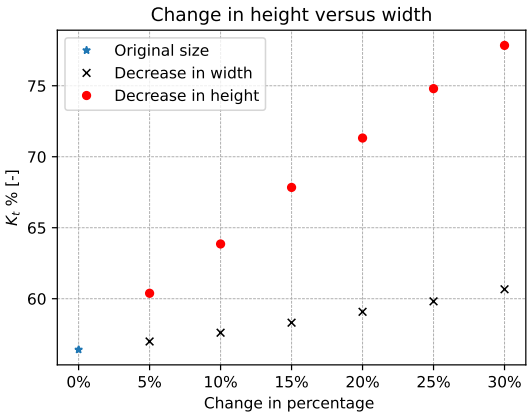

Figure 5.12.: Change in K_t for decreasing width or height.

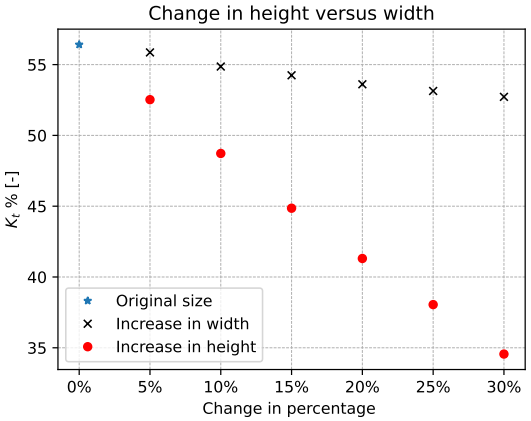

Figure 5.13.: Change in K_t for increasing width or height.

The above figures were made to validate the effectiveness of the structure height in regulating the transmitted wave height. A change of 30% in width or height can lead to a difference in the transmission coefficient up to 15%. This means that in real-life conditions, more focus can be given to defining the structure height rather than structure width.

6. Discussion

This chapter discusses the study methodologies and findings, as well as the implications for the key conclusions. After a critical analysis of each part, the limitations and strength of this thesis will be discussed, by analyzing and commenting on each element of the study.

6.1. Assessment of the study

The focus of this research was to use XBeach to model the flume experiments reported by van den Brekel [2021], and compare the computed wave heights and the recorded ones. The use of XBeach was decided based on its simplicity and the fact that is more user-friendly compared to other numerical models. Indubitably, this causes limitations on the level of detail. To understand the potential limitations and the impact they have, a thorough analysis of the existing literature was conducted to comprehend how submerged porous breakwaters behave and how can they can be represented within the chosen numerical model. By explaining the details of XBeach's inner workings, it was made clear that to model a porous submerged structure, a solution had to be found because there is no such option available within the numerical model. Followed by the selection of the data, wave conditions and the setup of XBeach, the breakwater was modeled as an impermeable structure, then its shape was modified and was even represented as vegetation. Another solution was to modify the suggested values of XBeach settings. In the end, after also validating the solution with more structures, it was proven that decreasing the structure height by 15% shows the best results. As a final step, a brief consistency check was done on XBeach to solidify that it behaves as intended when a simple impermeable structure is modeled.

XBeach

The most important element of the current thesis is the use of XBeach. This numerical model was initially constructed to model nearshore processes. With the addition of new modes and updates, the model has expanded its field of application. The version that was decided is XBeach Non-Hydrostatic+ (XB-NH+). This specific mode though, and XBeach in general, has been validated in reef hydrodynamics and scaled flume experiments [Pearson, 2016; de Ridder et al., 2021], but not for scaled porous breakwaters. Under these circumstances, attention was given to understanding the behavior of the numerical model and reporting where its performance is lacking.

Within XBeach, the layout of the physical model was fully re-created. On the left side the waves were generated while on the right side a slope was constructed to mimic exactly the real-life slope of the wave flume. XBeach Non-Hydrostatic+ which is used, is known to illustrate the best behavior when $kd<2$. This caused extra limitations on the input data. Of the 8 irregular wave conditions only 5 of them where satisfying this limit. Wave conditions 17,19 and 20 were decided to be discarded because they all had $kd>2$. An example is given for wave condition 17 in Figure 6.1.

After the decision was made on the wave conditions, the next step was to use the input data from the previous thesis to model the wave conditions, initially without the breakwater inside. From the wave gauges inside the physical model tests, the significant wave height that was measured at each wave gauge was used as an input. It was found that at the start of the numerical domain, there is a steep decrease in the modelled wave heights, resulting in an underestimation of the wave heights at the location of the wave gauges within the numerical model. This was visible in Section 3.2.1 and Figure 3.4. This behavior of the model had been recorded also in past studies. Therefore, new wave heights had to be used as an input, which were higher than the ones that were used in the physical model as an input for the wave maker. Nonetheless, in Figure 6.1, with increased wave height as an input, XBeach failed to compute within reasonable limits the significant wave height evolution for wave condition 17 (a wave condition with kd>2, boundary condition in deep waters). The steep decrease in height at the start is also prominent. On the other hand, for the rest of the wave conditions that had kd<2 (boundary condition within shallow waters), XBeach succeeded in calculating the significant wave height evolution, as shown in Appendix B Section B.5.

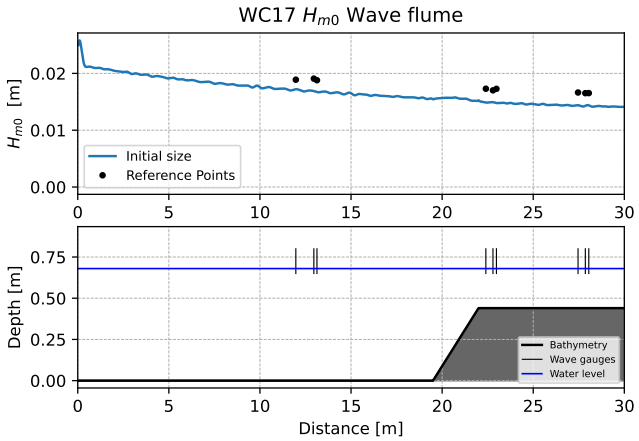

Figure 6.1.: Significant wave height evolution for wave condition 17. Input parameters: $T_{input} = 0.8$ [s], $H_{input} = 0.02$ [m].

Another input value that had to be changed, compared to what was used in the physical wave flume, was the spectral shape of the JONSWAP spectra that were defined. In the physical tests, a value of $\gamma = 3.3$ was used, while in this study it was found that $\gamma = 1$ demonstrated the best results on average for all wave conditions. In Appendix B Section B.2 a brief analysis was conducted, and it was shown that ideally for each wave condition the γ would have to be calibrated for each wave condition separately. Moreover, regarding the Nyquist frequency, which is the maximum frequency that can be accurately represented, a value of 3 hz was chosen, while the suggested values are 0.2-1. These values are usually observable in the seas, but the physical model was a scaled one and smaller wave heights were generated, meaning there is more energy in higher frequencies. In the present study the focus was on wave heights (wave transmission coefficients) rather than on spectral shapes. It is assumed that if the wave period $T_{m-1,0}$ would be modelled accurately, that the exact spectral shape is of lower importance.

For the settings of XBeach, the recommended values of XBeach User manual were used. A brief evaluation of the values of the friction coefficient and a sensitivity analysis was done in Appendix B Section B.4 where it was decided that the White-Colebrooke method resulted in the smallest errors,

with a geometrical roughness of Nikuradse $k_s = 0.01$ m, which is within the recommended limits. The RMSE for modeling the wave conditions without the breakwaters inside were on average 0.005 m for the total significant wave height H_{m0}, 0.337 sec for $T_{m0,1}$ and 0.222 sec for $T_{m-1,0}$. Therefore XBeach could simulate the wave heights with great precision but the error in the spectral periods is relatively large. This could be the effect of choosing a spectral shape with $\gamma = 1$. Another possible solution would be to change the wave steepness by modifying the wave steepness parameter setting *maxbrsteep*. In Figure 6.2, an example of a frequency spectra is given, for a test without a structure and for Wave gauge 9. XBeach overestimates the energy in lower frequencies and as a result the spectral periods are not computed accurately.

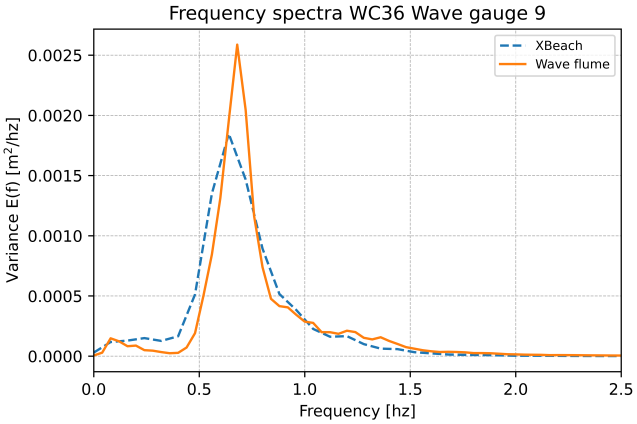

Figure 6.2.: Frequency spectra for wave condition 36, no structure. Input parameters: $T_{input} = 1.45$ [s], $H_{input} = 0.136$ [m].

XBeach computes the total significant wave height and does not distinguish between incoming and reflected signals. Structure design guidelines use mainly the incident wave height, and not the total, which also includes the reflected wave height. To do so, the simple Guza Split method [Guza et al., 1984] was used and will be elaborated on in the following paragraphs. The next step after the set-up of the wave flume was to find a way to model the breakwater.

XBeach has no specific option to simulate a submerged porous breakwater. The most simple solution was to simulate an impermeable structure. Throughout the literature review (Section 2), examples are given from previous studies that supported that when a porous breakwater is simulated as an impermeable one, wave breaking is stronger and thus lower wave heights are recorded. XBeach showcased exactly the aforementioned behavior with lower transmitted wave heights, and thus lower transmission coefficients. In light of this behavior, the focus was directed toward the breaking process itself, which was dominated by depth breaking. The impermeable structure was modified by having its height or width decreased. Moreover, it was explored whether changing the wave steepness parameter setting *maxbrsteep* could delay the breaking process. An attempt was also made to model the breakwater as vegetation, in hope that the model would be able to capture the wave evolution above it. A commentary on the solutions is given in the following paragraphs.

There were another 2 ways to simulate a porous breakwater that were not utilized in this study. The first one is porous in canopy flow, which is based on the vegetation module de Ridder et al. [2021], with the difference of using the velocity within the canopy, rather than the depth averaged velocity. A failure, or inconsistencies, of the vegetation to describe the wave evolution would most probably mean the same

is true for the porous in-canopy flow, and therefore was not tested. The second option would be to use the groundwater flow module. This module uses a parameterization of the Forchheimer equations for turbulent groundwater flow. It was constructed to model the water flow through coastal aquifers and beach profiles through vertical exchange of water. This module was extended to include also horizontal exchange of flow for steep profiles, like the one of a porous breakwater. The disadvantages are that someone would have to calibrate the conductivity parameters for each direction which can be very time consuming given the available data, and the fact that the module calculates only the flow through the porous media. What this means is that the module is not modelling the structure-wave interaction or wave breaking process through momentum equations. Given the fact that even more parameters would have to be defined, for example characteristics of an underground water level, a decision was made not to investigate this option. Likewise no available studies were available that have tested this module for submerged porous structures.

Simple Guza split

As it was previously discussed, XBeach only computed the total wave heights (or instantaneous water level), and does not separate the signal into incoming-reflected. To do so, the simple Guza split method was utilized, with an alteration in the wave celerity equation. The original formula assumes shallow water conditions and uses simple shallow water celerity. In this study, the method was modified to include the dispersion relationship, given the fact that most of the wave flume, for the given wave conditions, can be characterized as deep or intermediate (Section 3.1.1). Guza split computes both the incoming and reflected signals, which then are processed to compute the significant incoming and reflected wave heights. An example of the Guza split method is given in Figure 6.3, where the total, incoming and reflected significant wave height evolution is given for a specific wave condition. The modified version demonstrates favorable results. Only in the deep part of the wave flume, it seems like the method tends to slightly underestimate the incoming wave heights. This is not necessarily a miscalculation of the Guza split, but rather a result of the inability of XBeach to compute the depth average current in the deep part, which in turn affects the results of the wave decomposition method.

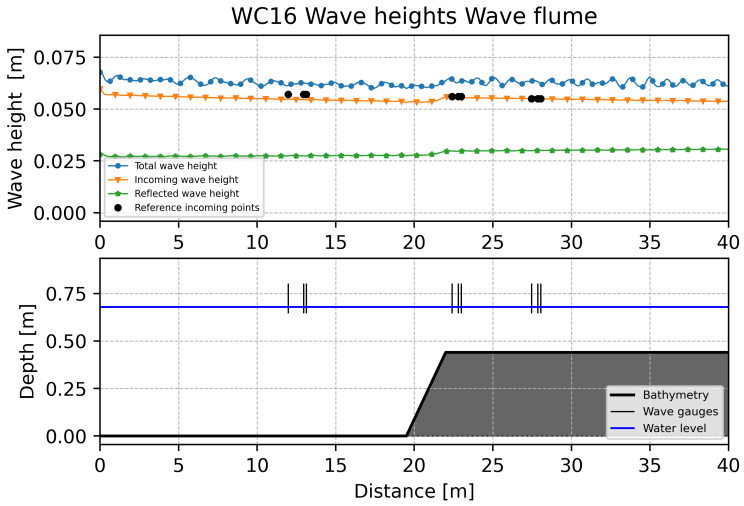

Figure 6.3.: Total, incoming and reflected significant wave height evolution for wave condition 16, with no structure. The slope at the end is located at distance x=55m. Input parameters: $T_{input} = 1.47$ [s], $H_{input} = 0.066$ [m].

Solution observations

There were three possible courses of action that could be taken. The first one was to represent the structure as an impermeable breakwater, which then would be modified shape-wise, using the recommended settings. The second course of action was to change the settings, namely the *maxbrsteep* parameter, to alter the breaking process. Lastly, the vegetation module of XBeach could be used to simulate the breakwater as vegetation. At the initial exploration phase of which solution works the best, only two structures were decided to be of interest, Structure 2 and Structure 8-I (Figure 2.3). Structure 2 was a simple structure with no change of shape along the width and data was available for 2 wave conditions. Structure 8-I on the other hand was a complex 3D structure, with varying orientation width-wise and a channel. There were 3 wave conditions that were available for Structure 8-I. Structure 2 had a porosity of 20% while Structure 8-I had 45%. Due to the availability of the data and the fact that these 2 structures had quite different shapes, it was decided to these conditions to select the optimal solution. For the rest of the structures, the available data was quite limited, with most structures being tested for only one wave condition.

The first step of representing the breakwaters as a simple impermeable change in the bathymetry, also referred as a Original case, was important for the evaluation of the numerical model. The expected behavior was clearly defined in the literature review, and if the model failed to demonstrate the same results, then either there would be problems with the choice of the model, or the available data was not correct. In the end, the result is the expected underestimation of the transmitted wave heights and transmission coefficient. The average MAPE and RMSE transmission coefficient errors were for the Original case 21.1% and 15.2% respectively.

The error plots of the Original case display a strong underestimation of the transmitted wave heights. Within the error plots, it is easy to see that Structure 2 performed better than Structure 8-I, indicating the fact that porosity affects the wave transmission since the structure with the smaller porosity percentage

presents better results when modeled as a simple bathymetry change. Nonetheless, for the given wave conditions and structure heights, the depth by breaking is the dominating factor of wave transmission, while porosity has a small effect on the end results. These results are in accordance with the Section 2.2.

The next step was to modify the impermeable structure in order to alter the breaking mechanism. The best results were obtained for either decreasing structure height by 15% or decreasing width by 20%. The latter did not lead to as good results as the change in structure height. Changes in the structure width had small effect on the wave transmission. Decreasing the structure height had a transmission MAPE error of only 5.9% and RMSE equal to 4.5%, for structures 2 and 8-I.

The second course of action was to change the *maxbrsteep* setting of XBeach. This parameter regulates the level of the wave steepness before the wave breaks. The bigger the value, the steeper the wave faces can become before breaking, shifting the breakpoint shoreward [Lashley et al., 2018]. The advantage of this option is that there is no need to modify the structure size, someone can easily change the value of the setting and then alter the bathymetry to represent the breakwater. The disadvantage is that this can result in unrealistic wave evolution and the need to increase the points per wavelength to better capture the wave steepening. For this reason, the setting was increased from the suggested value of 0.4 to a value of 1.4. The results were very promising. The MAPE error was equal to 10.9% and RMSE equal to 8.9% (for structures 2 and 8-I). Compared to a decrease in structure height, this solution also exhibits small errors of the spectral periods.

The last course of action was the vegetation module that failed to produce logical results and the error plots were not computed. In Appendix C, the wave height evolution of the vegetation module is given for the two structures. The results varied greatly not only between the structures, but also between different wave conditions of the same structure. The reason can be attributed either to the fact that unreasonable values for parameters were used (for example the drag coefficient) or that the width of the structures was not sufficient enough for the vegetation to have an impact on the incoming waves.

Because both decreasing in the structure height and changing the *maxbrsteep* setting displayed satisfactory findings, it was decided these two solutions for validation with more configurations and wave conditions that were not utilized before. 7 new structures were modeled again and their error plots were computed. In the end, decreasing the structure height was the most effective solution with a total MAPE of 9.9% and RMSE 8.2%, in the transmission coefficient. The errors are given in Table 4.2 and comparison between the two solutions is given in Figure 6.4.

Regarding the choice of the structures that were used for the validation, attention was given to use structures with different shapes, porosity values and that were tested for different wave conditions. Unfortunately, some of the structures were emerged, like Structure 12 and Structure 13. In Figure 6.5 one can see that when a structure is emerged, XBeach failed to produce reasonable outcomes, and thus Guza split method would also produce unreasonable results.

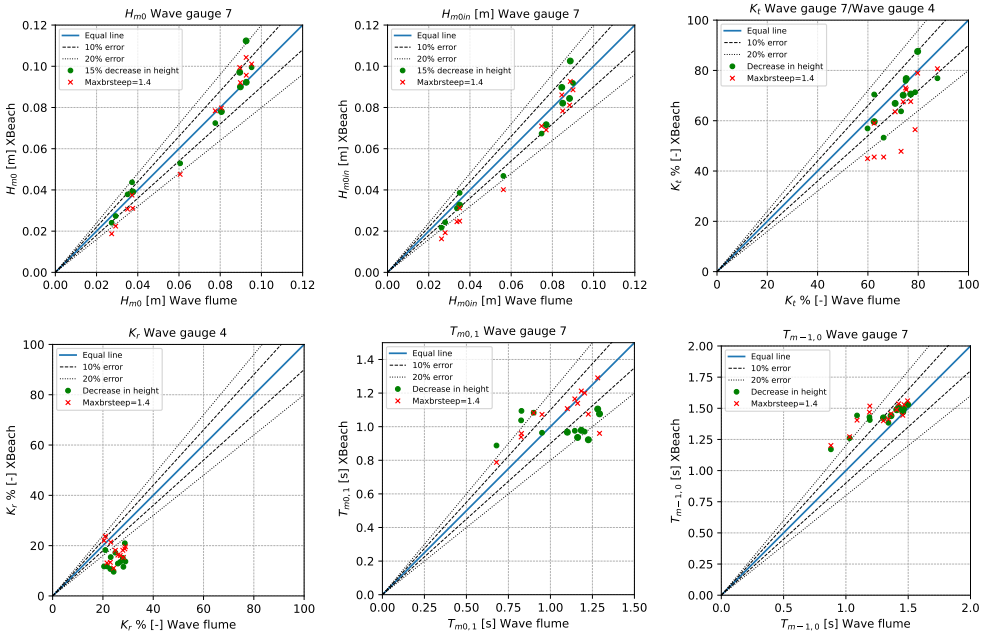

Figure 6.4.: Comparison between 15% structure height decrease and *maxbrsteep*=1.4 for all the structures and wave conditions that were tested.

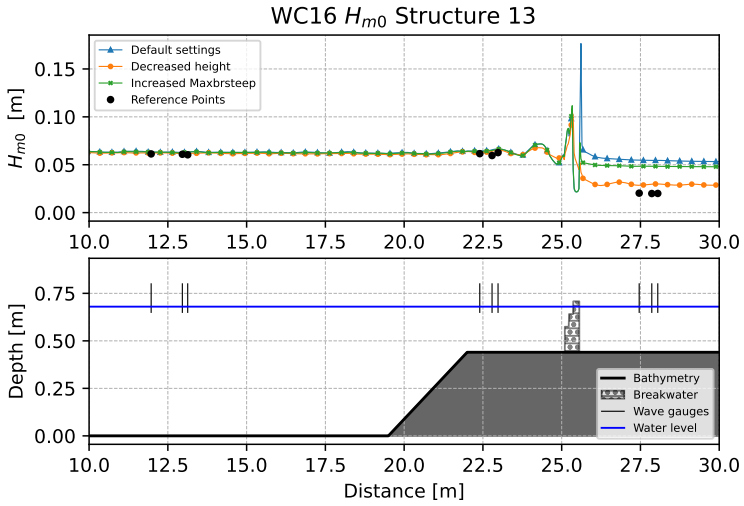

Figure 6.5.: Total significant wave height evolution for Structure 13. A decrease in structure height shows better results but this means that the structure had to be modeled as a submerged one.

Another possible solution would be to model structures that were simple (20% porosity) and structures that were complex (above 20% porosity) in different ways. In Table 6.1 a summary of the computed

errors for the two most promising solutions are given, but only for the simple structure. Likewise, in Table 6.2 the same information is given for only the complex structures.

Errors - Only simple 2D structures		H_{m0} [m]	H_{m0in} [m]	K_t % [-]	K_r % [-]	$T_{m0,1}$ [s]	$T_{m-1,0}$ [s]
Original case	MAPE [%]	7.7	12.6	14.7	46.6	23.9	9
	RMSE	0.008	0.01	11.5	13.1	0.275	0.184
15% Structure height decrease	MAPE [%]	10.4	7.7	6.8	47.8	19.1	6.3
	RMSE	0.01	0.007	5.8	13.4	0.225	0.116
Max steepness parameter = 1.4	MAPE [%]	6.8	5.3	5.1	35.5	7.2	8.2
	RMSE	0.007	0.004	4.8	9.9	0.107	0.141

Table 6.1.: Overview of the MAPE and RMSE errors for only simple structures. The results with the minimum error per parameter are coloured with green.

Errors - Only complex 3D structures		H_{m0} [m]	H_{m0in} [m]	K_t % [-]	K_r % [-]	$T_{m0,1}$ [s]	$T_{m-1,0}$ [s]
Original case	MAPE [%]	25.1	32.2	31.7	32.4	20.3	27.5
	RMSE	0.013	0.015	22.9	9.3	0.199	0.354
15% Structure height decrease	MAPE [%]	6.7	10.2	9.3	40.6	19.1	16.2
	RMSE	0.004	0.005	7.7	10.3	0.195	0.205
Max steepness parameter = 1.4	MAPE [%]	13.8	22.1	21.7	29.8	11.1	17.7
	RMSE	0.007	0.01	16.7	8.4	0.145	0.223

Table 6.2.: Overview of the MAPE and RMSE errors for only complex structures. The results with the minimum error per parameter are coloured with green.

Simple structures are modeled more efficiently when *maxbrsteep* is set at 1.4, while for the complex structures a decrease in the structure height is needed to have a MAPE error below 20% in the transmission coefficient. Interestingly enough, the negative spectral period $T_{m-1,0}$ is always better estimated when a decrease in height is chosen. An explanation is given in the next paragraph.

Errors		H_{m0} [m]	H_{m0in} [m]	K_t % [-]	K_r % [-]	$T_{m0,1}$ [s]	$T_{m-1,0}$ [s]
15% Structure height decrease	MAPE [%]	9.5	11.4	9.9	43.4	20.1	14.8
	RMSE	0.008	0.007	8.2	12.1	0.21	0.2
Max steepness parameter = 1.4	MAPE [%]	14.6	18	18	33.5	9.5	16.9
	RMSE	0.008	0.009	15.6	9.7	0.101	0.221
Combination of the above solutions	MAPE [%]	6.7	8.3	7.6	38.6	14.5	13.1
	RMSE	0.005	0.004	6.7	10	0.16	0.18

Table 6.3.: Overview of the MAPE and RMSE errors when the two solutions are combined. The simple structures modeled with *Maxbrsteep*=1.4 and the complex structures with 15% decrease in structure height. The results with the minimum error per parameter are coloured with green.

Table 6.3 shows the error if 2 solutions are combined. When the simple structures are modeled with *Maxbrsteep*=1.4 and the complex structures with a 15% decrease in structure height, the MAPE decreases to 7.6% and the RMSE to 6.7%, when the wave transmission is of interest. The combination of these two solutions though, is still not producing the smallest error for the reflection coefficient and spectral period $T_{m0,1}$.

Reflection coefficient and spectral periods

The focus of this thesis is not on the study of the reflection coefficient. Nevertheless, a short insight is given. The computed errors of the reflection coefficient are always quite big no matter the chosen solution. The best solution in regards to the transmission coefficient is also the solution with the biggest error in the reflection coefficient, namely 43.5% MAPE. In all the possible options, the reflection coefficient barely falls down from 30% MAPE. With a close look at the error graphs for the wave steepness parameter (Section 4.1.4), and more specifically at Structure 2, one can notice that the total significant wave height is overestimated, the incoming significant wave height is barely underestimated and the reflection significant height is also underestimated by more than 20%. The fact that both incoming and reflected signals are underestimated, but the total signal is overestimated can mean that the Guza split method is failing to accurately compute the reflected wave signal.

The spectral periods $T_{m0,1}$ and $T_{m-1,0}$ are important to design and building coastal structures, therefore it is important to know their values behind the breakwaters. The errors vary from 10% to 20% MAPE for the different solutions. $T_{m-1,0}$ seems to be overestimated and the numerical model tends to overestimate the energy carried by the lower frequencies (short waves). On the other hand, there seems to be no clear trend in $T_{m0,1}$, when the validation Section is taken into account. XBeach seems to struggle with energy allocation after the waves break on the structure. The variance spectra of Structure 14 are given in Figure 6.6 and Figure 6.7. In both figures XBeach has difficulties to accurately process the wave breaking above the breakwater and overestimates the energy in lower frequencies (longer periods), while in the first figure the peak is also located in lower frequencies. Shorter waves are better resolved compared to longer waves. Decreasing the structure height means long waves break less and therefore $T_{m-1,0}$ is overestimated. Compared to the solution of *maxbrsteep*=1.4, the error is smaller, as the latter overestimated the energy in the lower frequencies even more.

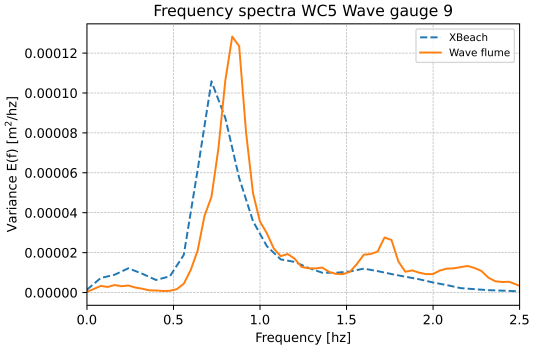

Figure 6.6.: Frequency spectra for WC5, Wave gauge 9 and Structure 14.

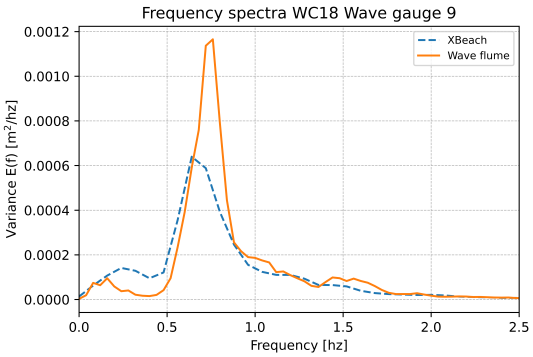

Figure 6.7.: Frequency spectra for WC18, Wave gauge 9 and Structure 14.

Application

An application of the model for different conditions was done to guarantee that the model properly simulates the physical processes that it is intended to reflect. For this reason, a simple structure was created, in the existing bathymetry layout, which was tested in various conditions. The objective was to validate that XBeach can produce the desired outcomes, as the ones recorded in the literature or the previous study of van den Brekel [2021].

The first element that was examined was the behavior of the breakwater under changes in the relative structure height h_c/d_f, followed by changes in the relative freeboard $R_c/H_{m0,i}$. Both investigations revealed that the results were in accordance with the trends that were found in the previous study. Moreover, it was highlighted that only changing the structure height to modify these ratios is wrong and can lead to wrong estimations of the transmission coefficient of more than 5%, at least when the bathymetry is complex.

With the relative width B/L, both the effect of the width and the effect of the wave steepness were examined. As stated in Section 2.2 width is not that effective in decreasing the transmitted wave heights, but it still influences the end results. An indefinitely long breakwater can decrease the transmitted wave height to zero. In this study, the behavior of the structure crest was validated. In the previous study of van den Brekel [2021] the width had a stronger impact on the transmission coefficient, but this can be attributed to the differences between the shapes of the structure and the tested wave conditions.

Through changing the wave period, the wave steepness is modified. The effect of the wave steepness was clear in XBeach. Increasing the wave period means longer waves in the domain. For the longer waves to "feel" the crest of the breakwater, the more the crest width should be increased, therefore less dissipation is observed. Increasing the ratio (decreasing wave period) the transmission coefficient was decreasing, until the $B/L_{m-1,0}$ ratio reached a value of about 0.306, where the transmission coefficient remained steady at about 57%.

The slope of the structure was also varied from 1:1 to 1:5 to assess the impact on the transmission coefficient. XBeach demonstrated predictable results in which the transmission coefficient remained relatively stable. Milder slopes had about 2% decrease in the transmission coefficient. In case the waves were not breaking for the given wave condition, the effect of the slope would be even less pronounced.

Lastly, a direct comparison was made between changing the structure height versus changing the structure width, with the aim of quantifying the difference in the transmission coefficient. Through this study, it was shown that changing the height was more effective than changing the crest width, and this was shown again in the consistency check. Even for 5% change of the value of the height or width, decrease or increase, the difference in the transmission can be up to 5%. For bigger percentage changes, it was calculated that the end results can vary by about 20%. It is important to quantify this effect so more efficient structures can be designed.

In short, whether or not XBeach is suitable to represent the wave flume experiments is going to be answered by expanding on the three factors that help to choose a porous flow model as suggested from Han and Wang [2022]:

1. Simplicity and robustness: The main advantage of XBeach is that it is simple to use, and compared to other numerical models that are verified in modeling porous structure characteristics, no advanced skill set is required. In this study, quantitative results were given while the complexity and computational time were kept minimum. This is caused by the fact that the focus is on the transmitted wave field, and not on the specific effects of porosity itself.
2. Flow regime: The flow regime was not of importance while modeling with XBeach, because the model does not solve the porosity and friction effects that a porous submerged structure would have. Consequently, no resistance terms had to be elaborately computed, as its done in previous research.
3. Comparison with experimental data: All the results that were computed in the present thesis were examined next to the results of the previous study of van den Brekel [2021]. The suggested solutions to model the wave flume and the submerged structures were all verified through data from the physical flume. XBeach was not previously verified for porous structures therefore attention was given to all the results to exhibit good agreement with the physical experiments.

All things considered, XBeach is suitable to represent the wave flume experiments as long as the focus remains on the transmitted wave heights. A different validation analysis would have to be done, if the focus would change to be on the reflection coefficient or a more thorough spectral analysis past the breakwater. Decreasing the structure height by 15% is on average the option with the best results regarding the transmission coefficient.

7. Conclusions

In this chapter the research question and sub-questions are answered. First, the answer of the main research question will take place,and then the sub questions will be answered:

Main research question

In what way and how accurately can we simulate the impact on wave transmission of a Reefy breakwater using the process-based numerical model (XBeach Non hydrostatic+)?

In order to accurately simulate the impact of a Reefy breakwater on wave transmission using XBeach, it is proposed modeling the breakwater as a change in bathymetry with a shape similar to the original structure, but with a 15% decrease in height to compensate for the omitted effect of porosity. The validation results show that this approach has a mean average percentage error (MAPE) of 9.9% and a root mean square error (RMSE) of 8.2% for the transmission coefficient, as well as a MAPE of 11.4% and an RMSE of 0.007m for transmitted wave heights. The results were validated against data from 13 wave experiments with range of validity $0.47 < R_c/H_{m0in} < 1.05$, $3.3 < B/H_{m0in} < 13.6$ and $0.015 < s_{m-1,0} < 0.04$.. This approach provides an effective and efficient solution for accurately simulating wave transmission over a Reefy breakwater using XBeach.

Subquestion 1

How does the physical geometry of the breakwater affect the accuracy of XBeach Non hydrostatic+ simulation results?

The physical geometry of the breakwater can considerably affect the accuracy of XBeach simulation results. The results showed that structures with lower porosity and simple geometry had better performance compared to the complex structures with higher values of porosity. The underestimation of the transmitted wave heights due to more breaking on the structure was observed for all structures, and the order of this underestimation was on average about 26.5% MAPE before any solution being applied. However, for simple structures with small porosity values (below 20%), this error was of the order of 13%. Therefore, it is crucial to consider the porosity effects when modeling complex structures, and the modeling approach needs to be carefully selected based on the physical characteristics of the breakwater to obtain accurate simulation results.

Subquestion 2

In what ways can the breakwater and the impact on the transmitted wave heights be simulated within XBeach and how accurate are these other strategies?

There are 4 main approaches for simulating the impact of a breakwater on the transmitted wave field using XBeach. The first approach involves modeling the breakwater as an impermeable structure with a 15% decrease in height, which resulted in the most accurate and efficient results according to the validation. The second approach involves modeling the breakwater as an impermeable structure again, but with decreased width. The calibration showed that decreasing the structure width had small effect on wave transmission, with MAPE 16.5% and RMSE 11.9% in the wave transmission, for a 20% decrease in the width. The next solution was to use the vegetation module, but it produced inconsistent results. The last approach involves modeling the breakwater as a change in bathymetry, but with an increased value of the *maxbrsteep* parameter in XBeach. While the latter approach does not require altering the dimensions of the breakwater, it resulted in slightly lower accuracy compared to the first approach, with an average MAPE error of 18% in the transmission coefficient (compared to 9.9% for the reduced crest height approach). However, this approach can be useful for modeling simple structures with low porosity. It is also possible to combine approaches, modeling structures with low porosity using an increased *maxbrsteep* value and structures with higher porosity using decreased structure height. The combination of these 2 solutions has the smallest MAPE and RMSE in the transmission coefficient, with 7.6% and 6.7% respectively. Overall, the choice of approach depends on the user's priorities and the specific characteristics of the breakwater being modeled.

8. Recommendations

After conducting a thorough analysis of the identified factors, limitations, and strengths, this chapter aims to provide recommendations for future research.

- The first proposal to better understand the effects of a Reefy structure would be to re-create the model again, now that the focus points are identified, and simulate the regular wave conditions also. 28 regular wave conditions were tested for even more structures. The set up of the model may be more difficult for regular waves given the fact that the calibrated settings and parameters of the simulated wave conditions should exactly match that of the physical model. To better understand the physics and increase the confident in the model, it would be important to examine whether the solutions proposed here could also be applied for regular waves. Regular waves are frequently observed on coral reefs in the form of swells.
- A validation of the model for both irregular and regular wave conditions will help to ensure that a porous structure can indeed be modeled under several sea states. Following the validation, the design can be altered and be optimized, both regarding the hydrodynamic and ecological impact. In this study it was shown that structure height has a strong impact on wave attenuation, while structure width not so much. In other words, the breakwater can become less wide and save costs, or become wider and provide more space for marine life to settle. Another advantage of verifying XBeach to regular conditions would be the ability to verify the empirical equations of van den Brekel [2021]. Verifying the equations would give the possibility to assess faster the possible impact of the structures.
- Reflection was not addressed in detail but it can also become important when structure stability becomes important, as well as when erosion can appear in the area in front of the structure. A more detailed study should investigate both transmission and reflection of the breakwaters, not only for structural purposes but also due to possible impact on the marine ecosystem.
- Regarding the chosen wave decomposition method, a comparison with other methods would help pinpoint the limits of the method as well as its validation to determine the reflected signal. A decomposition method that uses Fourier transform would be chosen because it discretize the wave to its components first, and then separates the signal to incident-reflected using the wave characteristics of the components.
- The XBeach model used to simulate the wave transmission was a 1D model where no sediment transport was available. Even though for a preliminary assessments this is sufficient, the next phase is to model the breakwaters in a 2D or even a 3D model. By doing so, the interactions between waves, currents, and subsequently erosion patterns, with the structure will be captured. Erosion and sediment transport should also be introduced to the model to confirm that the placement of the breakwaters relative to the shore are not actually causing undesirable erosion patterns. Since XBeach has shown an overestimation tendency of the long wave energy, an investigation should be conducted to determine the effect on the sediment transport.
- Last but not least is to model the breakwater with a Computational Fluid Dynamics (CFD) model that solves the interaction between the porous media and waves. Friction and porosity influence

the structure effectiveness, and depending on the level of detail, they can affect the results. CFD models can resolve flow and wave dynamics at a considerably finer scale than XBeach, which is critical for effectively reproducing the complicated flow patterns surrounding the porous breakwater. CFD models are more adaptable than XBeach when it comes to modeling different geometries and flow regimes, and they can also model overturning waves and the vertical structure of the flow. Therefore, the impact of the structure on the ecosystem will be better determined. CFD models can also represent turbulence with great detail and no need of parameterization, which is vital for modelling wave-breaking and energy dissipation in the porous breakwater, but also for the fauna and flora that would make the structure their habitat. Nevertheless, CFD models are computational expensive such that using XBeach also has its advantages.

A. Physical Model

In this appendix data and figures from the previous study [van den Brekel, 2021] will be given.

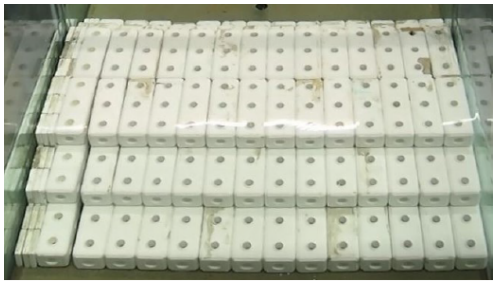

Figure A.1.: Structure 2

Figure A.2.: Structure 2 Blocked Holes

Figure A.3.: Structure 4

Figure A.4.: Structure 5

Figure A.5.: Structure 6

Figure A.6.: Structure 7

Figure A.7.: Structure 8-I

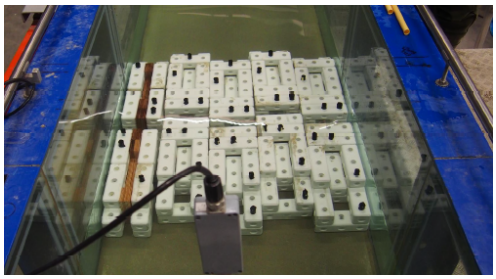

Figure A.8.: Structure 8-I-PVC(38)

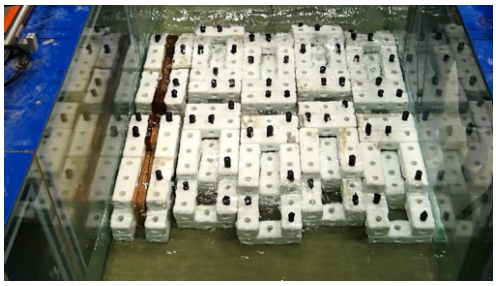

Figure A.9.: Structure 8-I-PVC(69)

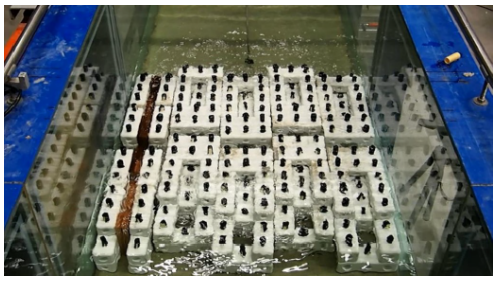

Figure A.10.: Structure 8-I-PVC(169)

Figure A.11.: Structure 8-I-3D

Figure A.12.: Structure 11

Figure A.13.: Structure 12

Figure A.14.: Structure 14

Figure A.15.: Structure 15

Wave condition number	d_o	T_{target} (s)	H_{target}(m)	s (-)	Regular (R)/Irregular (I)	Structure Number
1	0.61	1.47	0.06	0.02	R	11-I
2	0.61	1.16	0.04	0.02	R	11-I
3	0.61	0.8	0.02	0.02	R	11-I, 12-I
4	0.61	0.98	0.06	0.04	R	11-I
5	0.61	1.16	0.04	0.02	I	11-I,11-III,12-I,12-III,14
6	0.68	2.51	0.12	0.02	R	11-I
7	0.68	2.15	0.10	0.02	R	11-I
8	0.68	1.80	0.08	0.02	R	1,2,3,8-I,8-III,8-V,9,10,11-I,15
9	0.68	1.47	0.06	0.02	R	-
10	0.68	1.15	0.04	0.02	R	1,2,3,8-I,8-III,8-V,9,10,15
11	0.68	0.80	0.02	0.02	R	1,2,3,8-I,8-III,8-V,9,10,15
12	0.68	1.47	0.12	0.04	R	11-I
13	0.68	1.31	0.10	0.04	R	11-I
14	0.68	1.15	0.08	0.04	R	1,3,9,10,11-I
15	0.68	0.98	0.06	0.04	R	11-I
16	0.68	1.47	0.06	0.02	I	2,8-0,8-I,8-V,13,15,8-I-PVC(69&169)
17	0.68	0.80	0.02	0.02	I	8-I,15
18	0.68	1.31	0.10	0.04	I	11-I,11-III,12-I,12-III,14
19	0.68	1.15	0.08	0.04	I	8-I,13.8-I-PVC(69&169)
20	0.68	0.98	0.06	0.04	I	8-0,8-I,8-V,8-I-PVC(169&3D)
21	0.75	3.11	0.16	0.02	R	-
22	0.75	2.76	0.14	0.02	R	2
23	0.75	2.42	0.12	0.02	R	1,2,2-BH,3,4,5
24	0.75	2.09	0.10	0.02	R	1,2,2-BH,3
25	0.75	1.92	0.18	0.04	R	2,15
26	0.75	1.76	0.16	0.04	R	2,4,5,8-I,8-III,8-V,9,10,15
27	0.75	1.60	0.16	0.04	R	-
28	0.75	1.60	0.14	0.04	R	1,2,2-BH,3,4,5,8-I,8-III,8-V,9,10,15
29	0.75	1.45	0.12	0.04	R	1,2,2-BH,3,8-I,8-III,8-V,9,10,15
30	0.75	1.29	0.10	0.04	R	1,2,2-BH,3,8-I,8-III,8-V,9,10,15
31	0.75	1.14	0.08	0.04	R	1,2,2-BH,8-I,8-III,8-V,9,10,15
32	0.75	0.98	0.06	0.04	R	R,8-I,8-III,8-V,9,10,15
33	0.75	0.80	0.04	0.04	R	-
34	0.75	0.40	0.01	0.04	R	-
35	0.75	1.60	0.14	0.04	I	2,2-BH,4,5,6,7,8-I,8-I-PVC(32&69&169)
36	0.75	1.45	0.12	0.04	I	-

Table A.1.: A summary of the conditions that were used as inputs for the wave files. For the conditions where no structures are displayed it means that the tests took place but the results weren't investigated further either due to time constraints or due to unforeseeable circumstances [van den Brekel, 2021].

Structure number	h_c (m)	B_c (m)	α (°)	Φ	L_{ch} (m)	Blocks number
Structure 1	2	12	26.6	0.20	N/A	27
Structure 2	3	6	26.6	0.20	N/A	27
Structure 3	4	3	26.6	0.20	N/A	30
Structure 4	3	3	18.4	0.20	N/A	18
Structure 5	3	6	18.4	0.20	N/A	27
Structure 6	3	6	45	0.20	N/A	27
Structure 7	3	6	26.6	0.20	N/A	27
Structure 8-0	3	11	58.3	0.45	0	27
Structure 8-I	3	11	58.3	0.45	1	27
Structure 8-III	3	11	58.3	0.45	3	27
Structure 8-V	3	11	58.3	0.45	5	27
Structure 9	3	7	58.3	0.31	1	27
Structure 10	3	7	58.3	0.46	1	21
Structure 11-I	2	11	26.6	0.39	1	19
Structure 11-III	2	11	26.6	0.39	3	19
Structure 12-I	3	6	26.6	0.39	1	23
Structure 12-III	3	6	26.6	0.39	3	23
Structure 13	4	5	68.9	0.44	N/A	17
Structure 14	2	5	26.6	0.40	N/A	9
Structure 15	3	5	58.3	0.46	N/A	13

Table A.2.: Characteristics of the different configurations, in 1:1 scale. The number of blocks is per 3 meter flume width [van den Brekel, 2021].

Dimension	Model 1 : 15	real system 1 : 1
width x height x length	0.067 x 0.067 x 0.20 m	1 x 1 x 3 m
Volume holes	0.18 x 10^{-3} m^3	0.61 m^3
Volume material	0.71 x 10^{-3} m^3	2.39 m^3
Mean dry weight	1329 $g/block$	4485 $kg/block$
Mean dry density	1.88 g/cm^3	1.88 g/cm^3
Mean saturated weight	1378 $g/block$	4651 $kg/block$
Mean salt water saturated weight	1379 $g/block$	4655 $kg/block$
Mean salt water saturated density	1.95 g/cm^3	1.95 g/cm^3
D_{50}	8.9 cm	1.3m

Table A.3.: Dimensions of a Reefy module in 1:1 and in 1:15 scaled [van den Brekel, 2021].

B. Spectral analysis

B.1. Spectral Analysis

The spectral density of the water surface time series is computed with the Welch method [Welch, 1967]. By averaging the spectal density the total variance is computed. Welch's approach estimates the spectral density by dividing the time series data into overlapping parts (D_{block}). The length of these parts defines the spectral resolution (i.e the interval between frequencies in the spectrum $\Delta f = 1/D_{block}$). In the python script (part of the scipy library), the length of these parts is defined by the keyword: nperseg. Increasing the length means increasing the resolution of the spectrum on the expense of the accuracy. Here a number of different nperseg values where used to examine which one would produce the desired resolution with acceptable accuracy.

For the XBeach results, a value of 500 nperseg gives the best balance between accuracy and resolution (Fig. B.1). On the other hand, for the files produced at the wave flume, a value of 1000 nperseg was better than 500. In Fig. B.2 and in wave condition 17, it is easily visible that for values 2000 and 4000 the accuracy is quite low.

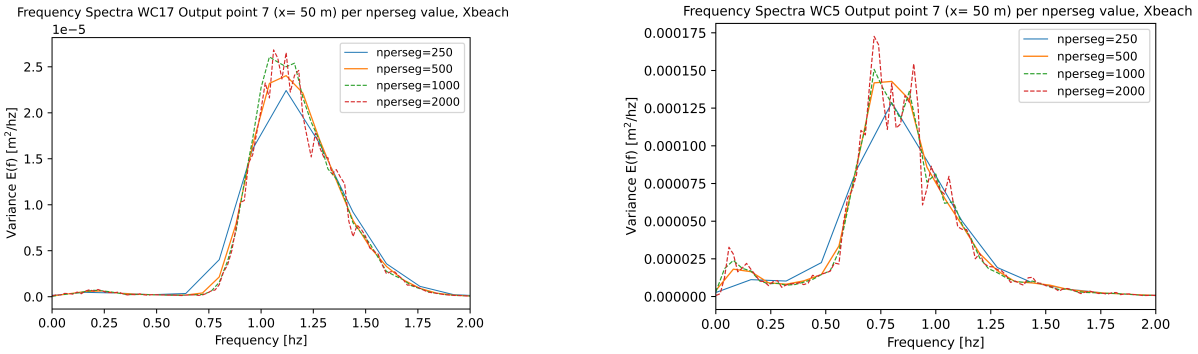

Figure B.1.: Example of different nperseg values for 2 wave conditions of the XBeach runs.

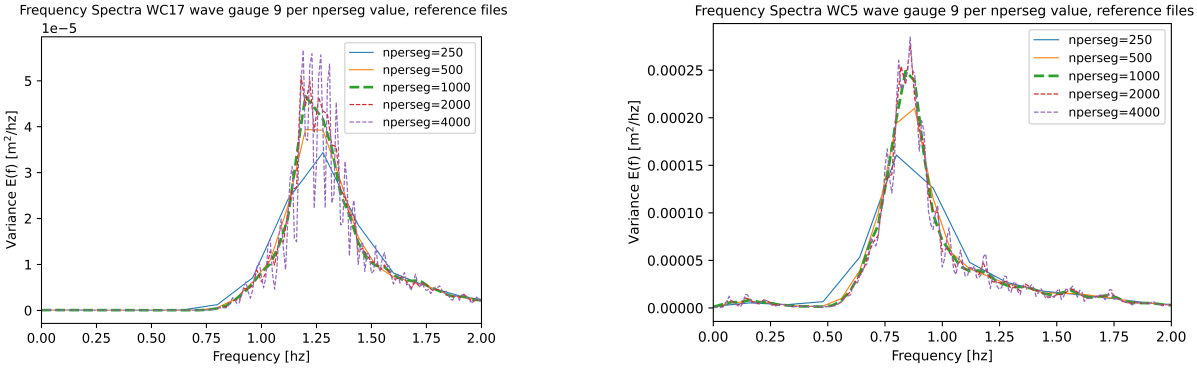

Figure B.2.: Example of different nperseg values for 2 wave conditions of the reference files of the wave flume experiments.

B.2. JONSWAP Calibration

To find whether changing the shape of the JONSWAP spectrum could decrease the error in the spectral periods, the spectral shape was varied from values $\gamma = 1$ till $\gamma = 12$. The higher the value, the more it transforms into a well peaked swell spectrum. In Figure B.3 and Figure B.4 two of the wave conditions show that the calibration of the γ value cannot produce the desired results. Small γ produce wider spectra that result in a slightly different shape and therefore negatively affect the spectral periods. On the other hand, higher γ values are more narrow and tend to approach the shape of the JONSWAP spectra produced by the reference files for the wave gauges 1-3. However, by the time they approach the shape, there is an overcompensation of energy at the peak frequency, impacting the end results. Different wave conditions show optimal results for different γ values. For Wave Condition 5 (Figure B.3) for example, $\gamma = 2$ produces a spectrum that fits over the referenced one, but for Wave Condition 35 (Figure B.4) $\gamma = 4$ produces the desired results.

The best approach would be to calibrate each wave condition individually, so as each one has a different γ value. Overall, a value of $\gamma = 1$ was found the best to represent all the conditions and it was the one used in this thesis.

γ	RMSE: H_{m0} [m]	RMSE: $T_{m0,1}$ [s]	RMSE: $T_{m-1,0}$ [s]
1	0.004	0.111	0.155
2	0.011	0.124	0.163
4	0.020	0.148	0.182
8	0.024	0.165	0.193
10	0.029	0.184	0.219
12	0.031	0.189	0.224

Table B.1.: Root mean square error for the different γ values.

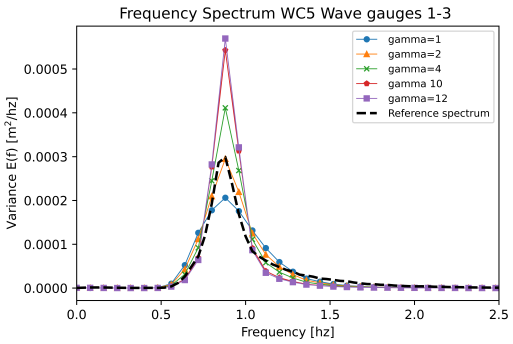

Figure B.3.: Frequency Spectrum for WC5 and different gamma values

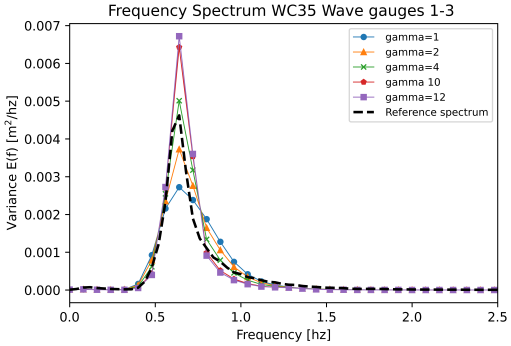

Figure B.4.: Frequency Spectrum for WC35 and different gamma values

B.3. Wave height damping

	Wave characteristics			Deep Part			Shallow Part		
	d_0 [m]	T_{target} [m]	H_{target} [m]	d/L [-]	kd [-]	ΔH%	d/L [-]	kd [-]	ΔH%
WC 5	0.61	1.16	0.04	0.30	1.90	18.06	0.12	0.78	9.09
WC 16	0.68	1.47	0.06	0.22	1.42	11.93	0.11	0.72	5.72
WC 17	0.68	0.8	0.02	0.68	4.27	41.83	0.25	1.63	16.72
WC 18	0.68	1.31	0.10	0.27	1.70	20.03	0.13	0.82	11.10
WC 19	0.68	1.15	0.08	0.33	2.12	26.93	0.15	0.97	9.07
WC 20	0.68	0.98	0.06	0.45	2.80	38.00	0.19	1.20	10.45
WC 35	0.75	1.60	0.14	0.21	1.34	13.59	0.12	0.76	8.89
WC 36	0.75	1.45	0.12	0.24	1.56	17.13	0.13	0.85	7.04

Table B.2.: The different wave conditions together with the computed characteristics including the decrease in wave heights ΔH.

In Table B.2 the limitations of XBeach-nh+ due to depth can be seen. The deep part of the model shows lot of numerical damping compared to the shallow part. The resolution of the model has been tuned in Section 3.2 while the surface roughness does not influence the results, at least for the deep part of the domain. However, wave conditions 17, 19 and 20 have 41%, 26% and 38% decrease in the wave heights respectively. The ΔH values on the shallow part are smaller than the respective deep part values, explained by the fact that XBeach-nh+ can capture better the short wave transformation for the given depths since the kd values are all smaller than 2. Ultimately, the big decrease in wave heights in these 3 wave conditions was the reason it was decided not to proceed with them.

B.4. Friction sensitivity analysis

For the bed friction coefficient two different approaches will be examined, the Chezy approach, with the respective Chezy value C (Equation B.1), and the White Colebrook approach where the geometrical

roughness of Nikuradse k_s is defined (Equation B.2). The different friction approaches are both semi-empirical formulas and both parameters have to be calibrated by comparing the water level as estimated from XBeach, and the water level as was measured from the gauges in the wave flume tests.

$$c_f = \frac{g}{C^2} \tag{B.1}$$

$$c_f = \sqrt{\frac{g}{(18log\,(\frac{12h}{k_s}))^2}} \tag{B.2}$$

In Table B.3 and Table B.4 the different values that were examined together with the RMSE of the wave characteristics are shown (for all the wave conditions without the structure). For both approaches, the value that results in the least possible friction gives the best result. This was expected as the model itself produces damping as explained in Section 3.2.1, and therefore minimizing the effect of friction would improve the results. The error on the wave height is small in both approaches (order of 0.01m), even though the White Colebrook method is more consistent among different k_s values. On the other hand, the error on the spectral periods is bigger than the respective wave height error for both approaches. Furthermore, there is not much variability in the error results despite the change in the values of C and k_s. For the spectral periods to change, the shape of the JONSWAP spectra at the boundary condition would need to change shape. Overall, both approaches illustrate the same behavior, but the RMSE was smaller for White Colebrook than the respective Chezy approach. Consequently, k_s=0.01 m was chosen.

C [$m^{1/2}/s$]	RMSE: H_{m0} [m]	RMSE: $T_{m0,1}$ [s]	RMSE: $T_{m-1,0}$ [s]
5	0.086	0.262	0.222
15	0.017	0.249	0.133
40	0.009	0.339	0.264
60	0.012	0.356	0.302
80	0.013	0.363	0.318

Table B.3.: Root mean square error for Chezy approach.

k_s [m]	RMSE: H_{m0} [m]	RMSE: $T_{m0,1}$ [s]	RMSE: $T_{m-1,0}$ [s]
0.01	0.005	0.337	0.272
0.15	0.006	0.290	0.165
0.4	0.009	0.274	0.144
0.6	0.009	0.275	0.143
2	0.010	0.275	0.143

Table B.4.: Root mean square error for White Colebrook approach.

B.5. Wave flume set-up

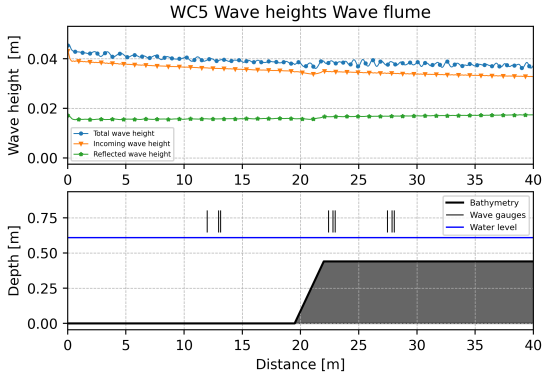

Figure B.5.: Wave condition 5, Significant wave heights

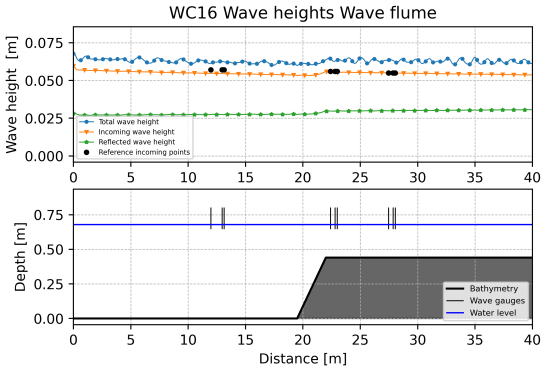

Figure B.6.: Wave condition 16, Significant wave heights

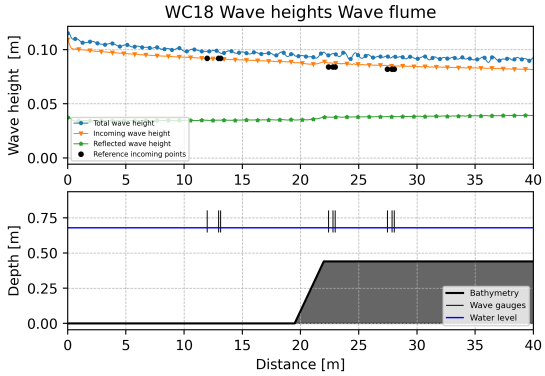

Figure B.7.: Wave condition 18, Significant wave heights

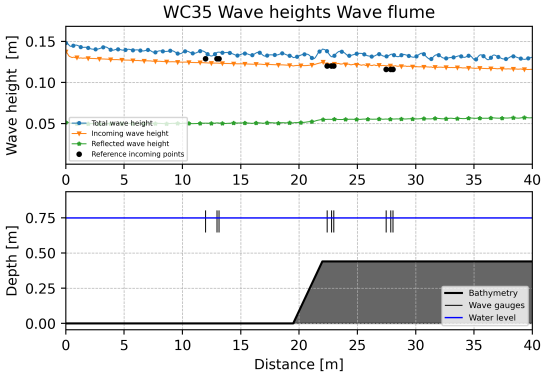

Figure B.8.: Wave condition 35, Significant wave heights

Figure B.9.: Total significant wave height evolution for the wave conditions that are going to be used, without the breakwater inside.

C. Results

In this appendix the evolution of the incoming wave heights will be given, from Section 4. In the first section, Section C.1 the results from the different solutions are presented. In Section C.2 the results from the validation with the different solutions are given.

C.1. Results from the solutions

The results for this section are given for wave conditions 16 and 35. These two wave conditions were chosen because both structures were tested for them, making the comparison easier.

Breakwater as a change in the bathymetry (Original case)

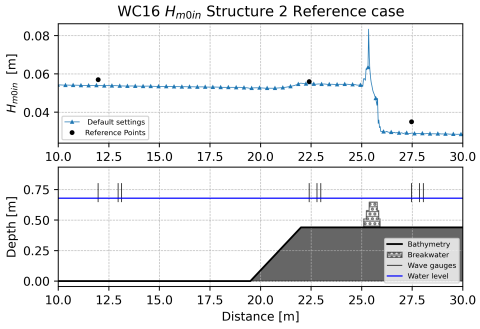

Figure C.1.: Incoming wave heights for WC16 Structure 2 Original case

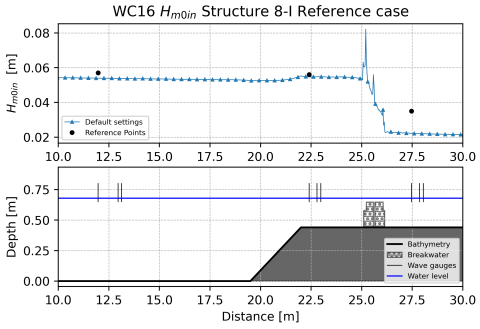

Figure C.2.: Incoming wave heights for WC16 Structure 8-I Original case

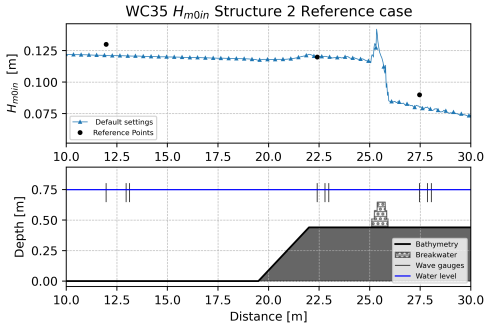

Figure C.3.: Incoming wave heights for WC35 Structure 2 Original case

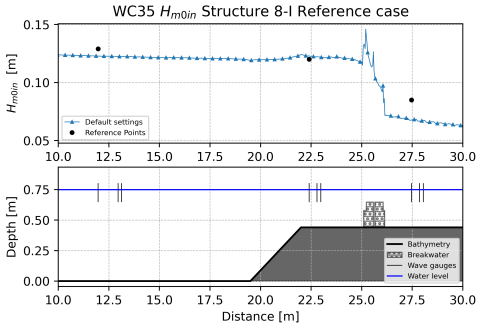

Figure C.4.: Incoming wave heights for WC35 Structure 8-I Original case

Decrease in the structure heights

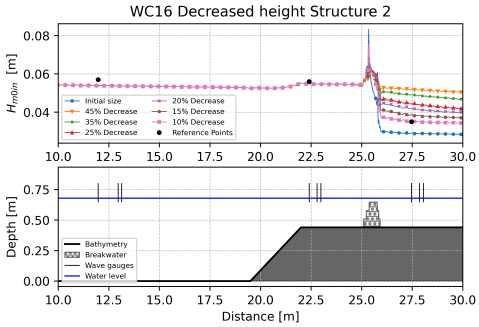

Figure C.5.: Incoming wave heights for WC16 change in heights Structure 2

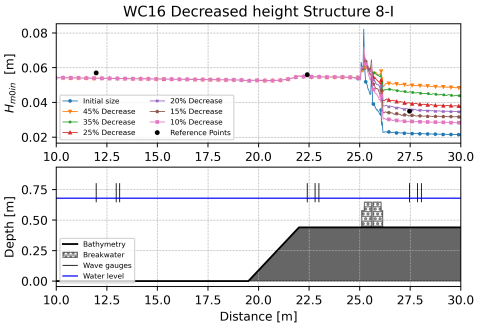

Figure C.6.: Incoming wave heights for WC16 change in heights Structure 8-I

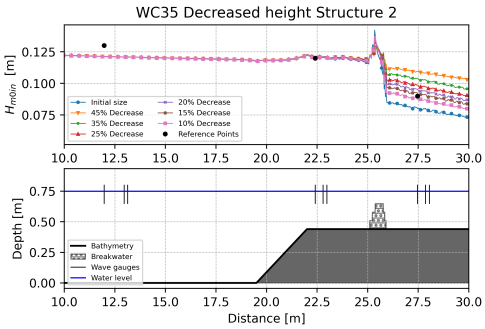

Figure C.7.: Incoming wave heights for WC35 change in heights Structure 2

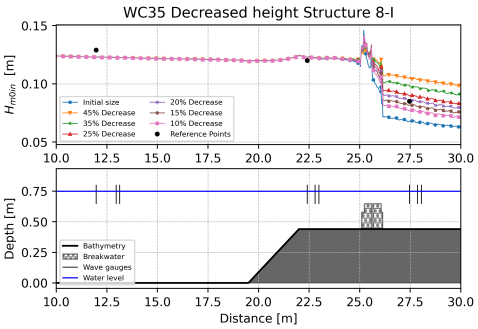

Figure C.8.: Incoming wave heights for WC35 change in heights Structure 8-I

Figure C.9.: Incoming wave height evolution for decreasing the structure height.

Decrease in the structure widths

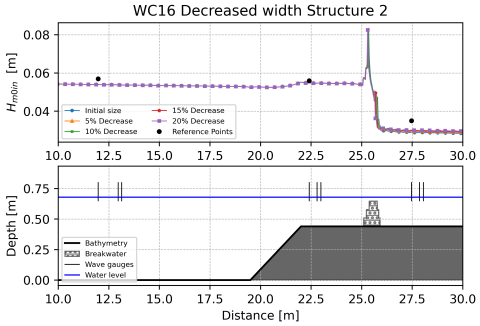

Figure C.10.: Incoming wave heights for WC16 change in widths Structure 2

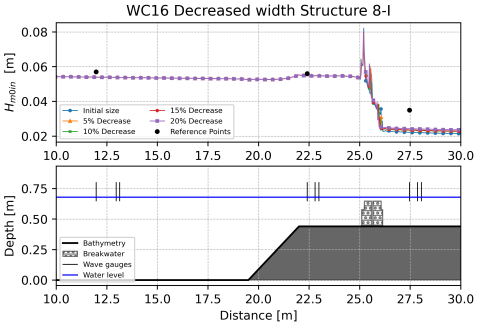

Figure C.11.: Incoming wave heights for WC16 change in widths Structure 8-I

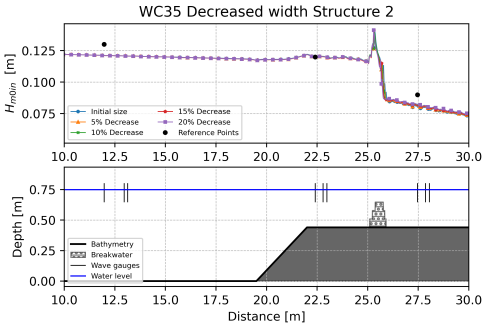

Figure C.12.: Incoming wave heights for WC35 change in widths Structure 2

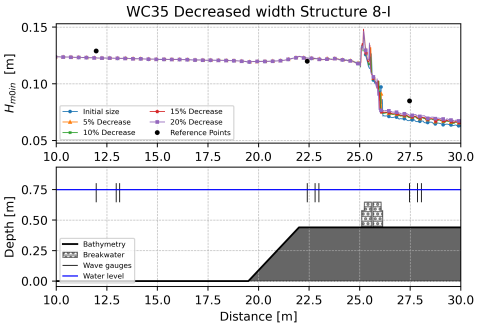

Figure C.13.: Incoming wave heights for WC35 change in widths Structure 8-I

Figure C.14.: Incoming wave height evolution for decreasing the structure width.

Change in wave steepness parameter

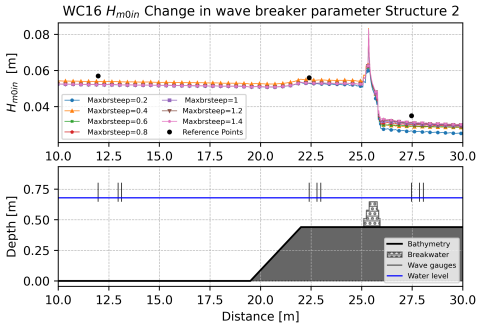

Figure C.15.: Incoming wave heights for WC16 change in Maxbrsteep Structure 2

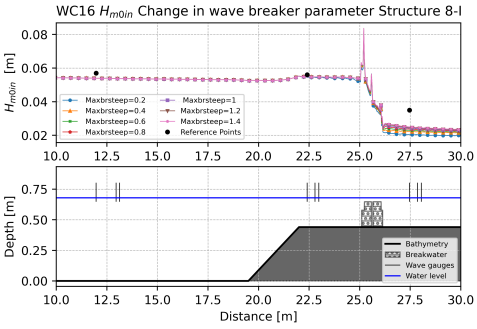

Figure C.16.: Incoming wave heights for WC16 change in Maxbrsteep Structure 8-I

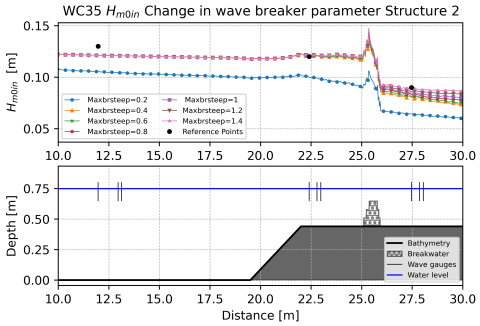

Figure C.17.: Incoming wave heights for WC35 change in Maxbrsteep Structure 2

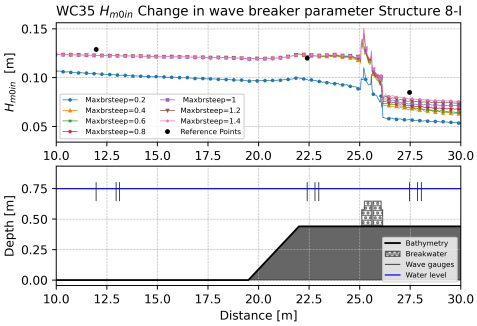

Figure C.18.: Incoming wave heights for WC35 change in Maxbrsteep Structure 8-I

Figure C.19.: Incoming wave height evolution for increasing the maximum wave steepness.

Vegetation Module

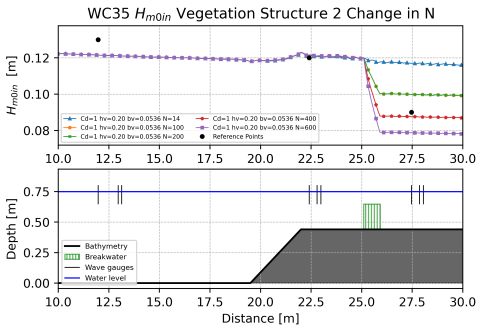

Figure C.20.: Incoming wave heights WC16 change in N Structure 2.

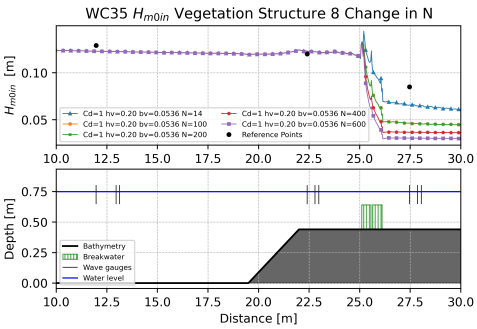

Figure C.21.: Incoming wave heights WC16 change in N Structure 8-I.

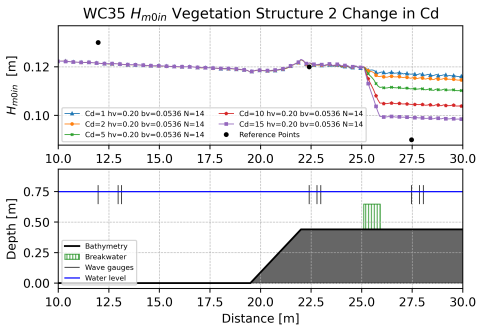

Figure C.22.: Incoming wave heights WC16 change in Cd Structure 2.

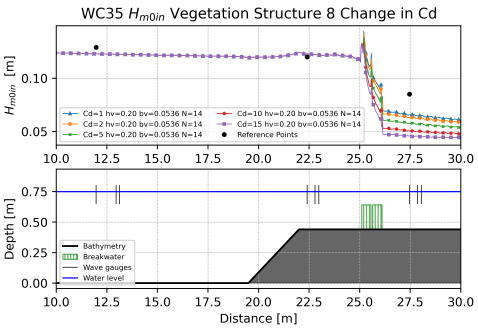

Figure C.23.: Incoming wave heights WC16 change in Cd Structure 8-I.

Figure C.24.: Incoming wave height evolution for vegetation module.

C.2. Results from the validation

Set-up of the breakwaters

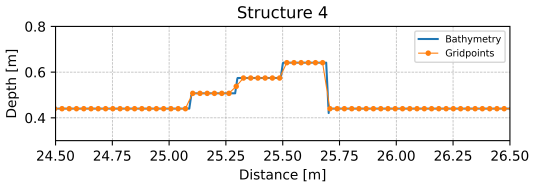

Figure C.25.: Bathymetry and grid points of structure 4.

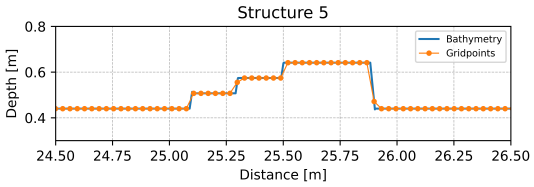

Figure C.26.: Bathymetry and grid points of structure 5.

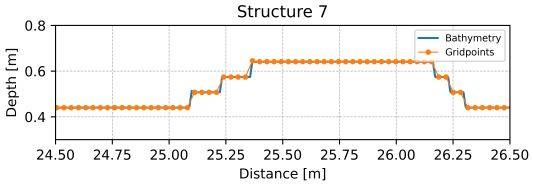

Figure C.27.: Bathymetry and grid points of structure 7.

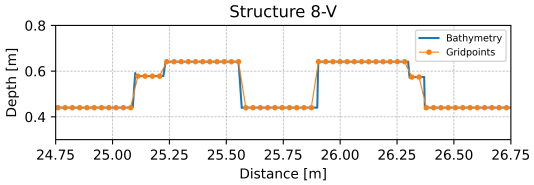

Figure C.28.: Bathymetry and grid points of structure 8-V.

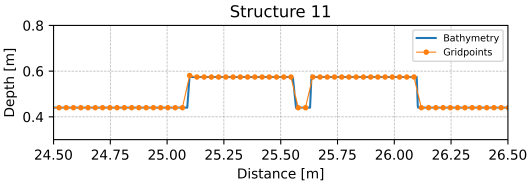

Figure C.29.: Bathymetry and grid points of structure 11.

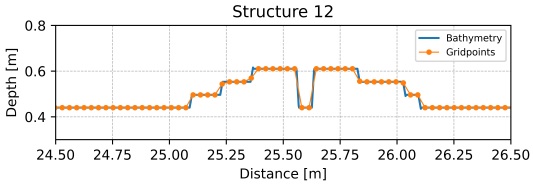

Figure C.30.: Bathymetry and grid points of structure 12.

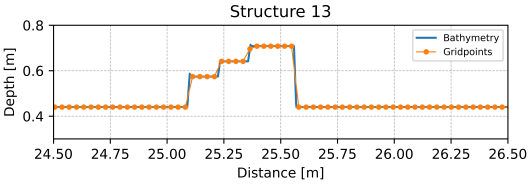

Figure C.31.: Bathymetry and grid points of structure 13.

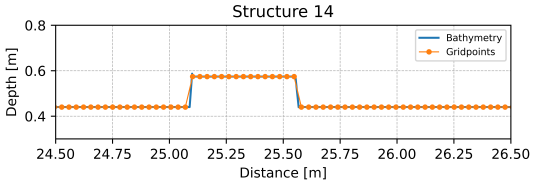

Figure C.32.: Bathymetry and grid points of structure 14.

Figure C.33.: Bathymetries of the extra structures that are going to be used for the validation.

Error plots

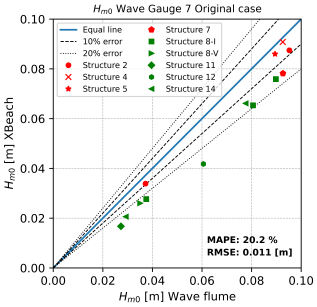

Figure C.34.: H_{m0} error for all structures.

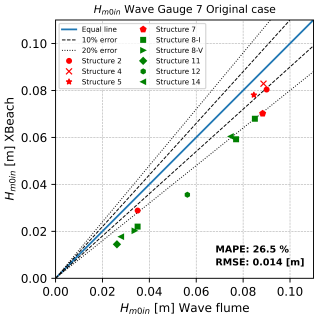

Figure C.35.: H_{m0in} error for all structures.

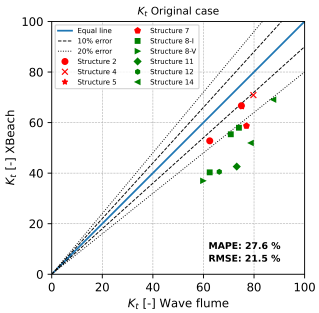

Figure C.36.: K_t error for all structures.

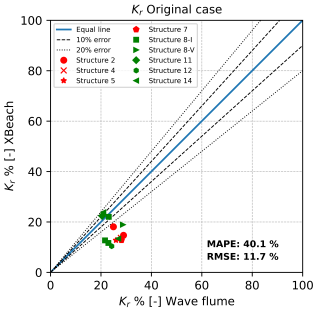

Figure C.37.: K_r error for all structures.

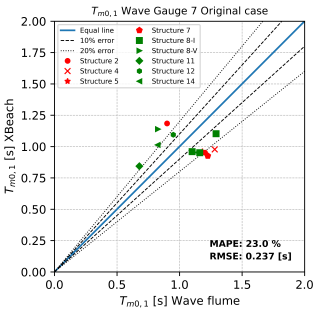

Figure C.38.: $T_{m0,1}$ error for all structures.

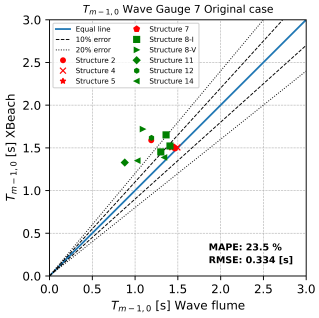

Figure C.39.: $T_{m-1,0}$ error for all structures

Figure C.40.: Error plots for all the structures used in the validation, for the Original case.

Significant wave height evolution

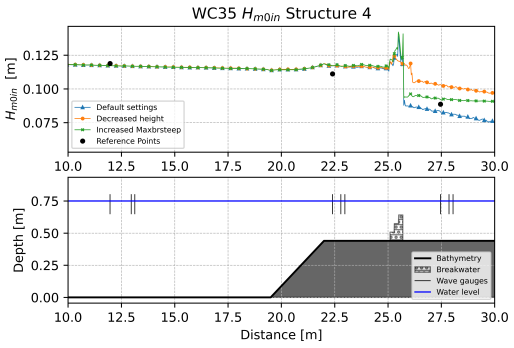

Figure C.41.: Incoming wave heights for WC35 Structure 4

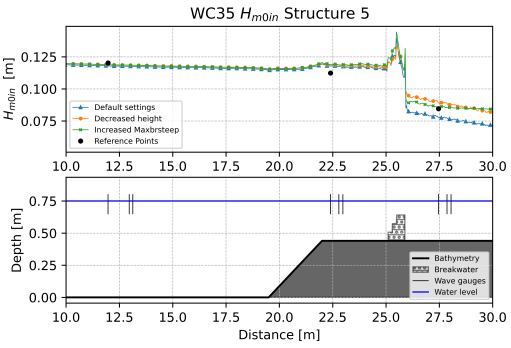

Figure C.42.: Incoming wave heights for WC35 Structure 5

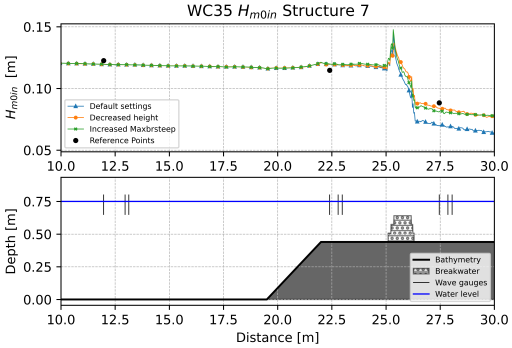

Figure C.43.: Incoming wave heights for WC35 Structure 7

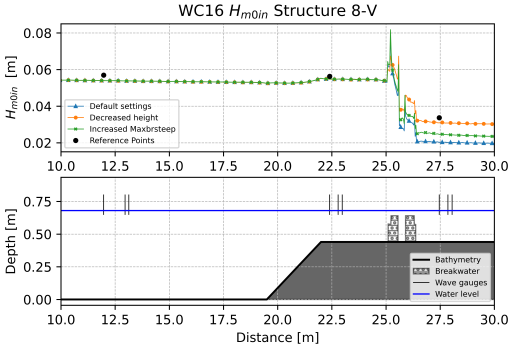

Figure C.44.: Incoming wave heights for WC16 Structure 8-V

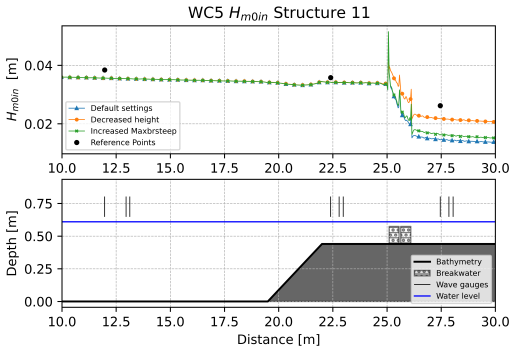

Figure C.45.: Incoming wave heights for WC5 Structure 11

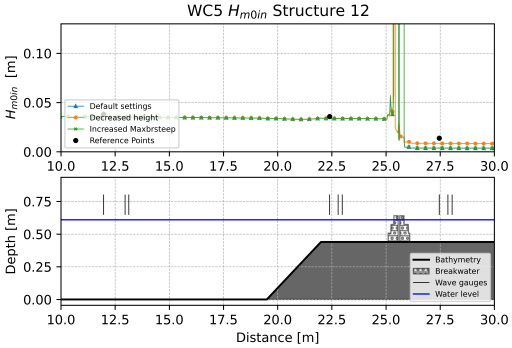

Figure C.46.: Incoming wave heights for WC5 Structure 12

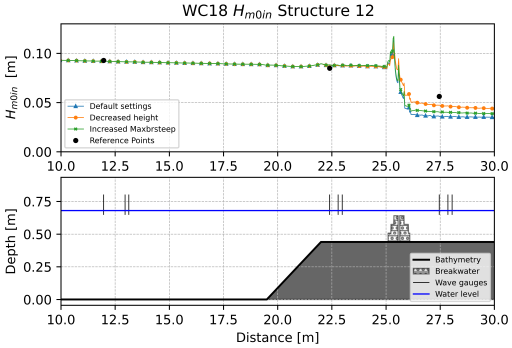

Figure C.47.: Incoming wave heights for WC18 Structure 12

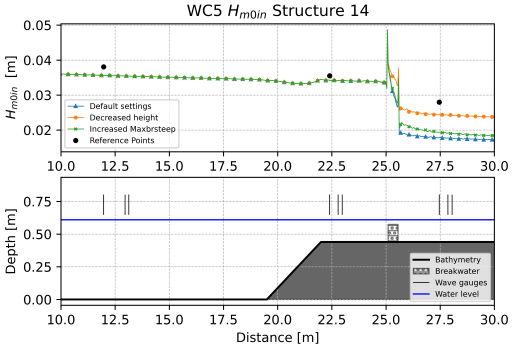

Figure C.48.: Incoming wave heights for WC5 Structure 14

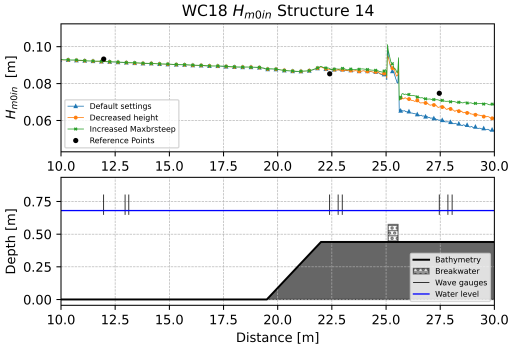

Figure C.49.: Incoming wave heights for WC18 Structure 14

Figure C.50.: Incoming wave height evolution for all the structures used in the validation. In the figures, the wave evolution is shown and compared for: the Original case, 15% decrease in structure height and Maxbrsteep=1.4.

Bibliography

Airoldi, L., Abbiati, M., Beck, M. W., Hawkins, S. J., Jonsson, P. R., Martin, D., Moschella, P. S., Sundelöf, A., Thompson, R. C., and Åberg, P. (2005). An ecological perspective on the deployment and design of low-crested and other hard coastal defence structures. *Coastal Engineering*, 52(10-11):1073–1087.

Beck, M. W., Heck, N., Narayan, S., Menéndez, P., Reguero, B. G., Bitterwolf, S., Torres-Ortega, S., Lange, G.-M., Pfliegner, K., Pietsch McNulty, V., and Losada, I. J. (2022). Return on investment for mangrove and reef flood protection. *Ecosystem Services*, 56:101440.

Bilkovic, D. M., Mitchell, M., Mason, P., and Duhring, K. (2016). The Role of Living Shorelines as Estuarine Habitat Conservation Strategies. *Coastal Management*, 44(3):161–174.

Bilkovic, D. M. and Mitchell, M. M. (2013). Ecological tradeoffs of stabilized salt marshes as a shoreline protection strategy: Effects of artificial structures on macrobenthic assemblages. *Ecological Engineering*, 61:469–481.

Brown, S., Jenkins, K., Goodwin, P., Lincke, D., Vafeidis, A. T., Tol, R. S., Jenkins, R., Warren, R., Nicholls, R. J., Jevrejeva, S., Arcilla, A. S., and Haigh, I. D. (2021). Global costs of protecting against sea-level rise at 1.5 to 4.0 °C. *Climatic Change*, 167(1-2).

Chen, Q. (2006). Fully Nonlinear Boussinesq-Type Equations for Waves and Currents over Porous Beds. *J. Eng. Mech.*, pages 220–230.

Cui, H., Pietrzak, J. D., and Stelling, G. S. (2014). Optimal dispersion with minimized Poisson equations for non-hydrostatic free surface flows. *Ocean Modelling*, 81:1–12.

Darcy, H. (1856). *Les fontaines publiques de la ville de Dijon: Exposition et application des principes à suivre et des formules à employer dans les questions de distribution d'eau: Ouvrage terminé par un appendice relatif aux fournitures d'eau de plusieurs villes, au filtrage des eaux et à la fabrication des tuyaux de fonte, de plomb, de tôle et de bitume*, volume 2. V. Dalmont.

Dattatri, Raman, H., and Jothi Shankar, N. (1978). PERFORMANCE CHARACTERISTICS OF SUBMERGED BREAKWATERS 12 3 J. *Coastal Engineering Proceedings*, 16:130–130.

De Lemos, M. J. (2012). *Turbulence in porous media: modeling and applications*. Elsevier.

De Ridder, M. (2018). Non-hydrostatic wave modelling of coral reefs with the addition of a porous in-canopy model. *Delft University of Technology. MSc Thesis. Retrieved from http://resolver. tudelft. nl/uuid: 4f738968-be52–4484-af1d-60a0e74fdbab*.

de Ridder, M. P., Smit, P. B., van Dongeren, A. R., McCall, R. T., Nederhoff, K., and Reniers, A. J. (2021). Efficient two-layer non-hydrostatic wave model with accurate dispersive behaviour. *Coastal Engineering*, 164.

del Jesus, M., Lara, J. L., and Losada, I. J. (2012). Three-dimensional interaction of waves and porous coastal structures. Part I: Numerical model formulation. *Coastal Engineering*, 64:57–72.

Dick, T. M. and Res, A. (1968). Solid and permeable submerged breakwaters. *Coastal Engineering Proceedings*, 11:72–72.

Diplarakos, N. (2016). Velocity measurements in and around a permeable breakwater. Student report, Delft University of Technology.

Er, E. ., Cruz, E. C., Isobe, M., and Watanabe, A. (1997). COASTAL ENGINEERING Boussinesq equations for wave transformation on porous beds. Technical report.

European Commission and Directorate-General for Research and Innovation (2015). *Towards an EU research and innovation policy agenda for nature-based solutions & re-naturing cities : final report of the Horizon 2020 expert group on 'Nature-based solutions and re-naturing cities' : (full version)*. Publications Office.

Ferrario, F., Beck, M. W., Storlazzi, C. D., Micheli, F., Shepard, C. C., and Airoldi, L. (2014). The effectiveness of coral reefs for coastal hazard risk reduction and adaptation. *Nature Communications*, 5.

Forchheimer, P. (1901). Wasserbewegung durch boden. *Z. Ver. Deutsch, Ing.*, 45:1782–1788.

Gracia, A., Rangel-Buitrago, N., Oakley, J. A., and Williams, A. (2018). Use of ecosystems in coastal erosion management. *Ocean & coastal management*, 156:277–289.

Gu, G. Z. and Wang, H. (1992). CHAPTER 90 NUMERICAL MODELING FOR WAVE ENERGY DISSIPATION WITHIN POROUS SUBMERGED BREAKWATERS OF IRREGULAR CROSS SECTION. *Coastal Engineering Proceedings*.

Guza, R., Thornton, E., and Holman, R. (1984). Swash on steep and shallow beaches. In *Coastal Engineering 1984*, pages 708–723.

Han, M. and Wang, C. (2022). Potential flow theory-based analytical and numerical modelling of porous and perforated breakwaters: A review. *Ocean Engineering*, 249:110897.

Harris, D. L., Rovere, A., Casella, E., Power, H., Canavesio, R., Collin, A., Pomeroy, A., Webster, J. M., and Parravicini, V. (2018). Coral reef structural complexity provides important coastal protection from waves under rising sea levels. *Science advances*, 4(2):eaao4350.

Hieu, P. D. and Tanimoto, K. (2006). Verification of a VOF-based two-phase flow model for wave breaking and wave–structure interactions. *Ocean Engineering*, 33(11):1565–1588.

Hofland, B., Chen, X., Altomare, C., and Oosterlo, P. (2017). Prediction formula for the spectral wave period Tm-1,0 on mildly sloping shallow foreshores. *Coastal Engineering*, 123:21–28.

Holthuijsen, L. H. (2007). *Waves in Oceanic and Coastal Waters*. Cambridge University Press.

Hsiao, S.-C., Hu, K.-C., and Hwung, H.-H. (2009). Extended Boussinesq Equations for Water-Wave Propagation in Porous Media. *J. Eng. Mech.*, pages 625–640.

Hsu, T.-J., Sakakiyama, T., and Liu, P. L.-F. (2002). A numerical model for wave motions and turbulence flows in front of a composite breakwater. *Coastal Engineering*, 46(1):25–50.

Hsu, T. W., Chang, J. Y., Lan, Y. J., Lai, J. W., and Ou, S. H. (2008). A parabolic equation for wave propagation over porous structures. *Coastal Engineering*, 55(12):1148–1158.

Huang, C. J., Chang, H. H., and Hwung, H. H. (2003). Structural permeability effects on the interaction of a solitary wave and a submerged breakwater. *Coastal Engineering*, 49(1-2):1–24.

Kobayashi, N., Otta, A. K., and Roy, I. (1987). Wave reflection and run-up on rough slopes. *Journal of Waterway, Port, Coastal, and Ocean Engineering*, 113(3):282–298.

Kurdistani, S. M., Tomasicchio, G. R., D Alessandro, F., and Francone, A. (2022). Formula for wave transmission at submerged homogeneous porous breakwaters. *Ocean Engineering*, 266.

Lamberti, A. and Burcharth, H. (2004). EU Fifth Framework Programme 1998-2002 Energy, Environment and Sustainable Development Environmental Design of Low Crested Coastal Defence Structures DELOS FINAL REPORT. Technical report, University of Bologna.

Lashley, C. H., Roelvink, D., van Dongeren, A., Buckley, M. L., and Lowe, R. J. (2018). Nonhydrostatic and surfbeat model predictions of extreme wave run-up in fringing reef environments. *Coastal Engineering*, 137:11–27.

Liang, B., Wu, G., Liu, F., Fan, H., and Li, H. (2015). Numerical study of wave transmission over double submerged breakwaters using non-hydrostatic wave model. *Oceanologia*, 57(4):308–317.

Lin, P. and Karunarathna, S. A. (2007). Numerical Study of Solitary Wave Interaction with Porous Breakwaters. *Journal of Waterway, Port, Coastal, and Ocean Engineering*, 133(5):352–363.

Losada, I. J., Lara, J. L., and del Jesus, M. (2016). Modeling the Interaction of Water Waves with Porous Coastal Structures. *Journal of Waterway, Port, Coastal, and Ocean Engineering*, 142(6).

Losada, M. A., Martin, P. A., and Dalrymple, R. A. (1991). Reflection and transmission from porous structures under oblique wave attack. *Journal of Fluid Mechanics*, 224:625–644.

Ma, G., Shi, F., Hsiao, S.-C., and Wu, Y.-T. (2014). Non-hydrostatic modeling of wave interactions with porous structures. *Coastal Engineering*, 91:84–98.

Madsen, P. A. and Sørensen, O. R. (1992). A new form of the boussinesq equations with improved linear dispersion characteristics. part 2. a slowly-varying bathymetry. *Coastal engineering*, 18(3-4):183–204.

Manson, T., Gilman, J. F., Perkol-Finkel, S., Sella, I., and Marrone, J. F. (2018). Multi-Purpose Breakwaters. pages 449–458. Thomas Telford Ltd.

Méhauté, B. (1976). *An Introduction to Hydrodynamics and Water Waves*. Springer Berlin Heidelberg, Berlin, Heidelberg.

Méndez, F. J., Losada, I. J., and Losada, M. A. (2001). Wave-induced mean magnitudes in permeable submerged breakwaters. *Journal of waterway, port, coastal, and ocean engineering*, 127(1):7–15.

Metallinos, A. S., Klonaris, G. T., Memos, C. D., and Dimas, A. A. (2019). Hydrodynamic conditions in a submerged porous breakwater. *Ocean Engineering*, 172:712–725.

Metallinos, A. S., Repousis, E. G., and Memos, C. D. (2016). Wave propagation over a submerged porous breakwater with steep slopes. *Ocean Engineering*, 111:424–438.

Narayan, S., Beck, M. W., Reguero, B. G., Losada, I. J., Van Wesenbeeck, B., Pontee, N., Sanchirico, J. N., Ingram, J. C., Lange, G. M., and Burks-Copes, K. A. (2016). The effectiveness, costs and coastal protection benefits of natural and nature-based defences. *PLoS ONE*, 11(5).

Pearson, S. G. (2016). Predicting wave-induced flooding on low-lying tropical islands using a bayesian network. Master thesis, Delft University of Technology.

P.Leatherman, S. (2000). Sea Level Rise Shown to Drive Coastal Erosion. Technical report.

Pomeroy, A., Lowe, R., Symonds, G., Van Dongeren, A., and Moore, C. (2012). The dynamics of infragravity wave transformation over a fringing reef. *Journal of Geophysical Research: Oceans*, 117(11).

Qu, K., Huang, J. X., Guo, L., and Li, X. H. (2022). Numerical Study on Hydrodynamics of Submerged Permeable Breakwater under Impacts of Focused Wave Groups Using a Nonhydrostatic Wave Model. *Journal of Marine Science and Engineering*, 10(11):1618.

Quataert, E. (2015). Wave runup on atoll reefs. Master thesis, Delft University of Technology.

Quataert, E., Storlazzi, C., Van Rooijen, A., Cheriton, O., and Van Dongeren, A. (2015). The influence of coral reefs and climate change on wave-driven flooding of tropical coastlines. *Geophysical Research Letters*, 42(15):6407–6415.

Reaka-Kudla, M. L. (1997). The global biodiversity of coral reefs: a comparison with rain forests. In Reaka-Kudla, M. L., Wilson, D. E., and Wilson, E. O., editors, *Biodiversity II: Understanding and Protecting Our Biological Resources*, pages 83–108. Joseph Henry Press, Washington.

Rijnsdorp, D. P., Smit, P. B., Zijlema, M., and Reniers, A. J. (2017). Efficient non-hydrostatic modelling of 3D wave-induced currents using a subgrid approach. *Ocean Modelling*, 116:118–133.

Roelvink, D., Reniers, A., van Dongeren, A., van Thiel de Vries, J., McCall, R., and Lescinski, J. (2009). Modelling storm impacts on beaches, dunes and barrier islands. *Coastal Engineering*, 56(11-12):1133–1152.

Rojanakamthorn, S., Isobe, M., and Watanabe, A. (1989). A Mathematical Model of Wave Transformation over a Submerged Breakwater. *Coastal Engineering in Japan*, 32(2):209–234.

Salman, A., Lombardo, S., and Doody, P. (2004). Living with coastal erosion in europe: Sediment and space for sustainability. *Eurosion project reports*.

Schoonees, T., Gijón Mancheño, A., Scheres, B., Bouma, T. J., Silva, R., Schlurmann, T., and Schüttrumpf, H. (2019). Hard Structures for Coastal Protection, Towards Greener Designs. *Estuaries and Coasts*, 42(7):1709–1729.

Sheppard, C., Dixon, D. J., Gourlay, M., Sheppard, A., and Payet, R. (2005). Coral mortality increases wave energy reaching shores protected by reef flats: Examples from the Seychelles. *Estuarine, Coastal and Shelf Science*, 64(2-3):223–234.

Singhvi, A., Luijendijk, A. P., and van Oudenhoven, A. P. (2022). The grey–green spectrum: A review of coastal protection interventions. *Journal of Environmental Management*, 311:114824.

Smit, P., Janssen, T., Holthuijsen, L., and Smith, J. (2014a). Non-hydrostatic modeling of surf zone wave dynamics. *Coastal Engineering*, 83:36–48.

Smit, P. B., Stelling, G. S., Roelvink, D., Van Thiel De Vries, J., Mccall, R., Van Dongeren, A., Zwinkels, C., and Jacobs, R. (2014b). XBeach: Non-hydrostatic model, Technical report. Technical report, Deltares, Delft, The Netherlands.

Sollitt, C. K. and Cross, R. H. (1972). Wave transmission through permeable breakwaters. In *Coastal Engineering 1972*, pages 1827–1846.

Spalding, M. D., Ruffo, S., Lacambra, C., Meliane, I., Hale, L. Z., Shepard, C. C., and Beck, M. W. (2014). The role of ecosystems in coastal protection: Adapting to climate change and coastal hazards. *Ocean and Coastal Management*, 90:50–57.

Toimil, A., Losada, I. J., Nicholls, R. J., Dalrymple, R. A., and Stive, M. J. (2020). Addressing the challenges of climate change risks and adaptation in coastal areas: A review. *Coastal Engineering*, 156:103611.

Twu, S.-W., Liu, C.-C., and Hsu, W.-H. (2001). WAVE DAMPING CHARACTERISTICS OF DEEPLY SUBMERGED BREAKWATERS. *Journal of waterway, port, coastal, and ocean engineering*, 127:97–105.

UNFCCC (2016). THE PARIS AGREEMENT. Technical report, United Nations / Framework Convention on Climate Change (2015) Adoption of the Paris Agreement.

van den Brekel, E. (2021). Hydrodynamic and ecological performance of a new modular unit for living breakwaters wave flume experiments and results. Master thesis, Delft University of Technology.

van der Meer, J. W., Briganti, R., Zanuttigh, B., and Wang, B. (2005). Wave transmission and reflection at low-crested structures: Design formulae, oblique wave attack and spectral change. *Coastal Engineering*, 52(10-11):915–929.

Van Dongeren, A., Lowe, R., Pomeroy, A., Trang, D. M., Roelvink, D., Symonds, G., and Ranasinghe, R. (2012). Modelling infragravity waves and currents across a fringing coral reef. In *Proceedings of the Coastal Engineering Conference*.

van Gent, M. R. (1994). The modelling of wave action on and in coastal structures. *Coastal Engineering*, 22(3-4):311–339.

Van Gent, M. R. A. (1993). Stationary and oscillatory flow through coarse porous media. *Communications on hydraulic and geotechnical engineering, No. 1993-09*.

Van Gent, M. R. A. (1995). Wave interaction with permeable coastal structures. Doctoral thesis, Delft University of Technology.

Welch, P. D. (1967). The Use of Fast Fourier Transform for the Estimation of Power Spectra: A Method Based on Time Averaging Over Short, Modified Periodograms. *IEEE Transactions on Audio and Electroacoustics*, 15(2):70–73.

Wu, Y. T. and Hsiao, S. C. (2013). Propagation of solitary waves over a submerged permeable breakwater. *Coastal Engineering*, 81:1–18.

Wu, Y.-T., Hsiao, S.-C., and Chen, G.-S. (2012). SOLITARY WAVE INTERACTION WITH A SUBMERGED PERMEABLE BREAKWATER: EXPERIMENT AND NUMERICAL MODELING. *Coastal Engineering Proceedings*, 33:1–14.

Wurjanto, A. and Kobayashi, N. (1993). Irregular wave reflection and runup on permeable slopes. *Journal of Waterway, Port, Coastal, and Ocean Engineering*, 119(5):537–557.

Zanuttigh, B. and van der Meer, J. W. (2008). Wave reflection from coastal structures in design conditions. *Coastal Engineering*, 55(10):771–779.

Zelt, J. and Skjelbreia, J. E. (1992). Estimating incident and reflected wave fields using an arbitrary number of wave gauges. In *Coastal Engineering 1992*, pages 777–789.

Zijlema, M., Stelling, G., and Smit, P. (2011). SWASH: An operational public domain code for simulating wave fields and rapidly varied flows in coastal waters. *Coastal Engineering*, 58(10):992–1012.

Colophon

This document was typeset using LaTeX, using the KOMA-Script class `scrbook`. The main font is Palatino.